INVESTIGATION OF ANTICORROSIVE PROPERTIES OF SOME IONIC LIQUIDS ON SELECTED METALS

Anitah Nkuna

Student number: 16023639

A dissertation submitted in fulfilment of the requirements for the degree of

Master of Science

in the

Department of Chemistry

School of Mathematical and Natural Sciences

University of Venda

Thohoyandou, Limpopo

South Africa

Supervisor: DR MA LEGODI

Co-supervisor: DR LC MURULANA

Co-supervisor: DR JK KIRUI

© University of Venda

DECLARATION

I hereby declare that the work in this dissertation is my own and was under the supervision of Dr M. Legodi, and Dr L.C. Murulana and Dr J.K. Kirui as my co-supervisors. The information derived from literature have been duly acknowledged in text and a list of references provided. This work is being submitted for the degree of Master of Science in Chemistry at the University of Venda and has not been submitted before for any degree or examination at any other university.

Full Names: ……..... Date: …….

Signature ……

© University of Venda

University of Venda
Creating Future Leaders

TABLE OF CONTENTS

© University of Venda

© University of Venda

ACKNOWLEDGEMENTS

First and foremost, I would like to thank my Father in heaven for this great opportunity to further my studies. I thank Him for the wisdom and health He gave me to do the work.

To my supervisor, Dr L.C. Murulana, you are an answered prayer. It has been such a great privilege to work under your supervision. I thank you for literally going out of your way to ensure that everything that needed to be done for this project was done. I am truly grateful for the guidance you offered throughout this project, and for the wisdom that you selflessly imparted on me.

I would like to thank my other supervisors, Dr M. Legodi and Dr J.K. Kirui for their contribution to this project. Your help is greatly appreciated!

To the Chemistry Department at the University of Venda, thank you for the help and support throughout this project.

I would like to extend my deepest appreciation to the Chemistry Department at North-West University (Mafikeng Campus) and Prof Eno E. Ebenso for opening their doors for me to do my electrochemical research. This project would be incomplete if it were not for your generosity. Thank you so much!
I would also like to thank Mr T.W. Quadri from NWU for taking the time to teach me how to operate the Potentiostat. I am grateful for your help.

I would like to extent my sincere gratitude to MINTEK for allowing me to collect SEM/EDS data.

My sincere gratitude also goes to the NRF and Sasol Inzalo Foundation for funding my studies. Words cannot fully describe how grateful I am for such great a financial assistance.

To my family, Mom, Dad, and Ntsako, thank you for believing in me and for the unending support throughout this project. You inspire me to become so much more than what I am right now. I love you all so much.

© University of Venda

ABSTRACT

The corrosion potential of three ionic liquids (ILs) namely, 5-(Trifluoromethyl)dibenzothiophenium tetrafluoroborate (TDTB), 5-(Trifluoromethyl)dibenzothiophenium trifluoromethanesulfonate (TDTM) and 1-Ethyl-3-methylimidazolium ethyl sulfate [EMIM][ESO_4] was studied for mild steel and zinc corrosion in 1.0 M hydrochloric acid using electrochemical, spectroscopic and gravimetric techniques. The studied ILs showed appreciable inhibition efficiencies at the considered concentration range. The highest inhibition efficiencies were observed at 30°C when inhibitor concentration was 8.0 × 10^{-2} M. The gravimetric data revealed that inhibition efficiencies decreased with an increase in temperature, the lowest inhibition efficiencies for mild steel and zinc were observed at 50°C. The potentiodynamic polarization results indicated that all three inhibitors are mixed-type inhibitors, with TDTM being a predominantly anodic inhibitor. The orders of inhibition efficiency at 8.0 × 10^{-2} M were TDTM > TDTB > [EMIM][ESO_4] and TDTB > TDTM > [EMIM]ESO_4] for mild steel and zinc, respectively. All inhibitors showed superior performance in mild steel than in zinc. The adsorption of the studied ILs on mild steel and zinc obeyed the Langmuir adsorption isotherm. The Gibbs free energy of adsorption (ΔG°_{ads}) indicated that the adsorption process was spontaneous, and that corrosion inhibition occurred by a physical adsorption process. Surface morphology analysis through scanning electron microscopy (SEM) and energy dispersive spectroscopy (EDS) revealed a great improvement in the surface morphologies of mild steel and zinc specimens in the inhibited systems. The Fourier transform infrared spectroscopy studies confirmed the chemical interactions between the metal surface and the ILs. This is observed by means of the disappearance of characteristic absorption bands in the adsorption film FTIR spectra.

© University of Venda

LIST OF ABBREVIATIONS

MS	Mild Steel
Zn	Zinc
ILs	Ionic Liquids
TSIL	Task-Specific Ionic Liquids
HCl	Hydrochloric Acid
MINTEK	Council for Mineral Technology
IE	Inhibition Efficiency
SCC	Stress Corrosion Cracking
TDTB	5-(Trifluoromethyl)dibenzothiophenium tetrafluoroborate
TDTM	5-(Trifluoromethyl)dibenzothiophenium trifluoromethanesulfonate
[EMIM][ESO_4]	1-Ethyl-3-methylimidazolium ethyl sulfate
GDP	Nation's Gross Domestic Product
SEM	Scanning Electron Microscopy
EDS	Energy dispersive spectroscopy
FTIR	Fourier Transform Infrared Spectroscopy
SCE	Saturated Calomel Electrode
CE	Counter Electrode
WE	Working Electrode
RE	Reference Electrode
OCP	Open Circuit Potential
PDP	Potentiodynamic Polarization
EIS	Electrochemical Impedance Spectroscopy
FRA	Frequency Response Analyzer
PGSTAT302N	Metrohm Autolab Potentiostat/Galvanostat
C_{dl}	Double Layer Capacitance

© University of Venda

$\mathbf{R_s}$	Solution Resistance
$\mathbf{R_{ct}}$	Charge Transfer Resistance
CPE	Constant Phase Element
IUPAC	International Union of Pure and Applied Chemistry

© University of Venda

University of Venda
Creating Future Leaders

LIST OF FIGURES

© University of Venda

© University of Venda

© University of Venda

© University of Venda

© University of Venda

© University of Venda

University of Venda
Creating Future Leaders

LIST OF TABLES

© University of Venda

1. INTRODUCTION TO CORROSION

1.1. Historical background

The term corrosion is of Latin origin; it stems from the word ‘corrodere’ which means to ‘gnaw away’ [1]. For many people corrosion is known as rust, although the term rust has been recently reserved specifically for the corrosion of iron. Although the occurrence of corrosion has been observed since the introduction of common metals, the idea that some philosophers (e.g. Aristotle (fourth century BC)) had of the universe being made up of a material continuum without any voids may have delayed the theoretical studies of the nature of solid surfaces. This led to very little curiosity when it came to the causes and mechanism of corrosion [2]. The earliest record of surface consideration is attributed to a Roman philosopher by the name of Pliny the Elder (23-79 AD) who wrote about the destruction of iron in his essay entitled ‘Ferrum Corrumpitar’. The reason for the interest in corrosion and solid surfaces was due to the extensive use of iron for weaponry and other artifacts (at that time the Roman Empire was established as the world’s foremost civilization) which then made corrosion a problem that could not be ignored any longer [2]. Corrosion studies were, at that time, only limited to prevention measures and not so much the causes and mechanism. So much time and effort were dedicated to developing prevention methods and evidence of this is seen in the Dhar Pillar in India which has withstood corrosion for over 700 years [1]. The earliest studies of the causes of corrosion were by Robert Boyle (1627−1691) who addressed these causes in two of his publications entitled ‘Of the Mechanical Origin of Corrosiveness’ and ‘Of the Mechanical Origin of Corrodibility’ [1].

One of the most important contributions were made by Michael Faraday (1791−1867) who established a quantitative relationship between electrical quantities (charge and current, its time derivative) and mass changes and material loss rates. It is through Faraday’s first and second laws that we have the basis for the calculation of corrosion rates for metals [3, 4, 5].
Rapid advancement in the study of corrosion occurred during the nineteenth and twentieth centuries. In the nineteenth century interest in this area was spiked by invention of the galvanic battery. The twentieth century, on the other hand, brought about the rediscovery and/or elaboration of theories and facts about corrosion that were established in the nineteenth century [3]. Examples include the electrochemical theory of corrosion which was proposed by Wollaston (1801), developed by de La Rive (1830), confirmed by Ericson-Auren and Palmer (1901) and later rediscovered by Whitney (1901) [1]. Later in 1923 U.R Evans proposed his classical electrochemical theory which provided a modern understanding of the causes and control of corrosion [3].

© University of Venda

U.R Evans, M. Fontana and H.H Uhlig are responsible for the progress towards modern understanding of corrosion [3]. To date, the study of corrosion is continuing to grow and develop. More tertiary institutions globally have made the study of corrosion an integral part of engineering education, with some universities having laboratories dedicated to the sole study of corrosion. Examples of such institutions include Massachusetts Institute of Technology (MIT) in America and University of Cambridge in the United Kingdom [3].

1.1.1. Definition of corrosion

Corrosion is a natural process like tornadoes, floods and volcanic eruptions in that it is equally as destructive [3]. For a long time, the term corrosion was reserved exclusively for metals and alloys. It was not until the 1960s that other materials (polymers, ceramics, composites and semi-conductors) were incorporated into the definition [3]. Metals and alloys, however, remain the principal materials which undergo corrosion.

Metals in service give an impression of permanence, but the reality is that most of them are thermodynamically unstable with the exception of noble metals such as platinum, titanium and gold [6]. This instability arises due to energy that is supplied during the extraction process which causes an increase in the free energy of the metal. The compositional elements within these metals therefore possess a natural tendency (i.e. a driving force which is the high free energy) to revert to their thermodynamically stable (primitive) state, resulting in the formation of corrosion products, i.e. oxides, carbonates, hydroxides or salts [7]. The greater the amount of energy supplied during the extraction process (metals that are more stable in their primitive state will require a lot of energy), the higher the tendency or driving force to corrode [8]. The International Union of Pure and Applied Chemistry (IUPAC) broadly defines corrosion as “an irreversible interfacial reaction of a material (metal, ceramic, polymer) with its environment which results in consumption of the material or in dissolution into the material of a component of the environment” [9, p. 340]. The International Standard (ISO 8044:2015) defines corrosion with respect to metals as the “physicochemical interaction between a metal and its environment that results in changes in the properties of the metal, and which may lead to significant impairment of the function of the metal, the environment, or the technical system, of which these form a part” [10, p. 1].

1.1.2. Corrosive environment

Engineering metals are used in a wide variety of applications in everyday life. For every application, the metallic material may be exposed to a unique environment. Practically every environment to which these metals are exposed are corrosive to some degree, with more severe corrosion being observed in high temperature and pressure environments (common in

© University of Venda

the chemical process industries; without the use of corrosion resistant materials operations would not be possible or economically viable) [11].

Three basic types of corrosive environments will be discussed below, these are atmosphere, water and soil.

- **Atmosphere**

In this environment metals undergo deterioration due to exposure to air and its pollutants at normal temperatures [12]. Corrosion in this environment is the oldest and most common corrosion problem, this is because metal structures are more commonly exposed to the atmosphere than any other corrosive environment [13]. The corrosivity of a particular atmosphere is influenced by several variables. These include: moisture (i.e. relative humidity, rain, dew or condensation), presence of contaminants (e.g. chlorides, NH_3, SO_2, NO_2, hydrogen sulphide, etc.) [14]. Another influencing factor is the geographic location, for example a steel part left in a desert will remain bright and without tarnish for a long time as opposed to one left in a coastal area which will rapidly undergo corrosion [15]. It is due to such variations that corrosion in the atmospheric environment has been found to be very complicated [7].

Atmospheres are generally divided into four major categories (however, most environments are mixed i.e. there is no clear demarcation) namely: industrial, marine, urban and rural [2, 12]. Marine areas are the most corrosive of the four types. In this type of atmosphere, the air is laden with chlorides from the seawaters as well as from the salts being carried by the wind [2, 14]. Industrial atmospheres normally consist of contaminates such as SO_2 and NO_x as pollutants [14]. Urban atmospheres are typically less corrosive than the marine and industrial atmospheres, they usually contain contaminants of the SO_x and NO_x variety emitted from motor vehicles and home fuels [2, 16]. Rural atmospheres are generally the most benign, they do not contain chemical contaminants, but contain organic and inorganic dust [16].

- **Water**

In the context of corrosion, two types of water can be distinguished: fresh water and sea water.

Fresh water

This is naturally occurring water which comes from lakes, rivers, brooks, rain and underground sources [17]. Water has the ability to dissolve every substance found on the Earth's crust to some degree; as a result, water from these sources is generally impure and consists of various constituents. The corrosivity of the water will, in turn, be controlled by the nature and concentration of these constituents (the various constituents have the ability to stimulate or suppress corrosion reaction) [2, 18]. The constituents or impurities can be classified as follows [12, 19]: (a) dissolved gases (e.g. O_2, CO_2, NH_3); (b) mineral constituents including calcium

© University of Venda

(Ca) and magnesium (Mg) salts (hardness salts), salts of heavy metals, sodium salts and silica; (c) organic matter, including that of animal and vegetable origin; (d) microbiological forms. Among the dissolved gases, oxygen plays a very important role in that it stimulates corrosion reactions. Dissolved CO_2 is also very important, however its effect on the corrosivity of fresh water is closely linked with bicarbonate content [12, 19]. The principal ions found in water are calcium, magnesium, sodium, bicarbonate, sulfate, chloride and nitrate. Ions such as chloride increase the electrical conductivity of water, hence facilitating the flow of corrosion currents [12].

Organic matter may exist in suspended or dissolved form. The major source is decaying animal and vegetable matter. Other sources may include domestic and industrial wastes [12]. The microbiological forms in fresh water are usually bacteria, fungi, algae and protozoans. Bacteria, fungi and algae stimulate the corrosion process by producing corrosive by-products, whereas protozoans suppress corrosion, in a way, by preying on the bacteria and algae [12].

Sea water

Due to the increase of offshore oil and gas exploration over the last few decades, sea water has increasingly become an important corrosive environment [17]. Sea water comprises most of the elements which are found on the earth. The chloride content in sea water gives maximum corrosion (as seen in Figure 1.1), however, due to the presence of Ca and Mg salts corrosion tends to be particularly low. These salts usually form deposits on metal structure hence providing a barrier to the diffusion of oxygen [17].

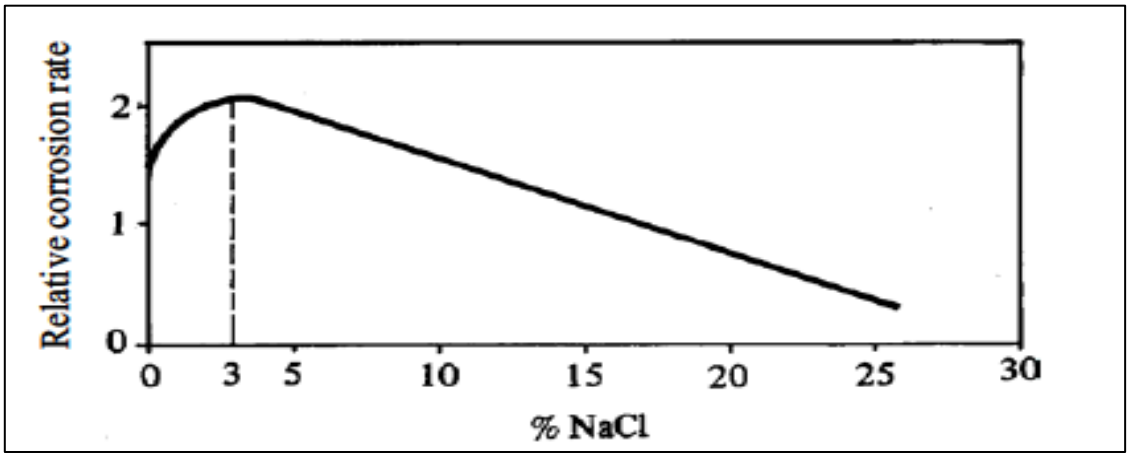

Figure 1.1: Effect of NaCl concentration on corrosion rate of steels in aerated solutions at room temperature [15].

© University of Venda

According to Figure 1.2, corrosion is usually higher at the splash zone where the high tide results in the washing away of corrosion product allowing for oxygen to be easily supplied to the surface [17].

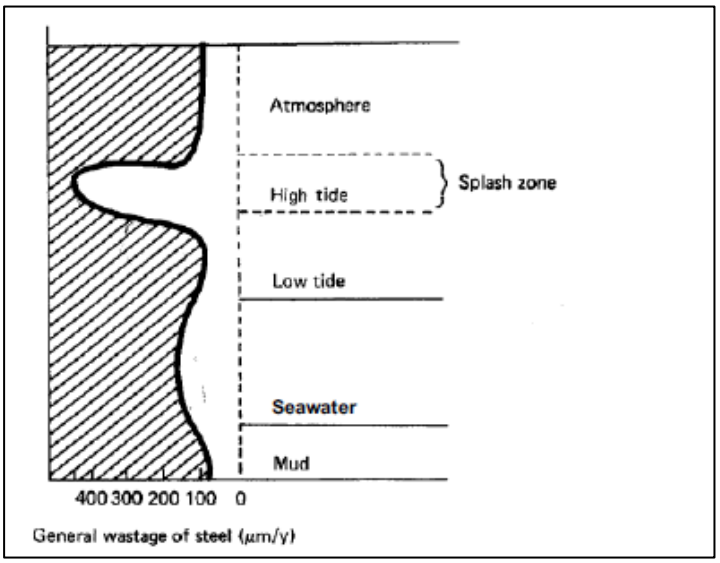

Figure 1.2: Relationship between corrosion rate on steel in sea water and depth [20].

- **Soils**

Many constructions which serve a vital role in the community are buried underground (across the United States alone, there are about 3.7 million kilometres of buried pipelines transporting natural gas and hazardous liquids from their sources to customers) hence, material degradation in soils is of major importance [15, 21, 22]. The corrosion process in soils is a complex one; it is affected by several variables which are still not fully understood. These variables include: degree of aeration, presence of soil moisture, electrical conductivity or resistivity, dissolved salts, pH value and microbial activity [21, 22]. Degree of aeration (oxygen concentration) and presence of soil moisture are very important parameters in controlling the rate of corrosion. Soils which are porous may retain moisture or oxygen over a long period. The content of the pores will be determined by the position of the soil relative to the water table i.e. soils at greater depths will be close to the water table and hence contain more moisture than oxygen in their pores [15]. There are certain instances where oxygen does not play a vital role. This occurs when microbes (such as sulfate-reducing bacteria) are present in the soil. When these microbes are present corrosion rates can be high even under poorly aerated conditions [12]. Variables such as the resistivity and the amount of dissolved salts have a mutual relationship (i.e. soil which has a high concentration of dissolved salts will have low resistivity, and hence typically very corrosive) [22].

© University of Venda

1.1.3. Cost of corrosion

Many sectors in a nation's economy experience losses associated with the corrosion of metallic materials. The phenomenon results in the loss of metals, materials, energy, labour, etc. [23]. Studies that have been carried out in various industrialized countries show consistent results of the economic losses that happen due to corrosion. These results show that corrosion costs for each studied country amount to about 3 − 5% of the Gross Domestic Product (GDP) [15, 24].

These losses can be divided into two categories [15, 23]

- Direct losses and
- Indirect losses.

Direct losses include [15, 23]:

- Cost of replacing corroded or failed structures and machinery (or their components such as condenser tubes, pipelines and metal roofing).
- Painting and repainting of structures for rust prevention,
- Costs for all other protective or control measures, such as inhibitor addition, galvanizing, cathodic protection, protective coating, etc.
- Extra costs for the use of corrosion-resistant metals and alloys (such as stainless steel, titanium, nickel base alloys, etc.) instead of carbon steel.
- Costs for dehumidifying storage rooms that store metallic equipment.

The value of indirect losses is more difficult to evaluate; however, these losses contribute substantially to the total cost of corrosion.

These indirect losses include [2, 15]:

- Plant shutdowns: Forced shutdowns of process plants, power plants, nuclear plants and refineries due to corrosion failure may result in the loss of thousands of rands due to lost production.
- Loss of product: Losses of water, gas or oil may occur due to leakage of corroded pipe systems. Leakage may result in severe accidents and hazards.
- Loss of efficiency: This may occur because of the reduction of heat transfer and pumping efficiency due to the accumulation of corrosion product scales on pipelines and on the heat transfer surfaces. Thus, the heat exchangers and pumps require increased power.

In addition, corrosion costs can be divided into those that can be reduced by application of available corrosion control practices (avoidable costs) and those for which saving requires new and advanced materials and technology (unavoidable costs) [2, 24].

Table 1.1 below illustrates how the cost of corrosion has increased from 1975 to 2005 in the United States, as well as the increase in the avoidable costs for different industries.

© University of Venda

Table 1.1: Cost of metallic corrosion in United States (in billions of dollars) [1].

Industry		**1975**	**1995**	**2005**
All industries	Total	82	296	403
	Avoidable	33.0	104	142
Automotive	Total	31.4	94.0	125.3
	Avoidable	23.1	65.0	86.7
Aircraft	Total	3.0	13.0	18.0
	Avoidable	0.7	3.0	4.2
Others	Total	47.6	159.0	260
	Avoidable	9.3	36.0	50

Studies conducted in 2005 by Mintek and the University of Witwatersrand estimated the direct cost of metallic corrosion in South Africa to be R154 billion per annum. This value is approximately 5% of the country's GDP [25]. Other independent studies show that about 25 – 30% of these costs associated with metallic corrosion could be saved by applying known technologies and methodologies [26].

1.1.4. Types of corrosion

Corrosion can be conveniently classified by the forms or types in which it manifests itself; the basis of this classification is the appearance of the corroded metal [11].

In his 1986 book entitled 'Corrosion Engineering', M.G. Fontana listed 8 basic types of corrosion, namely [11]: (1) uniform (or general) corrosion; (2) galvanic (two-metal) corrosion; (3) crevice corrosion; (4) pitting corrosion; (5) intergranular corrosion; (6) selective attack, selective leaching (de-alloying); (7) erosion corrosion; and (8) stress corrosion cracking.
The basic types of corrosion can be described and illustrated in the following way:

Uniform (or general) corrosion

This is the most common type of corrosion. It is also the most important type because it causes the greatest metal loss [2, 12]. This type of attack is characterised by corrosion which proceeds uniformly (i.e. about the same rate) over the entire surface, leading to relatively uniform thinning (as seen in Figure 1.3) of the metal piece until failure occurs [24].

© University of Venda

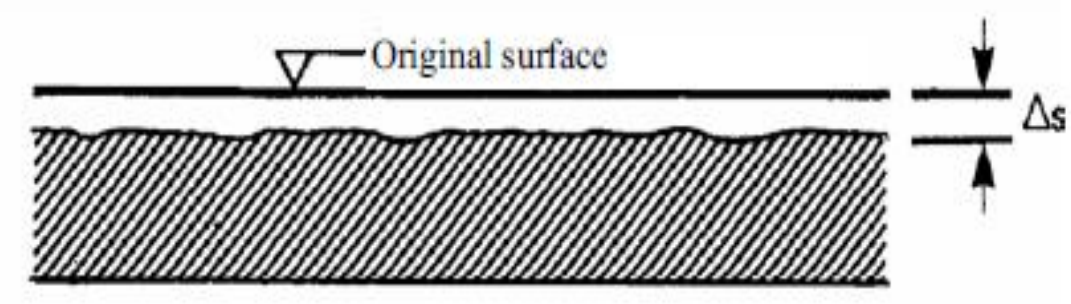

Figure 1.3: Schematic representation of uniform (or general) corrosion [17].

Galvanic (two-metal) corrosion

Galvanic corrosion (also called ‘dissimilar metal corrosion’ or ‘bimetallic corrosion’) refers to corrosion damage induced when two dissimilar metals (or alloys) are electrically connected to one another in a common corrosive electrolyte [1, 2, 16, 17]. When this coupling is in place, a potential difference (driving force) usually exists because of the dissimilar metallic materials having different electrode potentials (i.e. different tendencies to corrode). The less noble or active metal (anode) will therefore undergo dissolution while the more noble metal (cathode) will remain unaffected or protected [7, 16]. The galvanic series (Table 1.2) provides information about the relative nobility of metallic materials in seawater. This series, however, is good for first approximations since slight variations in service conditions will cause the values of potential to change. Hence, for accurate predictions, potential measurements in the environment of interest are necessary [2, 16]. In this type of attack, the area ratio between the cathode and anode is very important. An unfavourable ratio would consist of a large cathode and a small anode. The large cathodic area provides large surface area for the cathodic reaction which will in turn require large anodic reaction to maintain a balance. The anode will therefore undergo rapid dissolution [12].

© University of Venda

Table 1.2: Galvanic series of some metals and alloys in sea water [12].

Noble or cathodic	Platinum
	Gold
	Graphite
	Titanium
	Silver
	Chlorimet 3
	Hastelloy C
	18-8 Mo stainless steel (passive)
	18-8 stainless steel (passive)
	Chromium steel >11% Cr (passive)
	Inconel (passive)
	Nickel (passive)
	Silver solder
	Monel
	Bronzes
	Copper
	Brasses
	Chlorimet 2
	Hastelloy B
	Inconel (active)
	Nickel (active)
	Tin
	Lead
	Lead-tin solders
	18-8 Mo stainless steel (active)
	18-8 stainless steel (active)
	Ni-resist
	Chromium steel >11% Cr (active)
	Cast iron
	Steel or iron
	2024 aluminum
	Cadmium
Active or anodic	Commercially pure aluminum
	Zinc
	Magnesium and its alloys

Pitting corrosion

Pitting corrosion is an extremely localized form of attack, whereby corrosion is limited to certain fixed areas on the metal surface (or the rate of corrosion is greater at some areas of the metals than at others). This type of attack is observed in metals where the passivity is locally broken down, usually due to the action of chloride ions [17, 24]. The localization of the attack leads to the formation of craters or pits that may result in the complete perforation of the pipe or vessel within a short period, this is illustrated in Figure 1.4.

© University of Venda

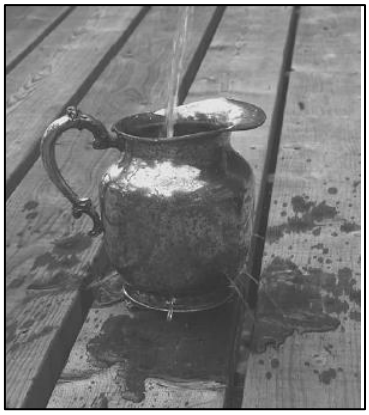

Figure 1.4: Perforations in a water jug caused by pitting corrosion [2].

Pitting corrosion is a destructive and insidious form of attack and is more dangerous than uniform corrosion. This is due to the following [11, 12, 17]:

- The pits that form on the surface are usually small in size and often covered by corrosion products making them difficult to detect.
- The number and size of pits may vary from region to region and within each region, therefore, carrying out quantitative measurements as well as the comparing of the extent of pitting become difficult.
- Laboratory testing for pit prediction is also difficult since these tests are short term while in reality pits may require several months or a year before they become visible. Additionally, the difference between corrosion microenvironments and the bulk environment make prediction of pits difficult.

As a result of the difficulty in detecting, predicting and designing against, pitting corrosion often gives rise to extremely sudden failures [2, 11, 12].

The different shapes that can be assumed by pits are illustrated in Figure 1.5.

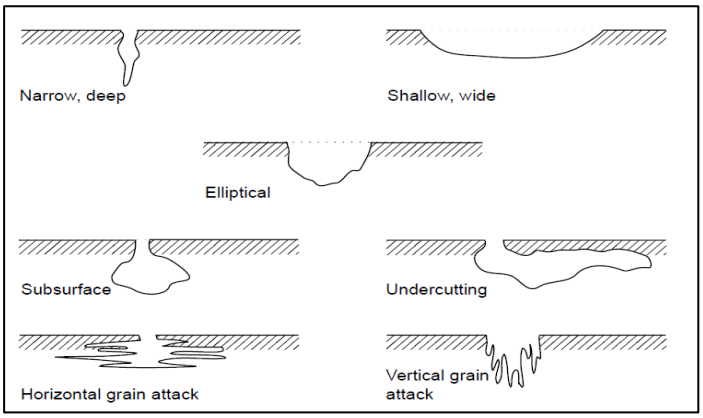

Figure 1.5: Characteristic shapes of pitting corrosion [12].

© University of Venda

Crevice corrosion

This is a type of localized attack that occurs in narrow gaps or openings formed by metal-to-metal or metal-to-non-metal contact. This type of attack can also occur in crevices produced by design such as those found under gaskets, insulation material, fastener heads and beneath coatings [7, 12, 16]. These openings or gaps are wide enough to allow entry of liquid and sufficiently narrow to maintain stagnancy of the liquid within the crevice [11, 17]. Figure 1.6 illustrates two types of crevices and indicates the areas which will experience attack. Crevice corrosion affects both active and passive metals, although passive metals (or metals that are easily passivated) are more prone to this type of attack particularly those in the stainless steel group [11]. The geometric configuration that exists when such attack is prevalent is one that restricts easy transportation (through convection and diffusion) of cathodic reactants (usually oxygen) into the crevice; whereas on the external surface, diffusion and convection of oxygen occurs easily [13]. This results in the creation of an oxygen concentration cell between the crevice and the external surface, causing the crevice area to be anodic while the external surface becomes cathodic (the oxygen reduction reaction can be sustained in the external environment) [12, 13].

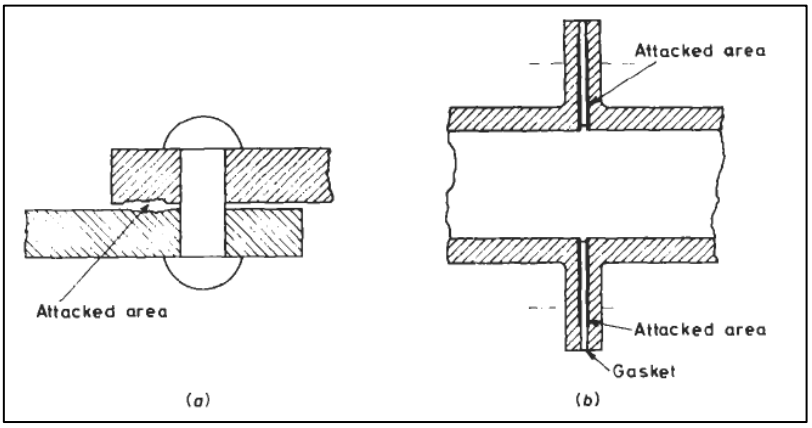

Figure 1.6: Crevice corrosion (a) Crevice caused by metal-to-metal contact; (b) Crevice due to design [13].

Selective attack, selective leaching (de-alloying)

Selective attack or de-alloying is a process that is observed in alloys whereby the less noble metal, having a significantly high fraction, is preferentially leached from the alloy when the alloy is exposed to certain environmental conditions [13, 16].

The most well-known example of this type of attack is the dezincification of brass (copper-zinc alloy). Copper-zinc alloys containing more than 15% zinc tend to be susceptible to this type of attack whereby, as the name suggests, zinc is selectively leached from the alloy leaving

© University of Venda

behind a weak, porous layer of copper and copper oxide [1, 16]. Dezincification can either occur uniformly (i.e. layer dezincification) or in a localized manner (i.e. plug dezincification) as shown in Figure 1.7. Additionally, a microstructural representation of the dezincification process is shown in Figure 1.8. A similar attack occurs in certain aluminium bronzes whereby aluminium is leached from the alloy; this process is called dealuminisation [21]. The remaining material may preserve the original shape. However, strength as well as other properties are often reduced mainly due to the alteration of the microstructure as seen in Figure 1.8 [17].

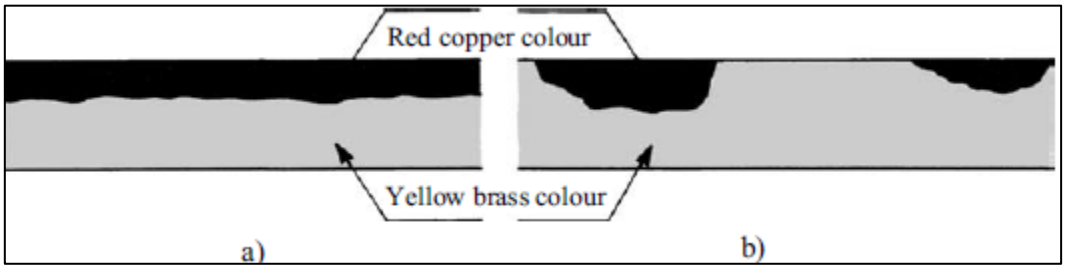

Figure 1.7: (a) Layer dezincification; (b) Plug dezincification [17].

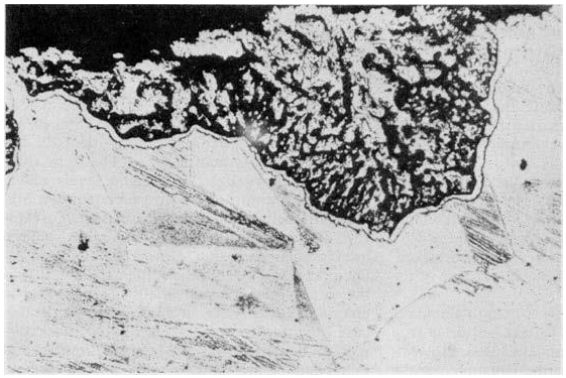

Figure 1.8: Microstructural representation of plug-type dezincification in α-brass (70Cu-30Zn) [16].

Erosion corrosion

Erosion corrosion is a form of attack whereby the metal surface is subjected to the conjoint action of erosion and corrosion [22]. Components (such as valves, propellers, heat exchangers, nozzles, etc.) that are exposed to a moving fluid are often susceptible to this form of attack [17]. Erosion corrosion is characterised by the presence of grooves, gullies, rounded holes and/or horseshoe shaped grooves, these features also indicate directionality [12]. In some metals (such as lead) corrosion resistance is achieved through the protective coating of corrosion products. This protective coating is stable in most static environments. However,

© University of Venda

when flow of corrosive fluid becomes turbulent the protective coating is worn off. As a result of the wear, the metal surface becomes unprotected and more active, and undergoes accelerated corrosion [17].

Cavitation and fretting are additional subsets of erosion corrosion. Cavitation corrosion is an attack which occurs as vapour bubbles in a moving fluid form and collapse near the metallic surface. As the bubbles collapse high pressures arise which cause damage of the protective film [7]. Fretting corrosion is experienced when two closely fitted components experience slight relative motion. This relative motion may cause damage to one metallic surface or both (i.e. protective film of one or both components may be damaged resulting in active surfaces). In the presence of corrosive fluid, erosion corrosion will then occur. Fretting corrosion is characterised by pits or grooves [7, 12]. Erosion-corrosion is more severe at high temperatures as well as when the solution contains suspended solid particles. Figure 1.9 represents erosion-corrosion and its subsets (cavitation and fretting) [8].

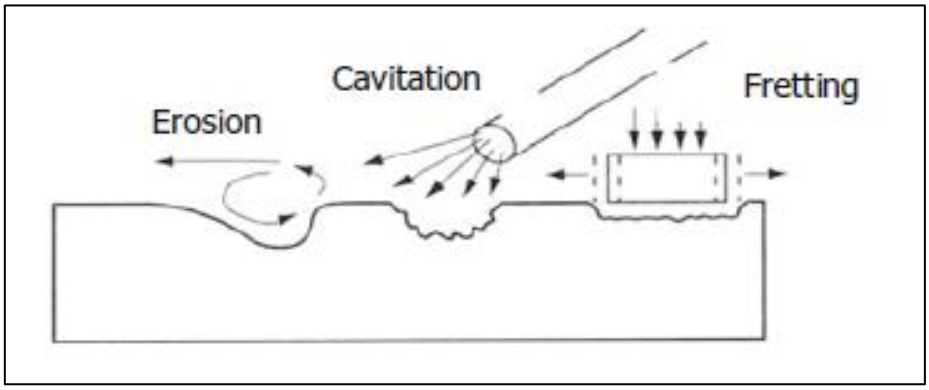

Figure 1.9: Illustration of erosion, cavitation and fretting corrosion [27].

Stress corrosion cracking (SCC)

SCC is a form of attack characterised by cracking induced by the conjoint action of static tensile stress and an exposure to an aggressive environment [11, 28]. The tensile stress can originate from external factors (such as external load, centrifugal forces or temperature changes) but in most cases, SCC is caused by residual (internal) stresses induced by cold working or heat treatment [17]. The metal is usually left unattacked over most of its surface while fine cracks progress through it. The cracks branch and proceed in a general direction normal to the tensile stresses contributing to their initiation and propagation [12, 16, 17]. The

© University of Venda

propagation of cracks may be intergranular or transgranular depending on the alloy system and corrodent combination [7].

For SCC to occur, the following conditions are necessary [7, 14, 17, 28]:

1. *Suitable environment*. SCC is normally observed in certain alloy-environment combinations. For example, copper-containing alloys experience SCC in an ammonia environment, whereas low-alloy austenitic stainless steels will undergo SCC in chloride-containing environments. Table 1.3 shows the different alloy-environment combinations susceptible to SCC.
2. *Tensile stress.* This is an essential feature of SCC; for SCC to initiate, the tensile stress should exceed the threshold value of the particular alloy. Normally, SCC will not occur if the part is in compression.
3. *Sensitive metal.* In certain alloys sensitivity or susceptibility to SCC is determined by alloy content. For example, in stainless steels an alloy with a nickel content greater than 30% is immune to SCC, whereas alloys with contents of nickel ranging between 7 – 10% are the most sensitive or susceptible to SCC.
4. *Appropriate temperature values.* SCC is accelerated by increasing temperature. Some alloy systems (e.g. magnesium alloys) undergo SCC at room temperature. However, most alloys which are susceptible to SCC will begin to undergo cracking at temperatures higher than 100°C.

The first three conditions are illustrated in Figure 1.10.

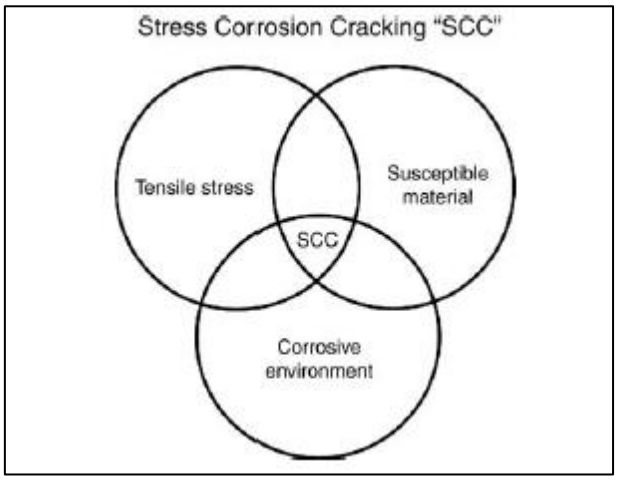

Figure 1.10: Simultaneous three conditions of SCC [1].

© University of Venda

Table 1.3: Alloy-environment combinations susceptible to corrosion [28].

ALLOY	ENVIRONMENT	INDUSTRIES MAINLY CONCERNED
Carbon steels	OH^- + H_2O NO_3^- + H_2O HCO_3^- + H_2O	power generation
Austenitic stainless steels	Cl^- + H_2O Br^- + H_2O I^- + H_2O OH^- + H_2O thiosulfate + H_2O	chemical and petroleum industries
Nickel alloys	H_2O	nuclear reactors
Aluminium alloys	Cl^- + H_2O $Br^- + H_2O$ $I^- + H_2O$	Aviation
Brass	$NH_3 + H_2O$ amines	power generation
Titanium alloys	$Cl^- + H_2O, Cl^- + CH_3OH$ $Br^- + H_2O, Br^- + CH_3OH$ $I^- + H_2O, I^- + CH_3OH$ N_2O_4 anhydride	aerospace industry

Figure 1.11 A shows stainless steel which has undergone SCC where the cracks propagated in a transgranular manner (i.e. through the grains) while Figure 1.11 B shows brass which has undergone intergranular (along grain boundaries) SCC.

© University of Venda

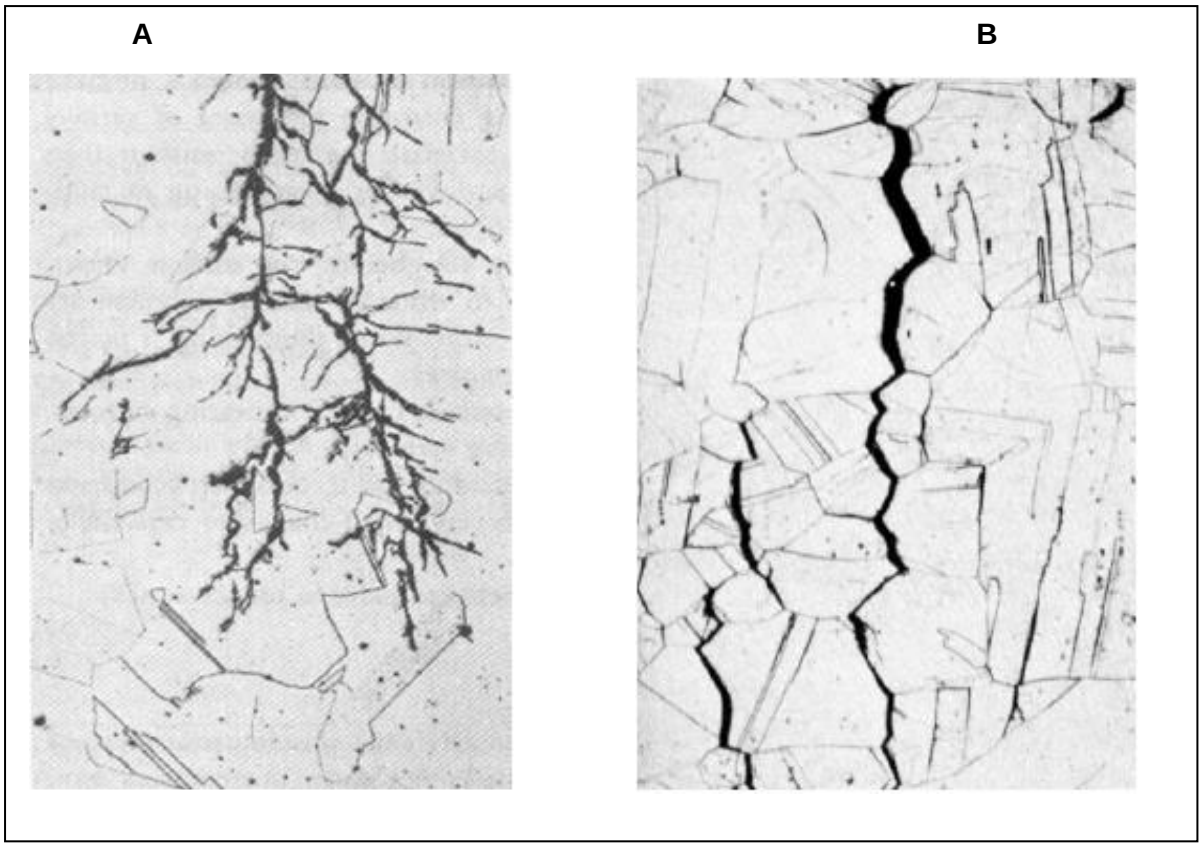

Figure 1.11: (A) Transgranular SCC of 304 stainless steel (B) Intergranular SCC of brass [1].

Intergranular corrosion

On a microstructural level, metals or alloys are made up of grains that are separated by grain boundaries. Intergranular corrosion is a form of localized attack which occurs preferentially along the grain boundaries or regions immediately adjacent to the grain boundaries. The main body of the grain experiences little or no attack [7, 12]. The driving force for this form of attack is the difference in corrosion potential that develops between the immediate vicinity of the grain boundaries and any precipitates, intermetallic phases, or impurities that form at the grain boundaries [16]. The factors that contribute to these differences in corrosion potential are the following [7, 12, 17]:

1. Migration of impurities or alloying elements to the grain boundaries (as in aluminium alloys),
2. Enrichment of a particular alloying element at the grain boundary (e.g. Zn in brass),
3. Local depletion of an alloying element (which serves as a corrosion-resisting constituent) at regions immediately adjacent to grain boundary.

A well-known example of intergranular corrosion relates to certain austenitic stainless steels, particularly the 304 alloy (304 contains 18 wt% Cr, 8 wt% Ni and 0.06−0.08 wt% C) [17]. When

© University of Venda

this alloy is exposed to temperatures in the 500 – 800°C range during welding, chromium carbide ($Cr_{23}C_6$) precipitates form at the grain boundaries. Due to the slow diffusion of Cr relative to carbon, Cr necessary for carbide formation is taken from the immediate vicinity. The immediate vicinity then becomes depleted of the corrosion-resisting constituent (as illustrated in figure 1.12), therefore making it more sensitive to corrosion [17]. Depending on the environment, the material may experience serious failure after different periods of exposure [17].

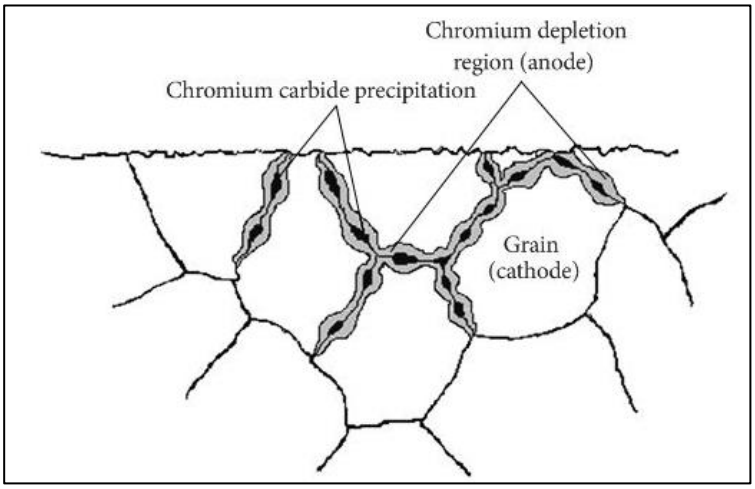

Figure 1.12: Mechanism for intergranular corrosion in austenitic stainless steels [29].

1.1.5. The rate of corrosion

During the corrosion process, the metallic material undergoes dissolution resulting in weight loss as well as change in thickness (i.e. the metal part becomes thinner). Corrosion rates, therefore, quantify the amount of metallic material that has been dissolved per unit time [21, 30].

There are a number of methods that are used to measure the corrosion rate. These measurements are essential when material selection is considered since they express the corrosion behaviour of a metallic material in a given environment [28].

The three main methods of measurement are [17, 21 – 28]:

1. Weight loss per unit area and unit time.

This method is commonly used when weight loss is a directly determined quantity in corrosion testing. Corrosion rate in terms of weight loss is usually given the following units: gm^{-2}/year or $mgdm^{-2}$/day (denoted as mdd).

© University of Venda

2. Thickness reduction of material per unit time.

This is the most practically significant method. It measures the thickness of the metal lost per unit time also known as the corrosion penetration rate (CPR) which can be determined from weight loss measurements using the following equation:

$$\mathrm{CPR} = \frac{(\text{mass of metal loss})}{(\rho \times A \times t)} \quad (1)$$

where ρ is the density of the metallic material, A is the area of the specimen exposed to corrosion, and t is the exposure time. The corrosion penetration rate is usually expressed in mm/year.

3. Corrosion current density.

This method involves the measuring of the anodic current (also called the corrosion current) causing the dissolution (oxidation) of the metal and subsequent calculation of the corrosion current density. Corrosion rate is then calculated using Faraday's laws. This method is usually employed in systems that cannot be subjected to weight loss tests, or those that cannot be visually inspected. Table 1.4 shows some of the corrosion rate units that are frequently encountered, including those of the methods discussed above.

Table 1.4: Frequently encountered units of corrosion rates [21].

Corrosion effect	**Unit**
Mass change	gm^{-2}/year mg dm^{-2}/day =mdd
Increase in corrosion depth	µm/year µm/year = 10^{-3}mm/year inch per year= ipy=25.4 mm/year mil per year = mpy = 10^{-3}ipy = 25.4 µm/year
Corrosion current	mA cm^{-2}
Decrease in ultimate strength, yield strength or rupture strain	per cent/year (of initial value)

1.1.6. Factors that affect the rate of corrosion

The factors affecting the rate of corrosion can be conveniently classified in terms of: (a) the nature of metals and (b) the nature of the environment.

© University of Venda

a) Nature of metal

Position on the galvanic series

Every metal tends to corrode. This tendency is expressed as the corrosion potential. Metals such as platinum and titanium have very little tendency to corrode and are termed noble metals. In the galvanic series of metals and alloys immersed in seawater, for example, these have the highest positive potentials. Metals such as magnesium and zinc have a high tendency to corrode and are termed active metals. These have the highest negative potentials in the noted galvanic series [1, 16].

When metals are coupled in the presence of an electrolyte (such as seawater), the less noble metal will be an anode and undergo dissolution; the rate of the dissolution will depend on the difference in the positions of the metals in the galvanic series [31]. The rate at which the anode undergoes dissolution (corrosion) will increase the further apart the metals are in the galvanic series.

Purity of metal

During melting and pouring, and other fabrication procedures (such as cold working), inclusions may be incorporated into the metal or alloy. When these impurities are exposed at the metal surface, local cathodes will form hence affecting the rate of corrosion [13]. The effects of inclusions exposed at the surface are shown in Figure 1.13.

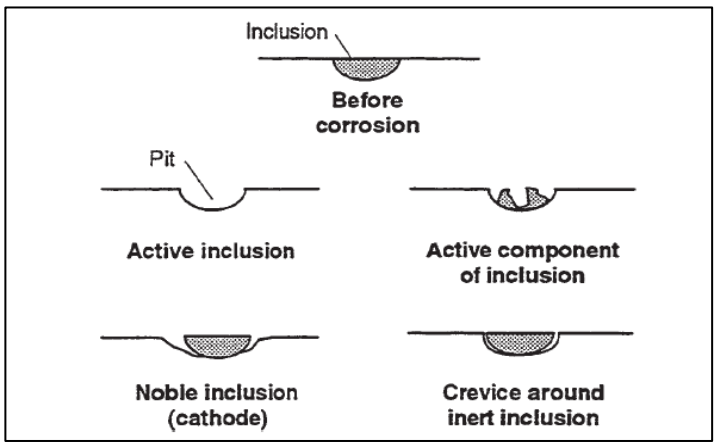

Figure 1.13: Effects of inclusions exposed at metal surface [16].

© University of Venda

Other effects of the presence of inclusions can be observed when comparing high purity nickel with commercial grade nickel after being exposed to identical anodic dissolution conditions in chloride solution. The two metals are shown in Figure 1.14 where (a) is the commercial grade nickel and (b) is the high purity nickel. The commercial grade nickel contains inclusions of sulfide which acts as preferential sites of dissolution giving rise to pits. On the other hand, the high purity nickel contains no inclusions and hence does not undergo pitting [28].

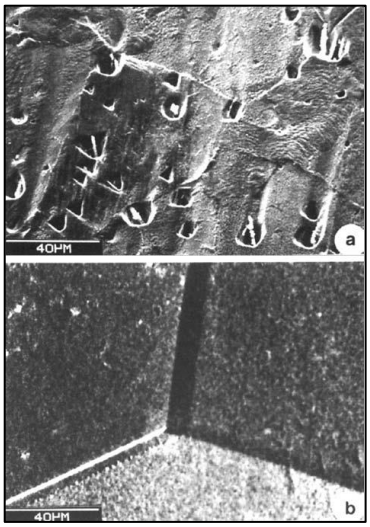

Figure 1.14: SEM images of nickel surfaces exposed to chloride solution: (a) commercial grade nickel (Ni 200) and (b) high purity nickel [28].

The rate of corrosion, therefore, generally increases as the purity of a metal decreases i.e. high purity metals tend to be more corrosion resistant than their commercial counterparts. This effect can also be shown in the Table 1.5 below, where corrosion rate increases as the purity of aluminium decreases [11].

Table 1.5: Effects of aluminium purity on corrosion in hydrochloric acid solution [11].

% aluminium	**Relative corrosion rate**
99.998	1
99.97	1,000
99.2	30,000

© University of Venda

Relative areas of the anode and cathode

When the area of the cathode is larger than that of the anode there is a greater demand for electrons. Thus, the anode will undergo rapid dissolution i.e. the greater the cathode area the greater the rate of corrosion [31]. This effect is illustrated in Figures 1.15 and 1.16, where Figure 1.15 shows steel rivets on a copper bar and Figure 1.16 shows copper rivets on a steel bar.

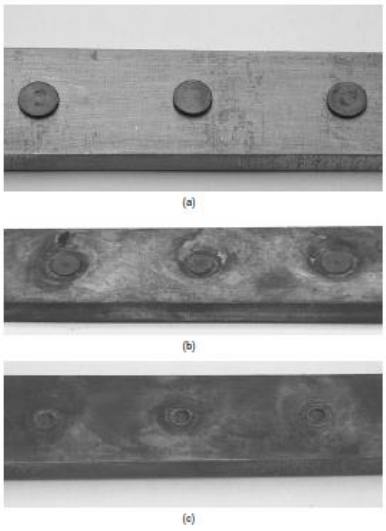

Figure 1.15: Steel rivets on a copper bar: (a) at start of experiment; (b) 6 months after being submerged in 3% NaCl solution; and (c) after 10 months in same solution [2].

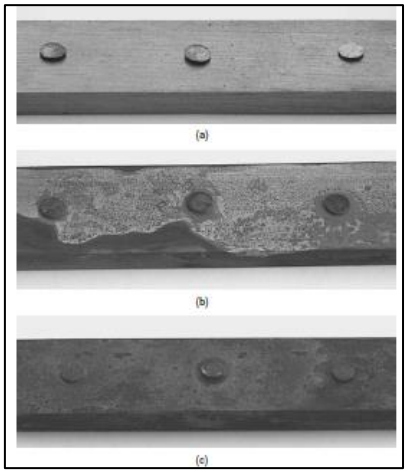

Figure 1.16: Copper rivets on a steel bar: (a) at start of experiment; (b) 6 months after being submerged in 3% NaCl solution; and (c) after 10 months in same solution [2].

© University of Venda

As per the galvanic series in Table 1.2, the steel rivets represent the anode while the copper bar is the cathode. This is an unfavourable area ratio and as can be seen from Table 1.2, iron is rapidly dissolved even after a short period of submersion (as indicated in Figure 1.15 b). A favourable area ratio is one seen in Figure 1.16 where the cathode (copper) has a smaller area than the anode (steel bar). In this case, the demand for electrons is much lower than in the previous case and as a result, the corrosion of the steel is only slightly accelerated [2].

Nature of oxide layer

When certain metals are exposed to air, oxygen or water, they spontaneously oxidize to form corrosion products in the form of metal oxides. If the metal oxides are not volatile or soluble, they form an oxide layer on the surface of the metal [13]. The oxide layer has the ability to act as a barrier restricting the interaction of the metal with its environment. Formation of an oxide layer, however, does not necessarily imply that a metal will be protected from further corrosion. A protective layer is one which is continuous, non-porous and well adhered [32]. The ability of an oxide layer to provide protection can be predicted using the Pilling-Bedworth ratio, which is the volume ratio of metal oxide to the metal it replaces [32]. Generally, if the volume ratio is less than 1 the layer will be too porous or discontinuous to protect the underlying metal against further corrosion. Metals such as magnesium, calcium and barium fall under this category. If the volume ratio is greater than 2, the oxide layer will spall off due to stresses accompanying the necessary volume expansion. In this case, the metal will also be poorly protected and hence the underlying metal will undergo rapid corrosion. An example of this effect is observed in iron. The favourable volume ratio is one that ranges between 1 and 2. In this case, an adherent, non-porous and protective layer is predicted to form. Metals such as aluminium, nickel and chromium (with oxide/metal ratios of 1.24, 1.6 and 2.0, respectively) fall under this category [32]. Figure 1.17 is a schematic illustration of the types of oxide layers depending on the ratio between metal oxide and metal.

© University of Venda

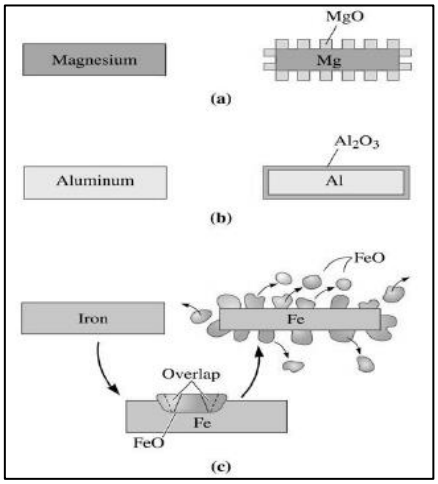

Figure 1.17: Three oxides that may form depending on the ratio between metal oxide and metal: (a) magnesium forms a porous oxide layer; (b) aluminium forms a non-porous and protective oxide layer; and (c) iron forms an oxide layer that spalls off providing poor protection [33].

b) Nature of environment

Temperature

Temperature can affect the rate of corrosion in several ways. The general trend, though, is that corrosion rate increases with an increase in temperature [34]. One of the ways that temperature affects corrosion is observed when an important corrosion constituent has limited solubility. An example of such a constituent is oxygen. The solubility of oxygen decreases as temperature increases which results in oxygen molecules being released from the liquid [34]. The implications of the release of O_2 molecules depends on the type of system in place.

Two systems can be used to illustrate the kind of alterations to corrosion rate that may occur; this is shown in Figure 1.18. The first system is one which is closed to the atmosphere. In this system, O_2 molecules which enter into the vapour phase above the liquid cannot escape into the atmosphere. With an increase in temperature, the water vapour pressure above the liquid increases. This, in turn, causes the O_2 molecules to re-enter the liquid phase resulting in an increase in concentration of O_2 in the electrolyte [24, 34]. The corrosion rate is, therefore, observed to increase monotonically from about 40°C to 160°C as illustrated in Figure 1.18 [24, 34]. The second system is one which is open to the atmosphere. In this system, oxygen molecules can escape from the immediate vicinity of the liquid and the water vapour pressure remains constant unlike in the previous system. In this system, corrosion rate initially increases with increasing temperature due to the increase of the diffusion coefficient D. However, above a certain temperature, corrosion rate decreases due to the decrease in oxygen concentration.

© University of Venda

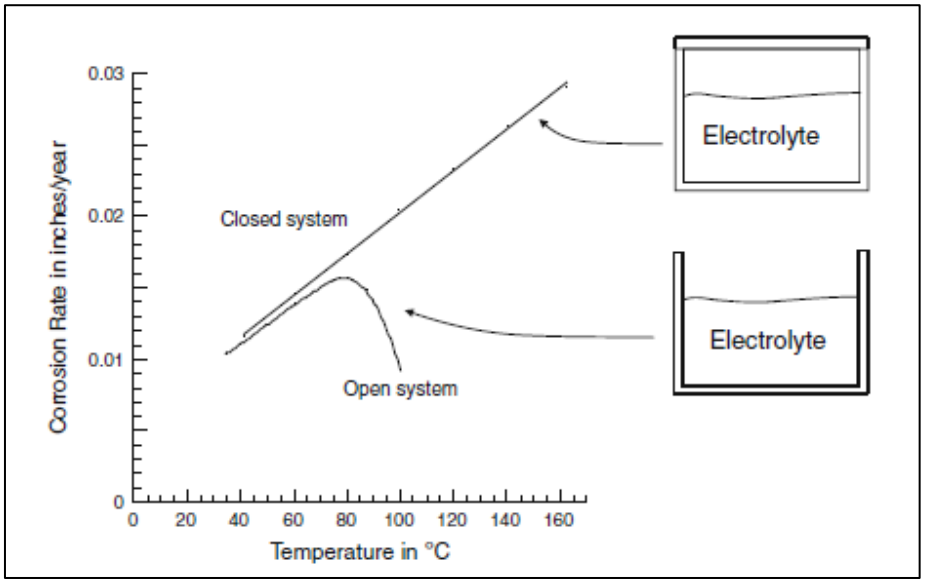

Figure 1.18: Schematic illustration of the effect of temperature on corrosion rate of a metal immersed in an aqueous solution in an open vs. closed system [24].

Effect of fluid velocity

The velocity of the solution has a major effect on the rate of corrosion. For example, certain types of corrosion (such as erosion-corrosion) come about mainly as a result of increased liquid velocity [2]. The main effect of the increase in velocity is that it causes mechanical disturbance of the oxide film to which most metals owe their corrosion resistance [2, 35]. The removal of the protective film leaves the metal in an active state hence its dissolution will be rapid (i.e. corrosion rate increases). Figure 1.19 is a schematic representation of the effects of increased velocity on the rate of corrosion.

© University of Venda

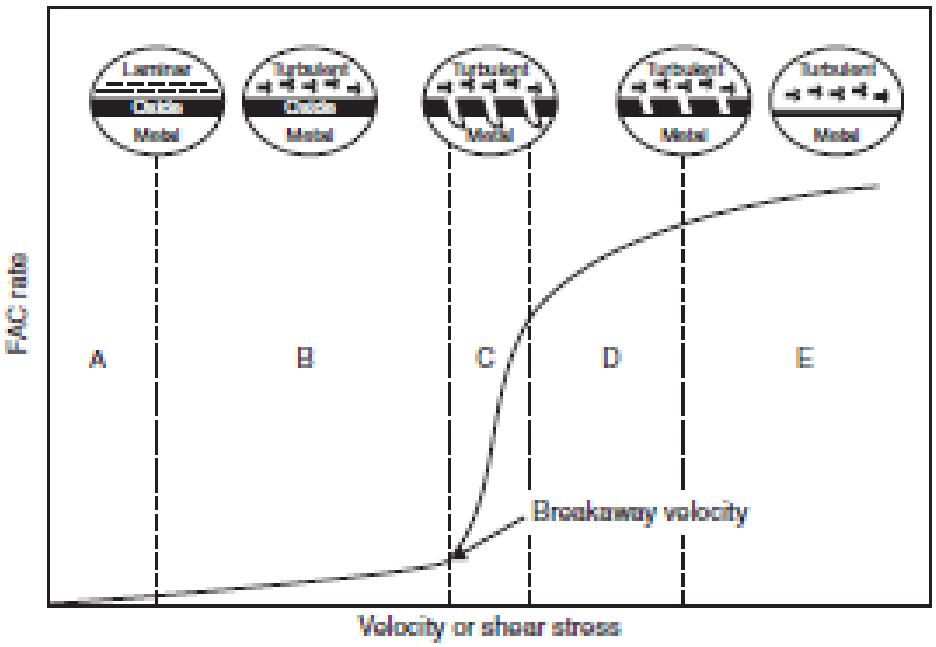

Figure 1.19: Illustration of the effects of velocity on the rate of flow accelerated corrosion (FAC) [2].

Humidity

This is an important factor for corrosion that occurs under atmospheric conditions. For corrosion to occur under these conditions, a moisture film needs to be present on the surface of the metal. The amount of moisture present on the metal surface depends, to a large extent, on the relative humidity of the air. Below a certain value of relative humidity (i.e. critical relative humidity), the moisture film on the metal surface is so thin that the corrosion is considered negligible. However, as the relative humidity increases beyond the critical value, the thickness of the moisture film also increases which in turn causes a noticeable increase in the rate of corrosion [21].

Nature of the electrolyte

Characteristics of the electrolyte such as the conductivity and pH, among others, have the ability to affect the rate of corrosion. The conductivity of the electrolyte is a measure of the electrolyte's ability to transport electric current. This ability is, to some extent, controlled by the concentration of dissolved salts (e.g. NaCl). Therefore, if the conductivity of the electrolyte is high the corrosion rate will be high [16]. This is especially true when comparing corrosion of metals in sea water versus distilled water. Sea water has a higher concentration of NaCl and hence has high conductivity. Metals immersed in sea water generally experience greater corrosion rates than those in distilled water [15, 16].

© University of Venda

The effect of pH is different for particular metals (or alloys). In iron, the effect of pH on corrosion rate in aerated, soft water is schematically illustrated in Figure 1.20. In the acidic region, the metal undergoes rapid dissolution due to dissolution of the protective oxide film. For pH values ranging between 4 and 10, the corrosion rate is constant. In this region, the rate depends only on how rapidly oxygen is transported to the metal surface. This leads to the continuous renewal of the ferrous oxide film [15]. At pH values above 10, the surface of iron changes from being active to being passive, resulting in a decrease in the corrosion rate [15].

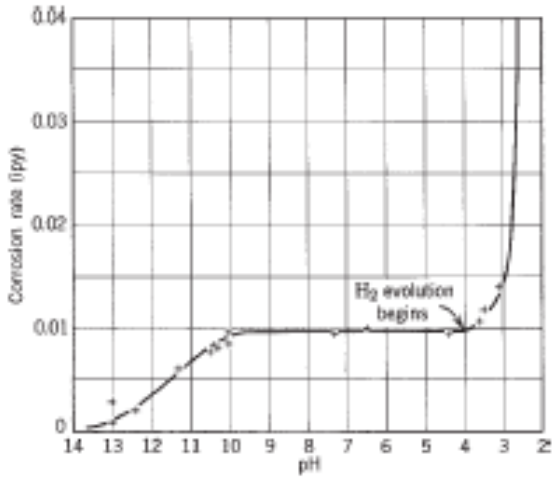

Figure 1.20: Schematic illustration of the effect of pH on corrosion rate of iron in aerated, soft water [15].

1.1.7. Mechanism of corrosion

Corrosion is most often an electrochemical process. It involves the simultaneous transfer of mass and charge across the metal/solution interface by the action of coupled electrochemical half-cell reactions [24]. For the corrosion process to occur, four constituents need to be present (absence of any one will prevent corrosion from occurring), namely: an anode, a cathode, a metallic conductor (providing an electronic path), and an electrolytic conductor (providing an ionic current path) [35].

The anode is the site where corrosion generally occurs. It is characterised by an oxidation (anodic) reaction which involves metals leaving the metal surface and entering the solution as metal ions (i.e. the metal is oxidised), and the subsequent generation of electrons [24].

Examples of the anodic reaction are [24]:

$$\mathrm{Al(s)} \rightarrow \mathrm{Al^{3+}(aq)} + 3\mathrm{e^-} \quad (2)$$

$$\mathrm{Cu(s)} \rightarrow \mathrm{Cu^{2+}(aq)} + 2\mathrm{e^-} \quad (3)$$

No corrosion occurs at the cathode. However, reactions that are essential for the operation of the corrosion cell occur. These reactions are reduction reactions also called cathodic

© University of Venda

reactions; they involve the consumption of electrons (these are electrons that were generated at the anode and transferred to the cathode through the metal conductor) by a given species (commonly occurring species include: dissolved oxygen and hydrogen ions) [16, 35]. The type of species present and hence the type of reduction reaction that takes place is dependent on the pH of the solution and will be discussed in the section to follow.

1.1.8. Corrosion in different media

Corrosion in different media is characterised by distinct cathodic (reduction) reactions. These reactions are dependent on the type of species present in the solution; the species in turn control the type of corrosion products that form.

In acidic media, there are two characteristic cathodic reactions; the predominant reaction will be determined by the availability of oxygen [16].

When oxygen is absent, the following cathodic reaction takes place:

$$2H^+(aq) + 2e^- \rightarrow H_2(g) \quad (4)$$

An example of metallic corrosion occurring in this type of solution is given below, where hydrogen gas is liberated, and a soluble salt is formed [2]:

$$2Al(s) + 6H^+(aq) \rightarrow 2Al^{3+}(aq) + 3H_2(g) \quad (5)$$

Another example is the corrosion of iron shown in Figure 1.21.

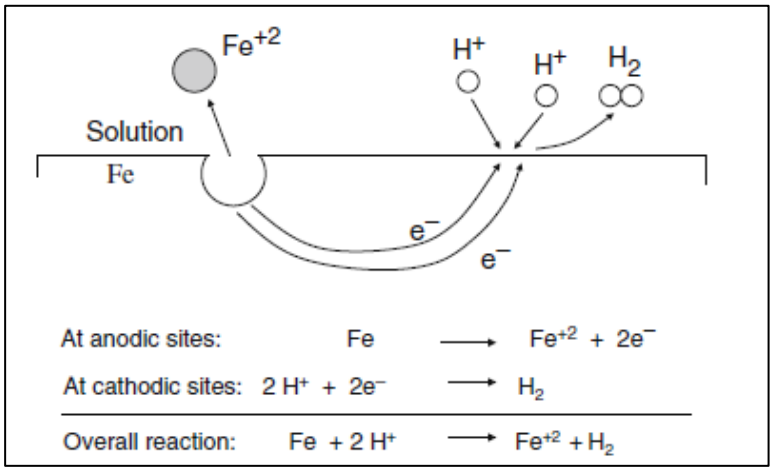

Figure 1.21: Coupled electrochemical half-cell reactions occurring at anodic and cathodic sites on metal surface immersed in an acidic solution [24].

© University of Venda

When oxygen is present the predominant cathodic reaction is the following [16]:

$$O_2(g) + 4H^+(aq) + 4e^- \rightarrow 2H_2O(l) \quad (6)$$

In most alkaline and neutral solutions corrosion will not occur if dissolved oxygen is absent. This is because the cathodic reaction involves the reduction of oxygen to form hydroxyl ions [24]:

$$O_2(g) + 2H_2O(l) + 4e^- \rightarrow 4OH^-(aq) \quad (7)$$

An example of such corrosion is shown below:

Anodic reaction: $2Zn(s) \rightarrow 2Zn^{2+}(aq) + 4e^-$ (8)

Cathodic reaction: $O_2(g) + 2H_2O(l) + 4e^- \rightarrow 4OH^-(aq)$ (9)

Overall reaction: $2Zn(s) + O_2(g) + 2H_2O \rightarrow 2Zn^{2+} + 4OH^- \rightarrow 2Zn(OH)_2$ (10)

1.1.9. Classification of corrosion process

The corrosion process can occur by a chemical, electrochemical or physical process.

Chemical corrosion

This is also called dry corrosion since it involves the destructive attack of a metal in a dry environment. Metals undergo oxidation as a result of the chemical attack of oxygen or other atmospheric gases such as CO_2, SO_2 and H_2S, with oxygen being the most common oxidant. This process can also involve degradation of metal due to direct chemical attack of anhydrous liquids [24]. When exposed to dry oxygen at ambient temperature, only alkali and alkali earth metals will readily be oxidised whereas at high temperatures, almost all metals except the noble metals are readily oxidised [36].

In the case of a divalent metal, the oxidation reaction can be expressed as follows [37]:

$$M(s) \rightarrow M^{2+}(aq) + 2e^- \quad \text{Oxidation of metal} \quad (11)$$

$$\frac{1}{2}O_2(g) + 2e^- \rightarrow O^{2-}(aq) \quad \text{Reduction of oxygen} \quad (12)$$

$$M(s) + \frac{1}{2}O_2(g) \rightarrow M^{2+}(aq) + O^{2-}(aq) \quad (13)$$

When M^{2+} and O^{2-} come into contact, a metal oxide (MO) is formed which acts as a barrier against further corrosion. A characteristic feature of this process is that the oxidation of the metal and the formation of the metal oxide must occur at the same place at the metal/gas interface [38].

© University of Venda

Electrochemical process

This process involves deterioration of a metal in the presence of moisture. A detailed explanation of this process has been given in section 1.1.7. A characteristic feature of this process is that the oxidation of the metal and the reduction of a species in solution occur at different areas on the metallic surface; these areas are the anodic and cathodic areas, respectively [38].

Physical process

Deterioration of a metal purely by mechanical action is not called corrosion but it is described as erosion, wear or deformation [39]. However, there are instances (in the presence of a corrosive environment) where the physical deterioration co-acts with the chemical or electrochemical deterioration processes. The physical deterioration participates in the disturbance of the protective film on the metallic surface, hence rapidly accelerating the corrosion process [39].

1.1.10. Thermodynamics and kinetics of corrosion

1.1.10.1. Thermodynamics

Thermodynamics is the science concerned with the changes that accompany chemical (or physical) reactions [11]. Thermodynamic information can be useful in determining if corrosion of a metal in a particular environment can occur spontaneously (i.e. without any external forces), and the nature of the corrosion products that are produced by the reaction between the metal and its environment.

As mentioned earlier, metals and alloys in service have a high free energy that is induced by the extraction process. It is a law of nature that any system will react spontaneously to reach its lowest energy state [16, 23]. Considering the reaction in Equation 14, a spontaneous direction of this reaction will be characterised by the relation given in Equation 15 [23].

$$\mathrm{M^{n+}} + \mathrm{ne^-} \leftrightarrow \mathrm{M} \tag{14}$$

$$\Delta \mathrm{G} = -\mathrm{ve\ (neg)} \tag{15}$$

In Equation 15, ΔG is the Gibbs free energy. Changes in ΔG provide the focal point of any thermodynamic analysis of corrosion reactions. ΔG cannot be directly measured but it can be related to the electrochemical potential by the following equation:

$$\Delta \mathrm{G} = -\mathrm{nFE} \tag{16}$$

where *n*, *F* and *E* , correspond to the number of electrons involved in the electrochemical reaction, Faraday constant (~96,500 coulombs), and the electrochemical potential,

© University of Venda

respectively. ΔG is related to the standard free energy change (ΔG°, which is the free energy at standard conditions: 298 K, with all the reactants and products at unity activity) and the equilibrium constant (K) in the following equation [23]:

$$\Delta G = \Delta G° + RT\ln K \quad (17)$$

Equation 17 can, therefore be written as:

$$E = E^{\circ} - \frac{RT}{nF}\ln K \quad (18)$$

Equation 18 is called the Nernst equation; prediction of the corrosion tendency of the metal can be determined based on this equation. It provides the equilibrium electrochemical potential for a half-cell reaction not occurring at standard conditions. A positive sign for E indicates spontaneity of the forward reaction i.e. oxidation of metal is favoured [23]. Corrosion, therefore, will not occur unless the spontaneous reaction direction indicates metal oxidation.

Thermodynamics data obtained from observing the corrosion behaviour of certain metal in an aqueous environment can be summarized in what are called Pourbaix (potential-pH) diagrams [15]. These diagrams are useful in (1) predicting the spontaneous direction of a reaction, (2) estimating the corrosion products formed and (3) predicting environmental changes (by controlling the electrochemical potential and/or adjusting the pH) that will prevent or reduce corrosive attack [11, 15]. These diagrams represent equilibrium and, just like any other thermodynamic calculation, cannot be used to predict the rate of a reaction [11]. An example of such a diagram is the Pourbaix diagram for the iron-water system as shown in Figure 1.22.

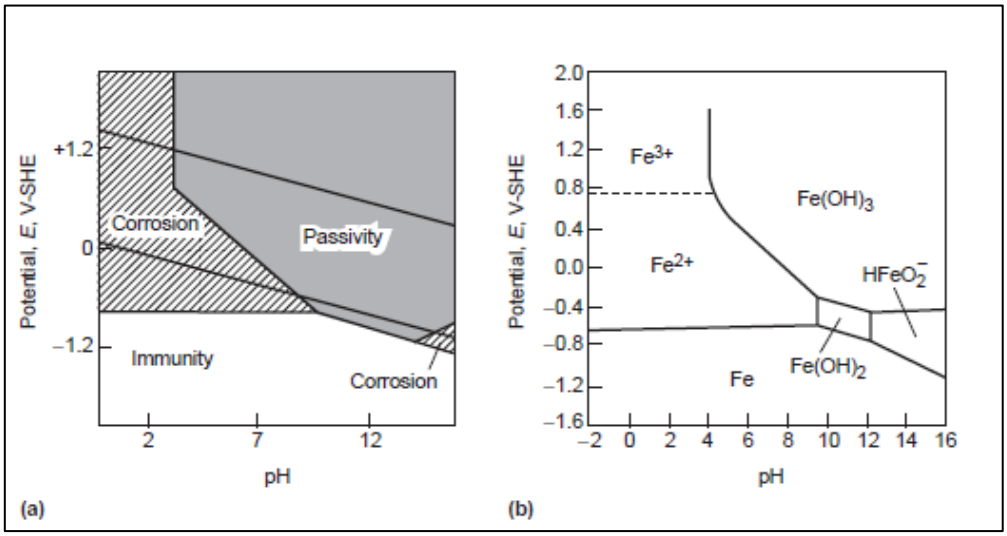

Figure 1.22: Simplified potential-pH for the iron-water system at 25°C showing (a) areas of corrosion, immunity (no corrosion) and passivity; and (b) corrosion products produced [16].

© University of Venda

1.1.10.2. Kinetics of corrosion

Corrosion reactions occur because equilibrium conditions have not been attained. It is for this reason that thermodynamic data cannot be used to predict the rate and extent of the corrosion process. Thus, kinetics data is necessary for making such predictions. Two kinetics concepts will be discussed in this section, namely: potentiodynamic polarization and Arrhenius equation

Potentiodynamic polarization

One of the most useful tools of conducting kinetics studies is potentiodynamic polarization. This involves applying a net current to the metal surface and observing how the potential value deviates from the equilibrium value. The study produces plots that are called potentiodynamic polarization (PDP) curves (i.e. plots of potential as a function of the logarithm of current density). These curves are made up of an anodic branch and a cathodic branch. The following four parameters can be determined from the curves: corrosion potential (E_{corr}), corrosion current density (i_{corr}), anodic (β_a) and cathodic (β_c) Tafel constants. The value of i_{corr} represents the corrosion rate when no external source of current is connected to the metal (i.e. applied current is zero) [40].

An example of such a curve is shown in the figure below:

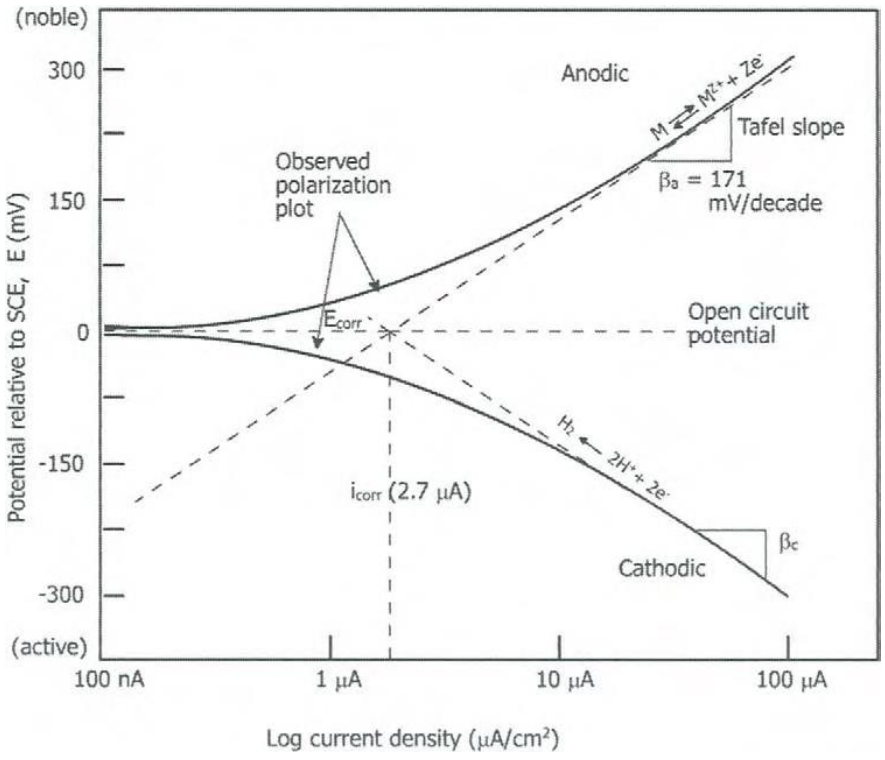

Figure 1.23: Example of PDP curve [3].

© University of Venda

Arrhenius equation

Corrosion rate is a function of many variables, one being the temperature at which the reaction occurs. Another variable is the activation energy; this is the energy barrier that the reacting species need to surmount to form the intermediate transition state that will then transform into the final products [6]. The corrosion reaction can be considered as an Arrhenius-type process represented by the following equation:

$$\mathrm{C_R} = \mathrm{A}\exp\left(-\frac{\mathrm{E_a}}{\mathrm{RT}}\right) \tag{19}$$

where E_a is the apparent activation energy, *R* is the universal gas constant, *A* is the Arrhenius pre-exponential constant and *T* is the absolute temperature [41].

Equation 19 can be rewritten in linear form as:

$$\mathrm{Log(C_R)} = \log \mathrm{A} - \frac{\mathrm{E_a}}{2.303\ \mathrm{RT}} \tag{20}$$

The changes that occur in corrosion rate because of changes in temperature can therefore be studied by plotting Arrhenius plots of $\log(\mathrm{C_R})$ vs. 1/*T*. These plots then allow for the determination of the activation energy associated with a particular reaction.

1.1.11. The effects of corrosion

The corrosion process gives rise to a lot of deleterious effects which affect the society in one way or another.

These effects can be classified as:

- Health and safety
- Conservation of materials
- Economic effects

Health and safety

The health and safety of humans can be put at risk in cases of corrosion failures. Collapsing of bridges, crashing of aircrafts and explosion of storage tanks due to corrosion failure have caused countless deaths and injuries of human beings. An example is that of the 1967 collapse of the ‘Silver Bridge” over Ohio River in the USA. The bridge collapsed while carrying 46 people, who all lost their lives. The cause of the failure was found to have been the effect of stress and corrosion [24]. Corrosion also raises health issues; potable water in particular can be contaminated by corrosion products as it flows through the corroded pipe system. One such incident occurred in Washington DC, USA, in 2004 when toxic levels of lead ions were found in drinking water. The lead ions were discharged into the drinking water as the lead pipe underwent corrosion [24].

© University of Venda

Conservation of materials

Corrosion is, by far, the number one consumer of metals known to man. Structures or components are continually removed from service to be repaired and maintained; this process consumes a portion of the total supply of the earth's natural resources [24].

The depletion process happens quicker than the discovery of new materials. Table 1.6 shows the limited supply of these resources, and loss of metals due to corrosion may soon result in a global metal crisis.

Table 1.6: Estimates of global reserves of various metals for years 1975 and 1995 [24].

	1975 Estimate of years of supply	**1995 Estimate of years of supply**
Aluminium	185	162
Iron	110	77
Nickel	100	43
Molybdenum	90	–
Chromium	64	–
Copper	45	22
Zinc	23	16

Economic effects

The type of impact corrosion has on the economy of South Africa and that of the world has been discussed in section 1.1.3. Studies show how the cost of corrosion continues to increase with an increase in development, meaning that nations will continue to lose money if better corrosion control methodologies are not put in place.

1.1.12. Corrosion of mild steel

Mild steel is an alloy of iron and carbon with small additions of elements such as manganese and silicon added to provide the necessary mechanical properties [12]. Iron is a naturally occurring metal which is found in the form of oxides; the ores of these oxides are then refined to produce steel. When the steel is in service, the iron has the tendency to revert to the oxide form by a process called rusting [7]. The environment to which mild steel is exposed plays a major role in determining the predominant cathodic reaction and hence the corrosion products. The anodic reaction of steel or iron undergoing dissolution is represented in Equation 21 and in Figure 1.24.

© University of Venda

$$Fe(s) \rightarrow Fe^{2+}(aq) + 2e^{-} \quad (21)$$

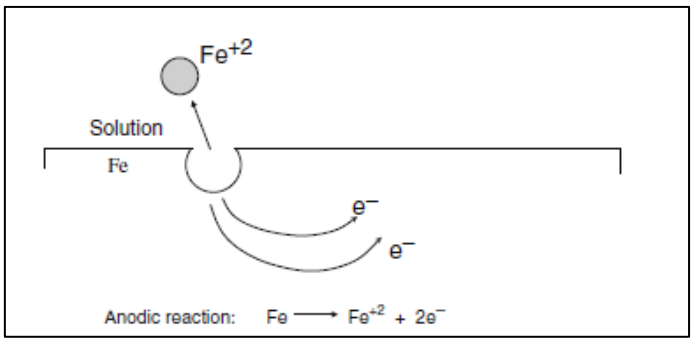

Figure 1.24: Anodic reaction of iron [24].

In the absence of water, such as in the case of a dry, clean atmosphere, mild steel is oxidized by oxygen to form a thin oxide film (made up of Fe_2O_3, formed according to Equation 22) of about 20 – 50Å in thickness.

$$4Fe(s) + 3O_2(g) \rightarrow 2Fe_2O_3(s) \quad (22)$$

The film protects the underlying surface against further corrosion. This film, when introduced to electrolytes, tends to breakdown and exposes the underlying metal to corrosive species [7]. The surface of mild steel can be subjected to various reactions; however, rust is commonly formed when the oxygen electrode is involved, i.e. when the following cathodic reaction is predominant:

$$½\ O_2(g) + H_2O(l) + 2e^{-} \rightarrow 2OH^{-}(aq) \quad (23)$$

The overall reaction being:

$$Fe(s) + \frac{1}{2}O_2(g) + H_2O(l) \rightarrow Fe^{2+}(aq) + 2OH^{-}(aq) \rightarrow Fe(OH)_2(s) \quad (24)$$

$Fe(OH)_2$ is unstable and tends to be oxidized to $Fe(OH)_3$ (also expressed as FeOOH) in the presence of excess water and oxygen, as shown in Equation 25 [3,17].

$$4Fe(OH)_2(s) + O_2(g) + 2H_2O \rightarrow 4Fe(OH)_3(s) \quad (25)$$

$Fe(OH)_2$ can also be converted, by oxygen, to form a hydrated ferric oxide $Fe_2O_3.nH_2O$ (as shown in Equation 26), which is the familiar reddish-brown product known as rust [3,17].

$$4Fe(OH)_2(s) + O_2(g) \rightarrow 2Fe_2O_3.nH_2O(s) + 2H_2O(l) \quad (26)$$

Figure 1.25 is a schematic representation of this corrosion process.

© University of Venda

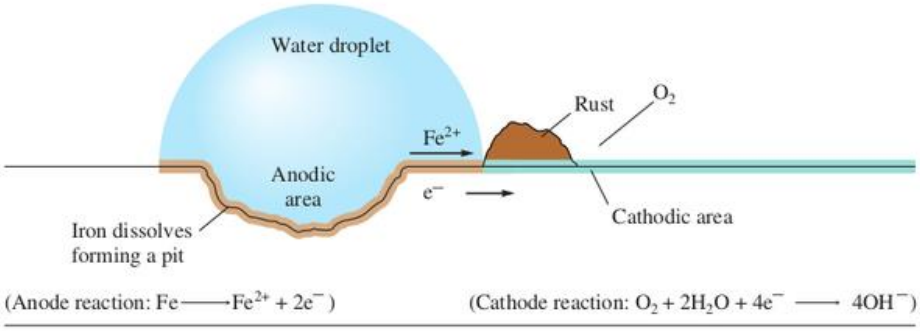

Figure 1.25: Rusting of mild steel [42].

1.1.13. Corrosion control measures

Corrosion control or prevention measures are those that provide the separation of a metal from its environment or allow modifying of the environment [18].

There are five primary methods for controlling or preventing corrosion, namely [16]:

- Design
- Materials selection
- Protective coating
- Cathodic protection
- Corrosion inhibitors

Design

This is a very important step in corrosion control, it should be known that corrosion control has to begin at the drawing board. A bad design is costlier than a good design, and if proper design considerations are adopted up to 20% of the costs associated with corrosion can be reduced. A proper design will, therefore, ensure that a material experiences long-term protection against corrosion [12, 43].

Material selection

Material selection is another important step in corrosion control. In order to do proper material selection, knowledge of how the actual conditions affect each material component is needed. That is, the material component's functional suitability as well as its ability to function safely in the given environment for the required period of time at a reasonable cost, needs to be evaluated [17,18]. In cases where combinations of materials are required, poor compatibility of these materials could lead to the formation of detrimental galvanic elements. Hence the consideration of not only the main structural materials but also the secondary material is important. There are also "natural" material-environment combinations that represent the

© University of Venda

maximum amount of resistance for the least amount of money, such as stainless steels in nitric acid, that provide guidelines for material selection [17].

Protective coatings

Application of coatings is the most common (and oldest) method of controlling corrosion. Coatings are used to provide long-term protection in a wide range of corrosive environments, by providing a continuous barrier between the metal substrate and the corrosive environment [12]. Any disruption or discontinuities can become the focal point for corrosion of the metal substrate [17].

Cathodic protection

In this case, protection of the metal is achieved by applying cathodic current to the surface so as to minimize anodic dissolution, hence, producing negative polarization [12, 21]. Cathodic protection can be achieved by using (i) a sacrificial anode (where the metal to be protected is attached to a more active metal which undergoes dissolution) or (ii) impressed current (where cathodic current is supplied through an external current source) [28].

Corrosion inhibitors

The use of corrosion inhibitors is very common in the oil extraction and processing industries. This technique forms the basis of the current study and will be discussed in greater detail in the section to follow.

1.2. INHIBITORS AND INHIBITION

1.2.1. Definition of corrosion inhibition

Corrosion inhibition is a method which involves the addition of chemical substances to a corrosive environment in small concentrations so as to reduce the corrosion rate of the metals to an acceptable level [1]. The inhibitor chosen has to be compatible with the environment in which it will be used, i.e. the inhibitor must be soluble and dispersible in the particular fluid [3]. This method is commonly used as an alternative where choosing a more corrosion resistant metal is prohibited by cost or when retaining mechanical strength is very important [24].

The way that inhibitors function is by modifying the electrochemical reactions from the solution side of the metal-solution interface, thereby increasing the resistance of the metal against corrosion [24].

© University of Venda

1.2.2. Types of inhibitors

Based on the definition above, corrosion inhibitors can be broadly divided into two main categories, namely: Environmental modifiers and Adsorption inhibitors [1].

Environmental modifiers are those inhibitors that interact with corrosive species in the environment. Such inhibitors include oxygen scavengers (e.g. sodium sulfite, hydrazine, etc.), which act to reduce the dissolved oxygen concentration thereby reducing the rate of the oxygen cathodic reaction [1].

The adsorption inhibitors, which will be under consideration in this current study, are those inhibitors which interact with the metallic surface where they modify the electrochemical reactions. These are further subdivided according to the type of electrochemical reaction they suppressed. The classification is as follows [21]: (i) Anodic inhibitors, (ii) Cathodic inhibitors; and (iii) Mixed inhibitors.

Anodic inhibition

These are generally effective in the pH range of about 6.5−10.5, and their chief role is to influence the anodic partial reaction and anodic polarization curve (by shifting the corrosion potential to the positive direction) [1, 21, 28]. The anodic inhibitors play a role in forming or facilitating the formation of passive films which impede or suppress the anodic dissolution reaction. The inhibition effect of these inhibitors is dependent on their concentration. There is a certain critical concentration below which the inhibitor will increase corrosion rate, through formation of pores and defects on the oxide film, instead of inhibition it [21, 22].

Cathodic inhibition

The role of cathodic inhibitors is to influence the cathodic partial reaction (i.e. hydrogen evolution and oxygen reduction) and the cathodic polarization curve (by shifting the corrosion potential to the negative direction) [21, 28]. Cathodic inhibitors influence the cathodic partial reaction by reducing the rate of cathodic reaction through the formation of a protective layer on the metal surface which limits the diffusion of reducible species to the metal surface [22].

Mixed inhibitors

Mixed inhibitors are those that reduce the rates of both anodic and cathodic reactions without having much of an effect on the corrosion potential [28]. Figure 1.26 is an illustration of the changes that occur in values of corrosion potential when the above-mentioned inhibitor types are introduced to a corrosive environment.

© University of Venda

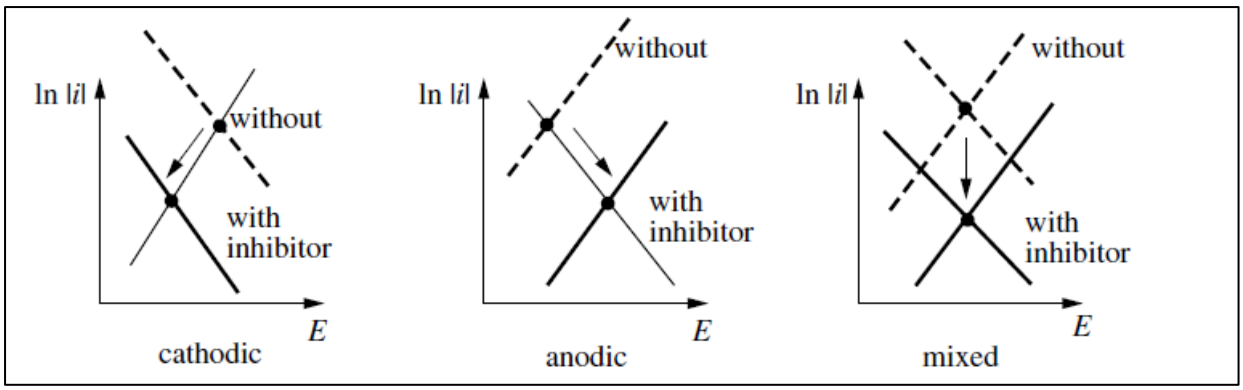

Figure 1.26: Evans diagrams showing the effect of different inhibitor types on the corrosion potential [28].

1.2.3. The mechanism of corrosion inhibition

When a metal is immersed into an electrolyte, a surface charge (positive or negative) is formed. This surface charge attracts oppositely charged ions from the electrolyte, the distribution of charge therefore gives rise to the electrical double layer. The electrical double layer (edl), as shown in Figure 1.27, comprises inner and outer Helmholtz planes within which water molecules, anions and cations are distributed. The sum of positive and negative charges is equal in the whole of the double layer [28, 44]. Water molecules form the first adsorbed layer on the metal surface, since the water molecule is polar it will be oriented according to the charge on the metal surface. If there are any adsorbable anions in the electrolyte such as Cl^- (or I^-), water molecules may be replaced by these anions (which approach the metal even when the charge on the metal surface is negative and are capable of chemisorbing on the metal surface) [24, 45]. When an inhibitor is added, inhibitor molecules interact with the metal surface hence changing the structure of the double layer [24].

In the case of organic inhibitors, the adsorption can either be competitive or co-operative as shown in Figure 1.28. Competitive adsorption involves the replacement of water molecules by the organic inhibitor (which has lost its proton). In this case, the inhibitor molecule adsorbs onto the metal surface through electron sharing. In the second case i.e. co-operative adsorption, the protonated inhibitor molecule does not lose its proton upon entering the double layer; however, it undergoes an electrostatic form of adsorption. In this case, the inhibitor adsorbs through its hydrogen unto the halide-covered surface [24, 45 – 47].

© University of Venda

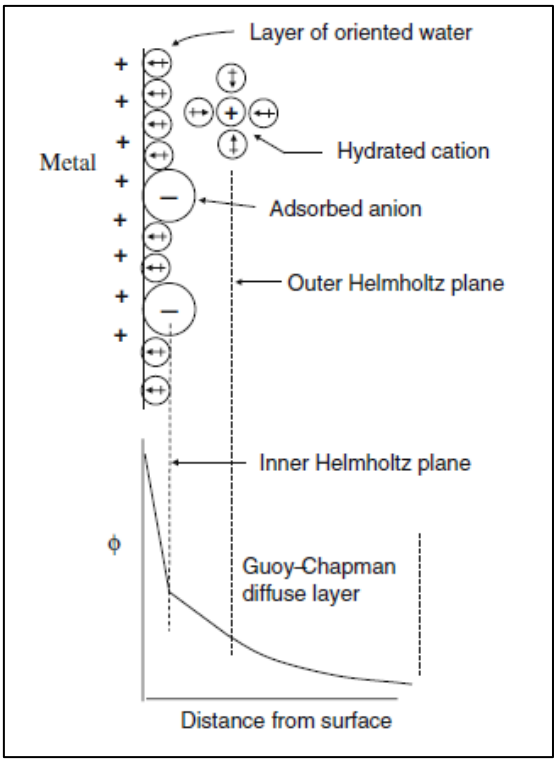

Figure 1.27: Electrical double layer [24].

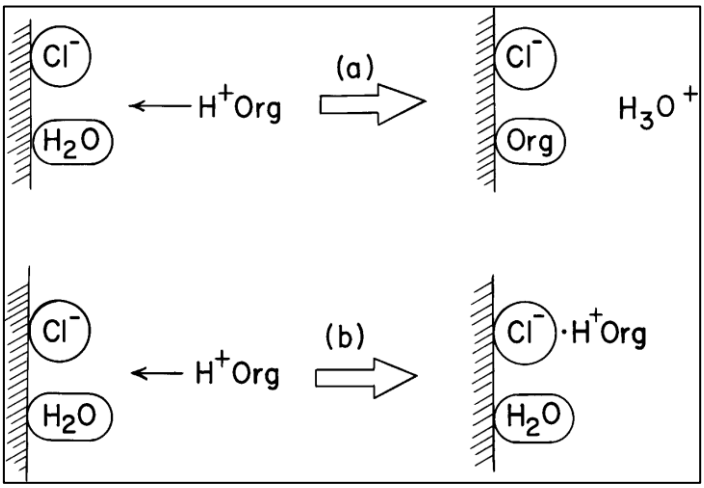

Figure 1.28: Adsorption of organic inhibitor: (a) Competitive adsorption and (b) Co-operative adsorption [24].

1.2.4. Techniques of application of corrosion inhibitors

A critical part of an inhibitor program is the application of the inhibitor to the metal surface to be protected, this is so crucial that even excellent inhibitors become ineffective if not applied properly [16, 22]. The system to be protected determines what kind of technique will be

© University of Venda

appropriate. The application techniques include: continuous injection, batch treatment, squeeze treatment and coatings [16].

Continuous injection

This process involves injection of inhibitors into the system, this is usually achieved by using an electric or gas driven chemical pump [3]. In this technique, a constant supply of inhibitor is injected throughout the lifetime of the equipment at a controlled rate [3, 48]. This is a cost-effective technique which is widely used in the oil industry; its use also helps in minimising scaling and corrosion problems especially for municipal water supplies and cooling towers [3].

Batch treatment

This method, unlike continuous injection, involves a periodic injection of a larger quantity of inhibitor. The frequency of inhibitor injection is dependent on the persistency of the film formed as the inhibitor adsorbs onto the metal surface [22]. In this method, occasional measurements of inhibitor concentration are important in ensuring that a safe level of inhibitor is maintained [22]. This method is commonly used to treat oil and gas wells [18].

Squeeze treatment

This is a method used for continuous treatment of oil wells, whereby a certain quantity of inhibitor is pumped into a well followed by pumping in of over-flush solvent which forces the inhibitor into the oil producing geological formation [3, 18]. The success of this method is centred on the continuous slow release of inhibitor from the formation. This method can offer protection which lasts for a year. The drawback of this method is that it is not cost effective and it can cause damage of the oil producing geological formation [3].

Coatings

This method is effective for coatings that are exposed to the open atmosphere [18]. The inhibitor is added to the protective coating or primer such that when moisture contacts the coating or primer some inhibitor is leached to protect the metal [22]. Incorporation of the inhibitor needs to be in such a way that the areas likely to undergo corrosion are protected, and also ensure that it does not leach completely from the coating or primer during the lifetime of the equipment [22].

© University of Venda

1.2.5. Aim of the present study

Acid solutions are widely used in the chemical industry to perform a variety of operations such as cleaning, descaling, pickling and oil well acidizing. Acids such as hydrochloric acid and sulphuric acid are usually chosen due to their low cost [49]. Mild steel is a common construction material in many industries. It is often chosen because of its excellent mechanical properties and low cost. [23]. Zinc is an important non-ferrous metal which is used extensively in metal coating [22].

All these metals are, however, easily corroded when exposed to the aggressive constituents of acidic solutions, particularly in HCl solutions where the presence of Cl^- promotes extensive localised attack [50]. Therefore, in order to minimise the attack of the metallic material, economical and efficient methods need to be developed [46]. The use of inhibitors helps in achieving this goal; with the use of organic inhibitors having gained much attention. The efficiency of organic inhibitors is dependent on the functional groups that adsorb onto the metal surface. The most effective organic inhibitors contain heteroatoms such as N, S, O and multiple double bonds in their molecules through which they adsorb onto the metallic surface [46]. However, most organic molecules are toxic and expensive. Hence, there exists a need to develop more environmentally friendly inhibitors which also have good inhibition efficiency [46]. Ionic liquids (ILs) have gained considerable attention in recent years, this interest stems from their eco-friendly nature which is due to properties such as low or negligible vapour pressure [51, 52].

The aim of the study is, therefore, to investigate the inhibiting behaviour of three ionic liquids (ILs) namely, 5-(Trifluoromethyl)dibenzothiophenium tetrafluoroborate, 5-(Trifluoromethyl)dibenzothiophenium trifluoromethanesulfonate and 1-Ethyl-3-methylimidazolium ethyl sulfate on the corrosion of mild steel and zinc in 1.0 M HCl.

The specific objectives are to:

1. Study the inhibition efficiency of the three ILs on the metals at different inhibitor concentrations and temperature using weight loss and electrochemical (Potentiodynamic polarization [PDP] and electrochemical impedance spectroscopy [EIS]) techniques;
2. Test the experimental data from gravimetric method with several adsorption isotherms in order to determine the thermodynamic functions for the adsorption process and thus obtain information about the mode of adsorption of inhibitor on the surface of mild steel and zinc;
3. Study the surface morphology/ interface interactions of the metals using SEM and FTIR spectroscopy in order to investigate the adsorption behaviour.

© University of Venda

2. LITERATURE SURVEY ON IONIC LIQUIDS

2.1. The historical background of ionic liquids

The history of ILs is generally believed to date back to 1914 when the first room temperature IL, ethylammonium nitrate, $[EtNH_3][NO_3]$, was synthesized [52]. Progress in this area was very slow; the next burst of interest was only in 1951 due to the discovery of haloaluminates. This discovery marked the beginning of the first generation of ionic liquids [52]. In 1963, synthesis of triethylammonium dichlorocuprate (which is a light-green oil at 25°C) was reported by Yoke III and co-workers. In the 1970s, Osteryoung and Wilkes successfully prepared room-temperature liquid chloroaluminate melts [53]. In 1982, the discovery of a "new class" of room temperature ILs, dialkylimidazolium chloroaluminates, was reported by Wilkes, Hussey and others. These haloaluminate ILs had challenges associated with their preparation, storage and handling, this is because of their hygroscopic and air sensitive nature. It was Wilkes and Zaworotko who, in 1992, successfully prepared ionic liquids which would solve this problem [53]. These were non-haloaluminate ILs, and they could be prepared, stored and handled outside a dry box [52, 54]. This discovery marked the second generation of ILs. The drawback that came with these non-haloaluminate ILs is that they were not as water stable as once believed. These ILs were later shown to undergo hydrolysis in certain conditions, forming toxic and corrosive hydrogen fluoride [52].

Other second generation ILs include those synthesized by Bonhôte, Grätzel and co-workers. Their work involved the synthesis of hydrophobic dialkylimidazolium ILs consisting of $[NTf_2]^-$ anions [52]. The third generation of ILs are the task-specific ionic liquids (TSIL) which emerged in the early 2000s. TSILs are those ILs which contain functional groups. As of 2008, the number of published papers relating to ILs was over 2500 compared to only 37 in 1996 and 76 in 2000, this shows that interest in ionic liquids is increasing exponentially [52].

2.2. The definition of ionic liquids

Ionic liquids are salts (organic or eutectic salts or eutectic mixtures of an organic salt and an inorganic salt) with melting points or glass-transition temperatures below 100°C. These salts consist entirely of ions, and as a consequence tend to exhibit conductivity [52].

Most ILs that meet the above definition happen to be liquid at or around room temperature; these are often called room temperature ILs. There are some ILs, however, which exist as solids at room temperature but still meet the current definition. Aqueous solutions of salts are not regarded as ionic liquids because they do not consist entirely of ions [52].

© University of Venda

2.3. Cations, anions and alkyl chains in ionic liquids

Ionic liquids are generally made up of large, low symmetry organic cations, and organic or inorganic anions [52]. The large organic cation usually involves a centre which contains positively charged phosphorus or nitrogen. This centre typically has linear alkyl chains attached to it. These cations are generally imidazolium, phosphonium, sulfonium, ammonium and pyridinium derivatives. Ionic liquids can be classified on the basis of the cation into five categories [55]:

- Five-membered heterocyclic cations e.g. imidazolium, pyrazolium and triazolium
- Six-membered and benzo-fused heterocyclic cations, e.g. pyridinium, benzotriazolium and isoquinolinium
- Ammonium, phosphonium and sulfonium based cations
- Functionalized imidazolium cations (Figure 2.1)
- Chiral cations, e.g. (1S, 2R)-(+)-*N,N*-dimethylephedrinium ion (Figure 2.2)

Generally, the melting point of the ionic liquid will be determined by the length of the alkyl chains. Longer, dissimilar alkyl chains usually cause packing constraints, hence lowering the melting point of the ionic liquid [55]. The water solubility of ionic liquids also generally depends on the length of the alkyl chain. Water solubility is generally decreased with an increase in alkyl chain length [55].

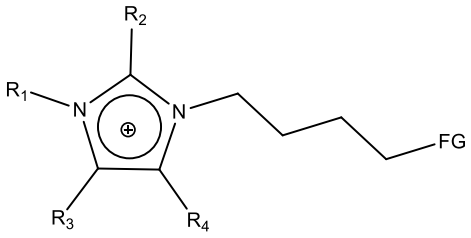

FG = OH, NH_2, SH, SO_3OH, $CONH_2$

Figure 2.1: Schematic representation of functionalized imidazolium cations [55].

© University of Venda

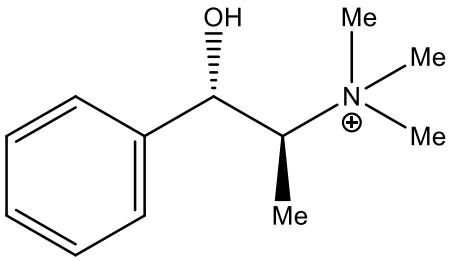

Figure 2.2: Chiral cation: (1S, 2R)-(+)-N,N-dimethylephedrinium ion [55].

Anions of ILs are inorganic or organic compounds possessing weak basic strength, and a diffuse or protected negative charge. ILs can be classified on the basis of the anion into six categories [55]:

- ILs based on $AlCl_3$ and organic salts
- ILs based on anions like BF_4^-, PF_6^- and SbF_6^-
- ILs with amide- and methanide-based anions
- ILs with phosphate-, phosphonate-, phosphinate-, sulphate- and sulphonate-based anions,
- ILs with anions such as tosylate $[CH_3PhSO_3]^-$, trifluoroacetate $[CF_3CO_2]^-$, and triflate $[CF_3SO_3]^-$; and
- ILs with borate- and borane-based anions

2.4. Aprotic and protic ionic liquids

The majority of research done on ILs has focused on aprotic ILs. These are a subset of ILs that consist entirely of non-protonated cations, and anions. The cations are usually formed by addition of a group (usually an alkyl group) to the basic site located on the parent base material [54]. Examples of aprotic ILs are 1-ethyl-3-methylimidazolium tetrafluoroborate $[C_2mim][BF_4]$ and 1-butyl-3-methylimidazolium bis(trifluoromethanesulfonyl)imide $[C_4mim][NTf_2]$ [52].

Protic ionic liquids are formed by proton transfer from a Bronsted acid (HA) to a Bronsted base (B) in the following way [52]:

$$HA + B \rightarrow [BH]^+ + A^- \quad (27)$$

Protic ILs may consist of a small amount of the molecular species (due to incomplete protonation) i.e. they do not necessarily consist exclusively of ions [52].

Examples of protic ILs as well as their formation processes are as follows [52, 53]:

a) Ethylammonium nitrate $[C_2H_5NH_3][NO_3]$

$$C_2H_5NH_2 + HNO_3 \rightarrow [C_2H_2NH_2]^+ + [NO_3]^- \quad (28)$$

© University of Venda

b) 1-methylimidazolium tetrafluoroborate [Hmim][BF_4]
Prepared from N-methylimidazole and tetrafluoroboric acid.

2.5. Organic and inorganic ionic liquids

Most commonly used ILs consist of an organic cation and an organic or inorganic anion. An examples of an IL with an organic cation and organic anion is [C_4mim][NTf_2]. An example of an IL with organic cation and inorganic anion is [C_2py][BF_4] [52].The ILs with organic cations and inorganic anions typically have lower melting points due to problems in efficiently packing the large irregular organic cations with the small inorganic anions [56].

There are ILs that consist entirely of inorganic entities, these are called inorganic ionic liquids. Examples are hydrazium nitrate, [N_2H_5][NO_3], and hydrazium bromide, [N_2H_5][Br], which melt at 70°C and 86.5°C, respectively [52]. Another example of inorganic ILs is observed in the $LiAlCl_4$ – $LiAlI_4$ system which has a eutectic temperature of 65°C (i.e. shows ionic liquid domain). The mismatching of large anions such as tetrachloroaluminate or tetrachloroiodide with Li^+ leads to the formation of an inorganic IL [56].

2.6. Task-specific ionic liquids

Task-specific ILs (TSILs) are also called functionalized ionic liquids since they contain functional groups which are covalently tethered to the cation and/or anion. Their function is to impart specific properties or reactivities (e.g. improved catalytic activity) to the IL [52, 57]. Most TSILs have the functional group covalently tethered to the cation [58]. Examples are imidazolium- or triphenylphosphine cations that are functionalized with sulfonic acid groups (-SO_3H) [52]. These imidazolium salts are called Brønsted acids, they can be used as catalysts for a wide range of acid-catalysed organic reactions such as Fischer esterification [52]. Although rare, there are some examples of anion-tethered TSILs such as 1-butyl-3-imidazolium cobalt tetracarbonyl, [C_4mim][$Co(CO_4)$] [52].

2.7. Synthesis of ionic liquids

The number of ways of forming ILs is increasing as the number of ILs increase. The simplest method for the formation of ILs is protonation. Protic ILs are prepared using this method which generally has starting materials such as amines and phosphines [52, 58]. An example is ethylammonium nitrate, which is formed by the protonation of ethylamine (present as aqueous solution), $C_2H_5NH_2$, by concentrated nitric acid (HNO_3). The final product after distillation (to remove water) is [$C_2H_5NH_2$][NO_3] [52, 58].

© University of Venda

This method, however, has a drawback i.e. the possibility of decomposition by deprotonation hence limiting the use of these protic ILs. More complex methods are generally required for preparing a wider range of useful salts, these are outlined below [58]:

Alkylation

This method is used for preparing ammonium-, imidazolium-, pyridinium- and phosphonium-based ILs. A suitable precursor (e.g. NR_3) is alkylated by an appropriate alkylation agent (RX), e.g. alkylsulfate or alkyl halide [52, 53]. An example of the alkylation reaction is the preparation of 1-butyl-3-methyl-imidazolium chloride [C_4mim]Cl from 1-methylimidazole and 1-chlorobutane, this reaction is carried out at 80°C for 2 – 3 days. This reaction is illustrated in Figure 2.3 below [53].

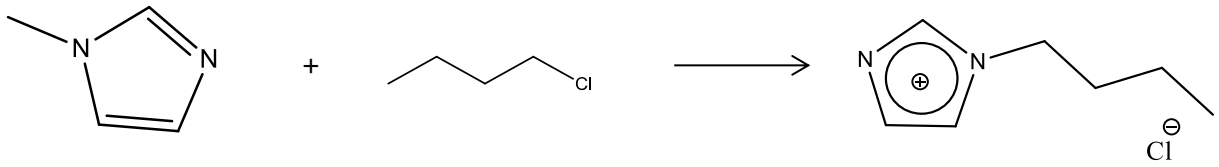

Figure 2.3: Preparation of 1-butyl-3-3-methylimidazolium chloride [53].

Tetraalkylphosphonium halide can be prepared by the nucleophilic addition of a tertiary phosphine to a haloalkane. For example, trihexyl(tetradecyl)phosphonium chloride [$P_{6\,6\,6\,14}$]Cl can be prepared by the reaction of trihexylphosphine, $P(C_6H_{13})_3$ with 1-chlorotetradecane, $C_{14}H_{29}Cl$ [52].

Anion exchange

When the IL with the desired anion cannot be obtained from the alkylation method, an anion exchange reaction is carried out. The previously formed IL (i.e. from the alkylation process) acts as a precursor and the halide anion is exchanged with the required anion, typically through a metathesis reaction [53]. The anion exchange occurs between an organic salt and an inorganic anion source (e.g. group 1 metal salt or a silver salt) [52].

In the preparation of [C_4mim][NTf_2], [C_4mim]Cl can be used as a precursor and reacted with lithium bis[(trifluoromethyl)sulfonyl]amide (Equation 29):

$$[C_4\text{mim}]\text{Cl} + \text{Li}[\text{NTf}_2] \rightarrow [C_4\text{mim}][\text{NTf}_2] + \text{LiCl} \qquad (29)$$

© University of Venda

Halide-free synthesis

Most imidazoles, alkylamines or phosphines are prepared by the two processes outlined above i.e. alkylation using alkyl halides as alkylating agents, followed by anion exchange. One advantage of this procedure is that a large number of ILs of good quality can be produced [55]. A major drawback of this procedure is the difficulty to obtain high purity ILs due to the following [52]:

- Difficulty of separating halogenoalkanes (particularly those of high boiling points) from the final products
- Contamination of ILs with the halide salts formed by metathesis reaction, possibly resulting in drastic change of the physical properties of the IL. When ILs are used as solvents for transition metal catalysts, the presence of halide impurities may result in the poisoning and deactivation of the catalysts.

Strategies for halide-free synthesis have therefore been explored since 2005. One such procedure involves the use of dimethyl carbonate, $(CH_3O)_2CO$, as an alkylating agent for the preparation of the halide-free ILs [55].

Another example of halide-free synthesis is the synthesis of halide-free phosphorus based ILs. These can be prepared by the direct reaction of [55]:

a) Phosphines with sulphates
b) Tertiary phosphines or imidazoles with alkylating agents e.g. monoalkylphosphinates, dialkylphosphonates and trialkylphosphates
c) Phosphines with acids

Microwave-assisted synthesis

Preparation of dialkylimidazolium halides by refluxing of 1-methylimidazole and a large excess of alkyl halide in organic solvents (e.g. toluene) as reaction media typically requires several hours in order to obtain reasonable yields [52]. In 2000, two researchers showed that a shorter reaction time, cleaner work-up procedure and unique transformations could be achieved by conducting microwave-assisted synthesis [52, 55]. A series of dialkylimidazolium based ILs were prepared (with reaction time of a few minutes) under solvent-free conditions in a common household microwave oven (equipped with inverter technology) [52 – 55.]. The $[C_n mim]$-type ILs were prepared by the reaction of 1-methylimidazole with alkyl halides or terminal dihalides [55].

© University of Venda

2.8. Properties of ionic liquids

The basic properties of ILs are the following:

Melting point

As mentioned in the definition of ILs, the melting point of ILs is generally below 100°C. Melting points of ILs are affected by a number of factors such as:

Size of cation and anion: Both the cations and anions contribute to the melting point of the IL. As the size of the cation or anion increases, the melting point tends to decrease. Examples of this are seen in $[C_2mim]Cl$ and $[C_2mim]AlCl_4$ which have melting points of 87°C and 7°C, respectively [52].

Length of alkyl chain: The length of the alkyl chains on the cation can affect the melting points. Generally, longer alkyl chains tend to decrease melting points of ILs; this is seen in $[C_4mim]Cl$ which has a melting point of 65°C compared to 87°C in $[C_2mim]Cl$ [52].

Symmetry of cation: A cation of low symmetry gives rise to packing constraints (effective packing of ions increases with increasing symmetry), as a result, melting points tend to decrease with decreasing symmetry. This can be illustrated in the following tetraalkylammonium bromide compounds: $[N_{5\,5\,5\,5}]Br$ (made up of four straight-chain pentyl groups) has a melting point of 101.3°C while $[N_{1\,5\,\,6\,8}]Br$ (made up of a methyl group and straight-chain pentyl, hexyl and octyl group) is a room temperature IL [52].

Vapour pressure

ILs, as mentioned in the definition are made entirely or almost entirely of ions. There exist, therefore, strong coulombic interactions between these ionic entities, and as a result, ILs have low or negligible vapour pressure. They do not evaporate in the reaction vessel; hence, they do not contribute to the pollution of air. It is for this reason that ILs are widely celebrated and considered as eco-friendly and less hazardous [46, 52].

There are, however, some ILs (particularly those with imidazolium cations with long alkyl chains and $[NTf_2]$ as anion) that have been successfully distilled at temperatures between their estimated boiling temperature and decomposition temperature [52]. Generally, ILs with shorter alkyl chains on the cations will have negligible vapour pressure at ambient temperatures and pressures [52].

© University of Venda

Liquidus range and thermal stability

The liquidus range is the temperature range where the IL is in the liquid phase. For most ILs, the liquidus range is the difference between the glass transition temperature and the thermal decomposition temperature [55]. Most ILs tend to slowly form glass at lower temperatures hence they have a glass transition temperature instead of a melting point. Since most ILs typically do not evaporate at high temperatures, they tend to undergo thermal decomposition. ILs typically exhibit a higher liquidus range than most common molecular solvents [52 − 58]. For example, 1-alkyl-3-methylimidazolium salts typically have a liquidus range of over 300°C (with glass transition temperatures usually ranging from −70°C to 90°C and decomposition temperatures usually ranging from 250°C to over 450°C), compared to dichloromethane, a common solvent, which has a liquidus range of 145°C (i.e. melting point of −95°C and boiling point of 40°C) and water which has a liquidus range of 100°C (melting point of 0°C and boiling point of 100°C) [52, 58].

The high thermal decomposition temperatures of ILs indicate high thermal stabilities, meaning that the ILs can potentially be used for high temperature applications. Thermal decomposition temperatures of some imidazolium-based ILs are shown in Table 2.1, these values show the effect of the alkyl chain length and anion on the decomposition temperature. Thermal stability is largely affected by the anion type and follows the general order of $Cl^- < [BF_4]^- \sim [PF_4]^- < [NTf_2]$ (weakly coordinating anions tend to be more resistant to thermal degradation) [53, 58].

Table 2.1: Thermal decomposition temperatures of some imidazolium-based ionic liquids [59].

$[C_n mim]X$[a]	**T (ºC)**
1-alkyl-3-methylimidazolium chloride	240 – 290
1-alkyl-3-methylimidazolium hexafluorophosphate	330 – 420
1-alkyl-3-methylimidazolium tetrafluoroborate	350 – 410
1-alkyl-3-methylimidazolium bis(trifluoromethylsulfonyl)imide	400 – 480

[a] Chain length of alkyl substituent, $C_n = C_2$ - C_{18}.

Electrochemical potential window

The electrochemical potential window is the difference between the anodic and cathodic potential limits. It indicates the range over which a material is neither oxidised nor reduced at an electrode i.e. indicates the range of electrochemical inertness. The potential window is primarily dependent on the resistance of the cation to reduction and the anion to oxidation [52, 58]. Generally, non-haloaluminate ILs have high electrochemical windows ranging from 2.0 to 6.0 V [52]. The presence of impurities such as halide ions have a large effect on the size of

© University of Venda

the electrochemical window. For example, the presence of easily oxidised halide ions (Cl^-, Br^-, I^-) in significant concentrations may cause an appreciable reduction of the anodic potential limit, hence reducing the size of the electrochemical window [58]. The size of the electrochemical window can also be affected by the presence of significant amounts of water which contaminates the IL. Water can be both oxidized and reduced and hence can affect both the anodic and cation potential limits [58].

Conductivity

Conductivity of an IL has to do with the available charge carriers and their mobility (i.e. their ability to conduct electric current). Since ILs consist entirely or almost entirely of ions which can act as charge carriers, it would be expected for them to have high conductivities. However, this is not the case [52, 58]. ILs, as a class, generally have higher conductivities when compared to conventional non-aqueous solvent/electrolyte systems. However, when compared to concentrated aqueous solvents, their conductivities are lower than expected. The reasons for the lower than expected conductivities are the ion-ion interactions which lead to ion pairing and/or ion aggregation (i.e. neutral entities), and reduction in ion mobility due to large sizes of ions (which correspond to high viscosity) [52, 58]. Conductivity of ILs will generally increase with a decrease in cation size and an increase in temperature [52].

2.9. Major applications of ionic liquids

ILs are considered to be ‘designable’ or ‘fine-tunable’ therefore the applications in which they can be used are vast. Initially, ILs were introduced as alternative green solvents in the place of volatile organic solvents which are commonly used in the industrial synthesis of organic chemicals [60]. The ‘designable’ characteristic of ILs means that a solvent can be designed in order to optimize a reaction, hence having control over both the percentage yield and selectivity [60]. This characteristic also means that a solvent can be designed or selected to dissolve a wide range organic or inorganic molecules hence reducing the volume of solvent required for a certain reaction [60].

ILs have progressively marched beyond the border of green solvents and are now playing a significant role of controlling chemical reactions as catalysts. Ranu et al [61] designed a task-specific basic IL, [Bmim]OH, which was used as a catalyst for Knoevenagel condensation of some aliphatic and aromatic carbonyl compounds. This IL proved to be a very efficient catalyst for the reaction process [61].

© University of Venda

2.10. Handling of ionic liquids

The hazards associated with ILs have not yet been fully explored. However, there are some well-established precautions when it comes to the handling of ILs such as haloaluminate ILs and those with fluorinated anions i.e. $[PF_6]^-$ and $[BF_4]^-$. The haloaluminate ILs are unstable in the presence of water or moisture and will decompose to form corrosive hydrogen halide fumes. Hence, they should be handled in a dry-box. ILs with fluorinated anions are also unstable in water and tend to decompose to form a toxic and corrosive hydrogen fluoride plus a colourless solid [52].

2.11. Ionic liquids as corrosion inhibitors

One of the main advantages of a good corrosion inhibitor is its low toxicity. As mentioned earlier, one of the most celebrated properties of ILs is their low to negligible vapour pressure. It is, therefore, this property which makes ILs an eco-friendlier and less hazardous alternative for the widely used organic inhibitors [47]. Non-toxic imidazolium compounds are the most commonly studied ILs. These have shown good corrosion inhibitory behaviour on mild steel, copper and aluminium [50]. This is attributed to the lone pair of electrons found on the nitrogen atoms, these help in the facilitation of adsorption of the IL on the metal surface [62]. Other widely studied ILs for corrosion inhibition are the pyridinium-based ILs. The use of ILs as corrosion inhibitors is fairly recent and hence there is limited information available. We cite below some of the work that has been done regarding ILs as corrosion inhibitors.

Likhanova et al [63], studied 'the effect of ionic liquids with imidazolium and pyridinium cations on the corrosion inhibition of mild steel in acidic environment'. In this study, two ILs were synthesized, namely: 1,3 dioctadecylimidazolium bromide ($ImDC_{18}Br$) and *N*-octadecylpyridinium bromide ($PyC_{18}Br$). These ILs were subsequently tested as corrosion inhibitors for mild steel in 1 M H_2SO_4. Both ILs showed efficient inhibition when present in higher concentrations (with average inhibition efficiency within the range of 82 − 88%). $ImDC_{18}Br$, particularly, showed better inhibition efficiency due to its larger esteric body [63]. The inhibition efficiency of these ILs were observed to increase as IL concentration increased.

Shukla et al [46], studied the 'inhibitive effect of imidazolium based aprotic ionic liquids on mild steel corrosion in hydrochloric acid medium'. The ILs in this study were: $[C_4MIM][NO_3]$, $[C_4MIM][BF_4]$ and $[C_4C_1MIM][BF_4]$. Weight loss and hydrogen evolution techniques were used, and it was reported that $[C_4MIM][NO_3]$ had the highest inhibition efficiency followed by $[C_4MIM][BF_4]$. For all the ILs, the inhibition efficiency was reported to increase with increasing IL concentration. Thermodynamic parameters such as the Gibbs free energy indicated that

© University of Venda

the adsorption process was a spontaneous reaction which followed the physical adsorption mechanism and obeyed the Langmuir adsorption isotherm model [46].

The corrosion inhibition properties of [EMIM][BF_4], [BDMIM][BF_4] and [C_{10}MIM][BF_4] were investigated by Sasikumar et al [64], using experimental techniques (i.e. electrochemical and spectroscopic techniques) and theoretical techniques (i.e. quantum chemical calculations and Monte Carlo simulations). Results obtained from the experimental techniques indicated a spontaneous adsorption process which obeyed the Langmuir adsorption isotherm model. In addition, the adsorption process followed both physisorption and chemisorption mechanisms. All ILs were reported to have an appreciable inhibition efficiency which increased with an increase in IL concentration, with [C_{10}MIM][BF_4] having the highest inhibition efficiency (reported as 98.8% at 500 ppm). At the concentration of 500 ppm, [EMIM][BF_4] and [BDMIM][BF_4] had inhibition efficiencies of 77.93% and 90.84%, respectively. This increase in inhibition efficiency is attributed to the increase in the alkyl chain length [64].

© University of Venda

3. EXPERIMENTAL

3.1. Materials

The mild steel specimens utilized in all the procedures were of the composition 0.02% Phosphorus (P), 0.37% Manganese (Mn), 0.03% Sulphur (S), 0.01 Molybdenum (Mo), 0.039% Nickel (Ni), 0.21% Carbon (C) and the remaining part being Iron (Fe). The zinc specimens used were of a 99.90 (wt%) purity. In the weight loss measurements, the metals specimens were supported by glass hooks and rods.

3.2. Reagents

The hydrochloric acid used for this study was obtained from MERCK CHEMICALS.

3.3. Corrosion inhibitors

The following ionic liquids obtained from SIGMA ALDRICH were used without further purification: 5-(Trifluoromethyl)dibenzothiophenium tetrafluoroborate, 5-(Trifluoromethyl)dibenzothiophenium trifluoromethanesulfonate and 1-Ethyl-3-methylimidazolium ethyl sulfate. Stock solutions in the concentration range of 1.0×10^{-2} M to 8.0×10^{-2} M were prepared for each inhibitor and were used for all the procedures. The names and structures of the ionic liquids used are listed in Figure 3.1.

3.4. Electrochemical techniques

All electrochemical measurements were carried out using a Metrohm Autolab PGSTAT302N which employs a conventional 3-electrode cell. Ag/AgCl with 3 M KCl was used a reference electrode (RE), platinum rod was used as a counter electrode (CE) and metal specimens (i.e. mild steel and zinc) were used as the working electrode (WE). A stabilization period of 30 minutes was allowed prior to all electrochemical measurements. This period was sufficient to obtain a stable open circuit potential (OCP) value. The potentiodynamic curves were generated at the potential range of −250 to +250 mV (SCE) at a scan rate of 1 mV s^{-1}. The electrochemical impedance spectroscopy measurements were carried out in a frequency range from 100 kHz to 0.1 Hz at 10 mV amplitude. All electrochemical measurements were conducted under atmospheric conditions without stirring at 30°C.

© University of Venda

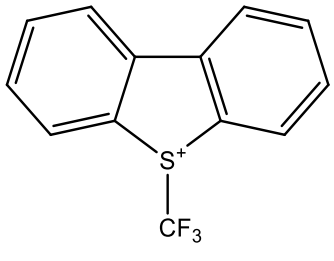

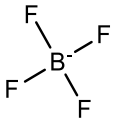

5-(trifluoromethyl)dibenzothiophenium tetrafluoroborate

$C_{13}H_8BF_7S$ Molecular weight: 340.07 g/mol

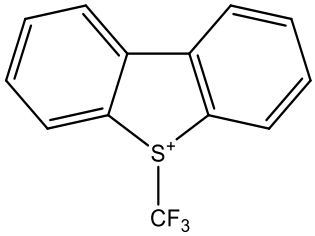

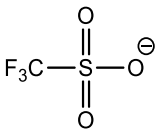

5-(trifluoromethyl)dibenzothiophenium trifluoromethanesulfonate

$C_{14}H_8F_6O_3S_2$ Molecular weight: 402.33 g/mol

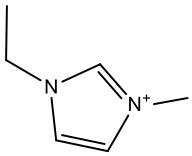

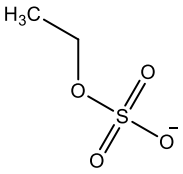

1-Ethyl-3-methylimidazolium ethyl sulfate

$C_8H_{16}N_2O_4S$ Molecular weight: 236.29 g/mol

Figure 3.1: Molecular structures of the ionic liquids used as corrosion inhibitors in this study.

3.4.1. Potentiodynamic polarization (PDP)

The potentiodynamic polarization method was used to obtain electrochemical parameters such as corrosion potential (E_{corr}), corrosion current density (i_{corr}), anodic and cathodic Tafel slopes (β_a and β_c, respectively). The percentage inhibition efficiency for each inhibitor was evaluated from the measured i_{corr} values using the relationship below:

$$\%IE_{PDP} = 100\left(\frac{i^0_{corr} - i^i_{corr}}{i^0_{corr}}\right) \quad (30)$$

where: i^0_{corr} and i^i_{corr} are the corrosion current densities in the absence and presence of inhibitor molecules, respectively.

© University of Venda

3.4.2. Electrochemical impedance spectroscopy (EIS)

The corrosion of mild steel and zinc in 1.0 M HCl was further studied using EIS. Electrochemical parameters such as the resistance to charge transfer (R_{ct}), capacitance of the double layer (C_{dl}), the constant phase element (*CPE*) and exponents (n) were obtained and used to calculate the percentage inhibition efficiency (%IE_{EIS}) using the equation below:

$$\%IE_{EIS} = 100\left(\frac{R_{ct} - R_{ct}^{0}}{R_{ct}}\right) \quad (31)$$

where R_{ct}^{0} and R_{ct} are the charge transfer resistances in the absence and presence of inhibitor molecules, respectively.

3.5. Adsorption film analysis

Adsorption films formed on the mild steel and zinc metal coupons after the metals were immersed in aggressive solution containing 8.0 × 10^{-2} M of each inhibitor were scraped off with a sharp pair of scissors. The resultant powders were analysed using the Bruker FTIR spectrometer Alpha II.

3.6. Surface analysis

Mild steel and zinc metal specimen with surface area of 6 cm^2 were immersed in 1 M HCl both in the absence and presence of varying concentrations of corrosion inhibitor at 30°C for a period of 15 hours. After this period, the coupons were retrieved from the solutions, cleaned with a bristle brush, rinsed thoroughly with distilled water, and dried with acetone. The surface morphology and Energy Dispersive Spectroscopy (EDS) were performed using the JOEL JSM-7500F Field Emission Scanning Electron Microscope.

3.7. Weight loss measurements

This method is commonly used for corrosion studies because it can be carried out with ease, accuracy and at low cost [65]. Two sets of tests were conducted by totally immersing the metal coupons (i.e. mild steel and zinc) in corrosive solutions. The first set involved immersing the metal coupons in corrosive solutions which did not contain inhibitor molecules and the second set of experiments involved the metal coupons being immersed in corrosive solution which had varying concentrations of the corrosion inhibitors. The metal coupons were immersed such that their surface area was completely covered by a 80 ml solution carried by a 100 ml capacity beaker. Specific temperatures (30, 40 and 50°C) were maintained with the help of a thermostated water bath during each test for a period of 15 hours. The metal coupons were accurately measured using a sensitive analytical balance; glass rods and hooks were used to support the metals and keep them suspended inside the solutions. After the 15-hour period,

© University of Venda

the metal coupons were removed from the solutions, cleaned with a bristle brush, rinsed thoroughly with distilled water, dried with acetone and re-weighed.

The corrosion rates for the metals in the acidic environment were obtained using the equation below:

$$\rho = (\Delta W/St) \tag{32}$$

where: ρ = corrosion rate

W = average weight loss of metal specimens (in grams, g)

S = total surface area of metal coupon (in cm^2)

t = total immersion time (in hours)

The rate of corrosion is therefore given in the units of $gcm^{-2}hr^{-1}$. The calculated corrosion rate values can be used to calculate the percentage inhibition efficiency ($\%IE_{WL}$) and the degree of surface coverage (θ) using the equations that follow.

Percentage inhibition efficiency ($\%IE_{WL}$):

$$\%IE = 100\left(\frac{\rho^0 - \rho^1}{\rho^0}\right) \tag{33}$$

where: %IE = the percentage inhibition efficiency

ρ^0 = corrosion rate in the absence of the inhibitor molecules

ρ^1 = corrosion rate in the presence of inhibitor molecules

Degree of surface coverage (θ):

$$\theta = \frac{\rho^0 - \rho^1}{\rho^0} \tag{34}$$

where: θ = degree of surface coverage

ρ^0 = corrosion rate in the absence of inhibitor molecules

ρ^1 = corrosion rate in the presence of inhibitor molecules

© University of Venda

4. RESULTS AND DISCUSSION

4.1. Mild Steel

4.1.1. Potentiodynamic polarization (PDP)

The corrosion process of mild steel in immersed in 1.0 M HCl solution at 30°C, in the absence and presence of various concentrations of the studied ILs i.e. 5-(Trifluoromethyl)dibenzothiophenium tetrafluoroborate (TDTB), 5-(Trifluoromethyl)dibenzothiophenium trifluoromethanesulfonate (TDTM) and 1-Ethyl-3-methylimidazolium ethyl sulfate ([EMIM][ESO_4]), can be illustrated by cathodic and anodic polarization curves. These curves are shown in Figures 4.1 – 4.3.

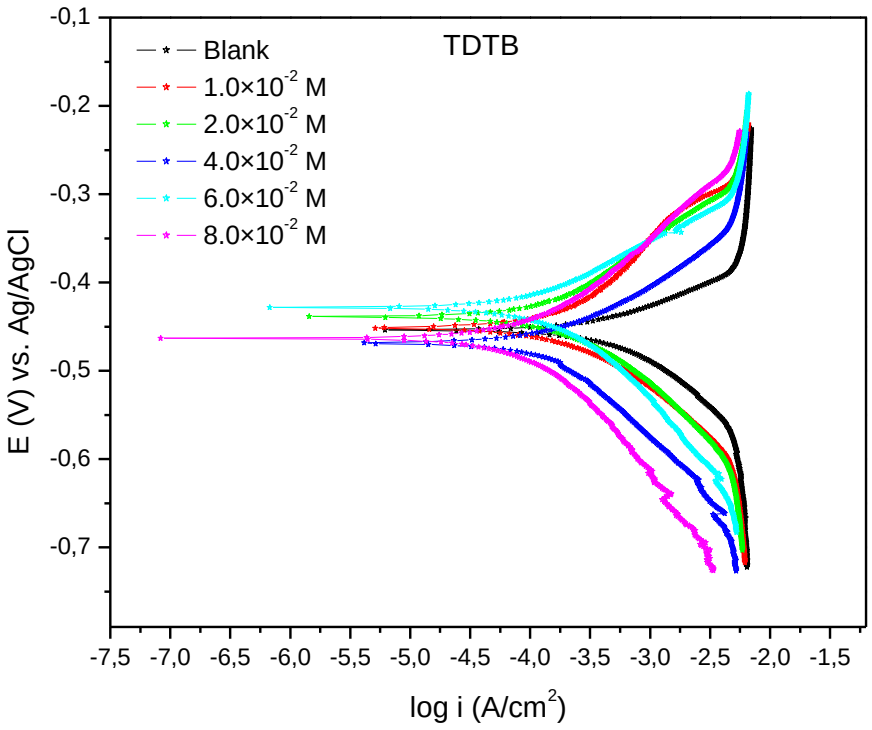

Figure 4.1: Tafel plots for mild steel in 1.0 M HCl in the absence and presence of different concentrations of TDTB inhibitor compound.

© University of Venda

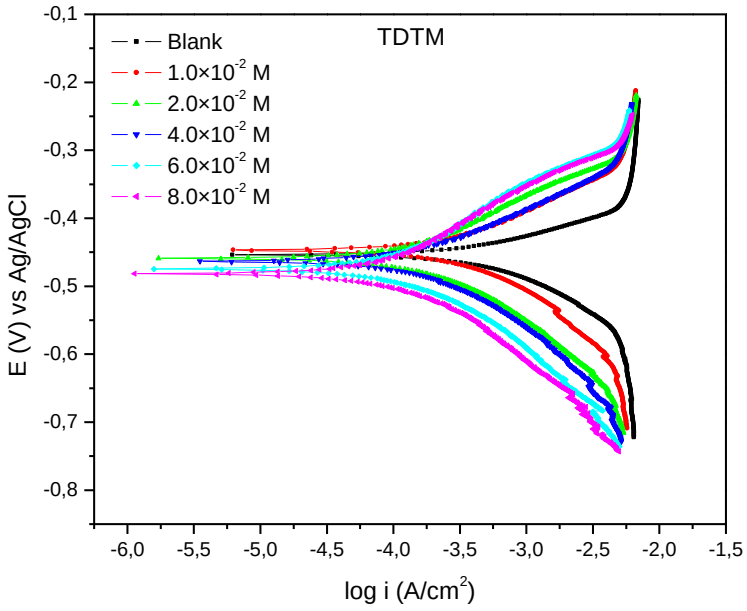

Figure 4.2: Tafel plots for mild steel in 1.0 M HCl in the absence and presence of different concentrations of TDTM inhibitor compound.

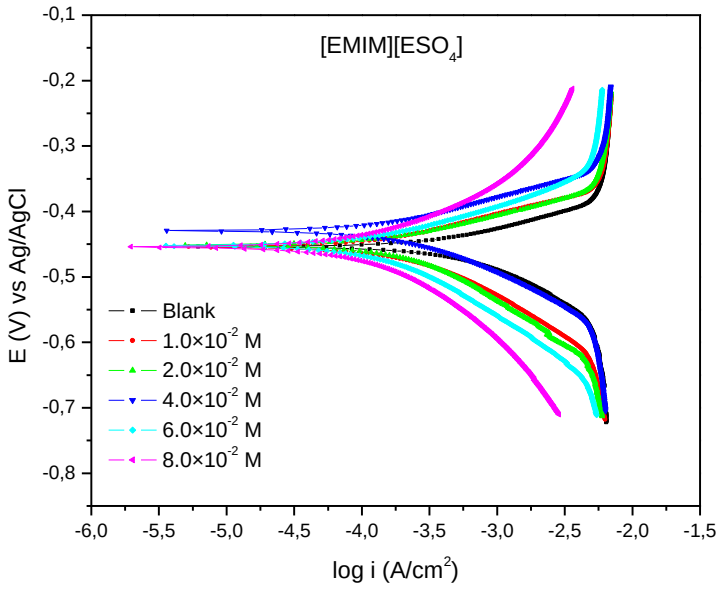

Figure 4.3: Tafel plots for mild steel in 1.0 M HCl in the absence and presence of different concentrations of [EMIM][ESO_4] inhibitor compound.

© University of Venda

The linear Tafel segments of the anodic and cathodic curves were extrapolated to obtain corrosion potential (E_{corr}), corrosion current density (i_{corr}), anodic and cathodic Tafel slopes (β_a and β_c, respectively). These parameters as well as the percentage inhibition ($\%IE_{PDP}$) calculated from Equation 30 are listed in the Table 4.1 below.

Table 4.1: Potentiodynamic polarization (PDP) parameters using different inhibitors.

Inhibitor	**Inhibitor conc. (M)**	**-E_{corr} (mV vs. Ag/AgCl)**	**i_{corr} (mA cm^{-2})**	**R_p (Ω cm^2)**	**b_a (mV dec^{-1})**	**b_c (mV dec^{-1})**	**%IE_{PDP}**
Blank	–	454	0.51	34.99	69	97	–
TDTB	1.0 × 10^{-2}	451	0.29	99.674	203	127	43.14
	2.0 × 10^{-2}	439	0.14	116.83	127	116	72.55
	4.0 × 10^{-2}	469	0.12	120.47	91	171	76.47
	6.0 × 10^{-2}	428	0.07	145.59	103	116	86.27
	8.0 × 10^{-2}	464	0.04	240.56	120	171	92.16
TDTM	1.0 × 10^{-2}	447	0.31	69.76	128	129	39.22
	2.0 × 10^{-2}	459	0.13	137.90	162	128	74.51
	4.0 × 10^{-2}	464	0.11	131.55	114	134	78.43
	6.0 × 10^{-2}	475	0.09	202.84	213	135	82.35
	8.0 × 10^{-2}	482	0.05	238.66	174	126	90.20
[EMIM][ESO_4]	1.0 × 10^{-2}	451	0.23	89.14	83	114	54.90
	2.0 × 10^{-2}	453	0.20	88.13	64	113	60.78
	4.0 × 10^{-2}	430	0.16	94.71	62	77	68.63
	6.0 × 10^{-2}	452	0.13	141.01	68	111	74.51
	8.0 × 10^{-2}	456	0.13	204.63	101	147	74.51

It is shown in Figures 4.1 – 4.3 that the polarization curves in the presence of the inhibitors are shifted towards regions of low current density relative to the uninhibited system. In all three inhibitor systems, a similar nature of polarization curves is observed which suggests that a similar inhibition mechanism is occurring. As reported in Table 4.1 there is no definite trend in the E_{corr} values of all the inhibitor systems. The displacement of these E_{corr} values relative to the E_{corr} values of the uninhibited system suggests that the inhibitors are mixed-type inhibitors (an anodic or cathodic inhibitor will have a shift in E_{corr} values greater than 85 mV; in this current study the maximum shift in E_{corr} is 28 mV) [66, 67]. These mixed-type inhibitors cause a reduction in the anodic dissolution of mild steel as well as a retardation of the hydrogen evolution reaction (i.e. cathodic reduction). The values of the Tafel slopes (β_a and β_c) can be used to further confirm the type of inhibition mechanism exhibited by the inhibitors in this study. Although the results in Table 4.1 show that there is no definite trend in the values of β_a and β_c with an increase in inhibitor concentration, a modification of the β_a and β_c values is observed to occur in the inhibited systems when compared to their uninhibited counterparts. For TDTB and [EMIM][ESO_4] inhibitors there are no significant differences between the changes in β_a and β_c values suggesting that the inhibitors have similar influence on both the

© University of Venda

anodic and cathodic reactions. Results for the inhibitor TDTM, however, show that changes in β_a are more significant than the changes in β_c. This indicates that while TDTM is a mixed-type inhibitor, it is predominantly anodic in nature since it has more influence on the anodic metal dissolution reaction.

4.1.2. Electrochemical impedance spectroscopy (EIS)

EIS measurements were used to investigate the anticorrosive behaviour of the ionic liquids on mild steel in 1.0 M HCl at 30°C after an exposure period of 30 minutes. The obtained Nyquist, and their corresponding Bode (phase angle and impedance modulus) plots are presented in Figures 4.4 – 4.9.

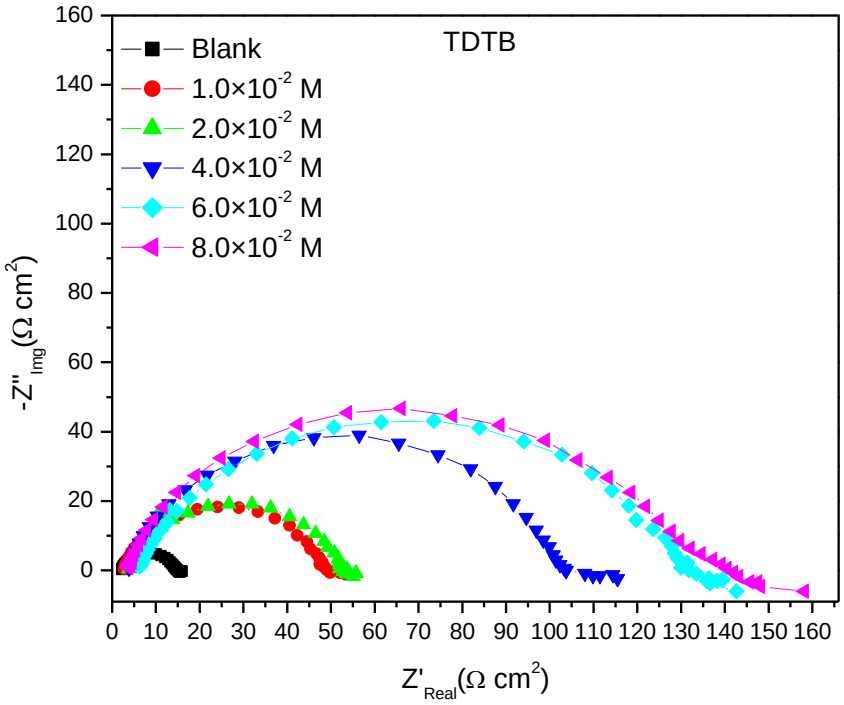

Figure 4.4: Nyquist plot of mild steel in 1.0 M HCl in the absence and presence of different concentrations of TDTB inhibitor compound.

© University of Venda

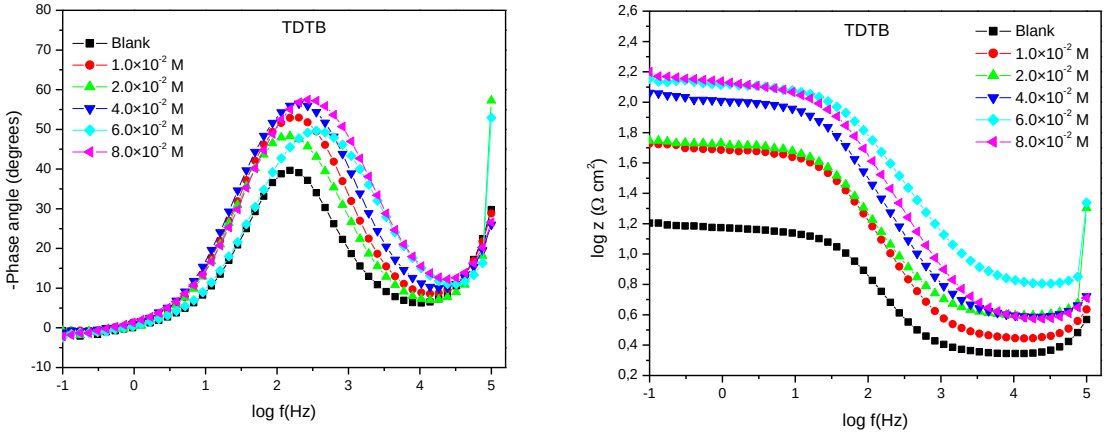

Figure 4.5: Bode plots of mild steel in 1.0 M HCl in the absence and presence of different concentrations of TDTB inhibitor compound.

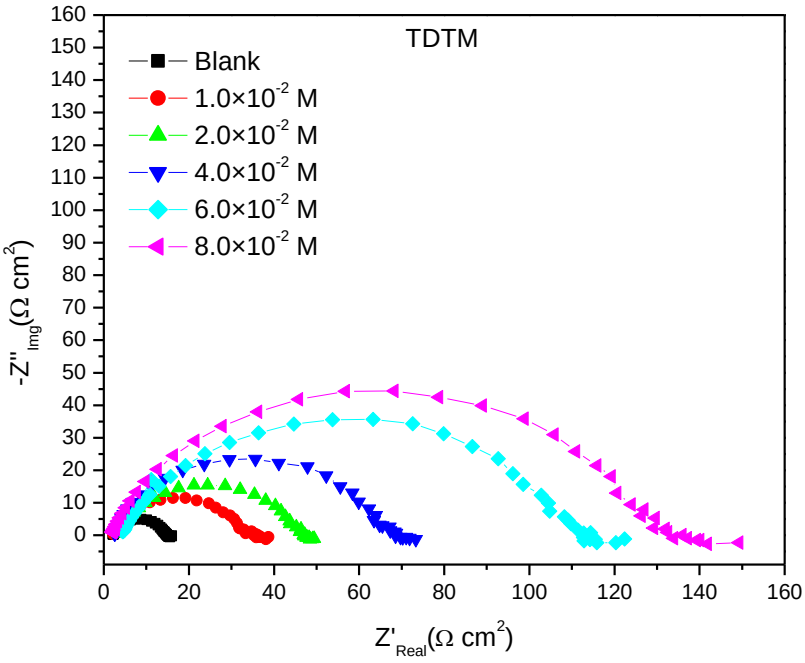

Figure 4.6: Nyquist plot of mild steel in 1.0 M HCl in the absence and presence of different concentrations of TDTM inhibitor compound.

© University of Venda

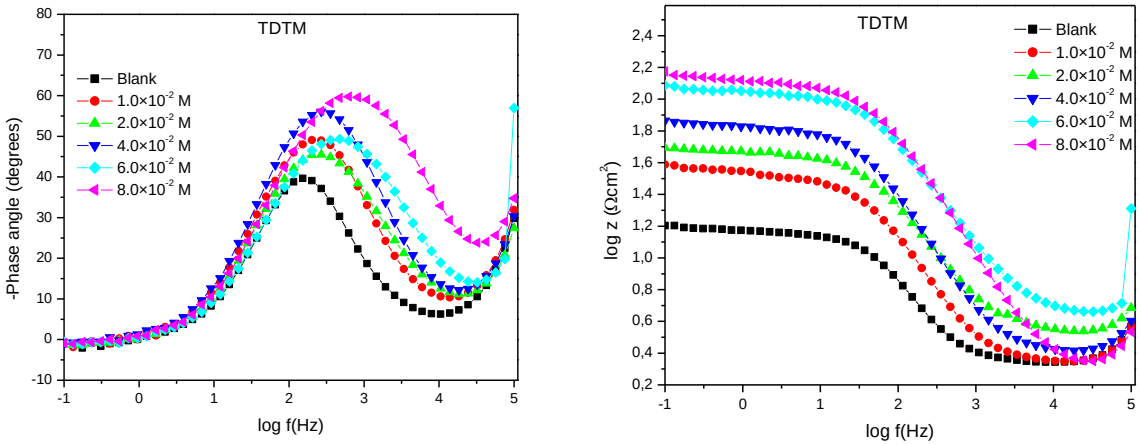

Figure 4.7: Bode plots of mild steel in 1.0 M HCl in the absence and presence of different concentrations of TDTM inhibitor compound.

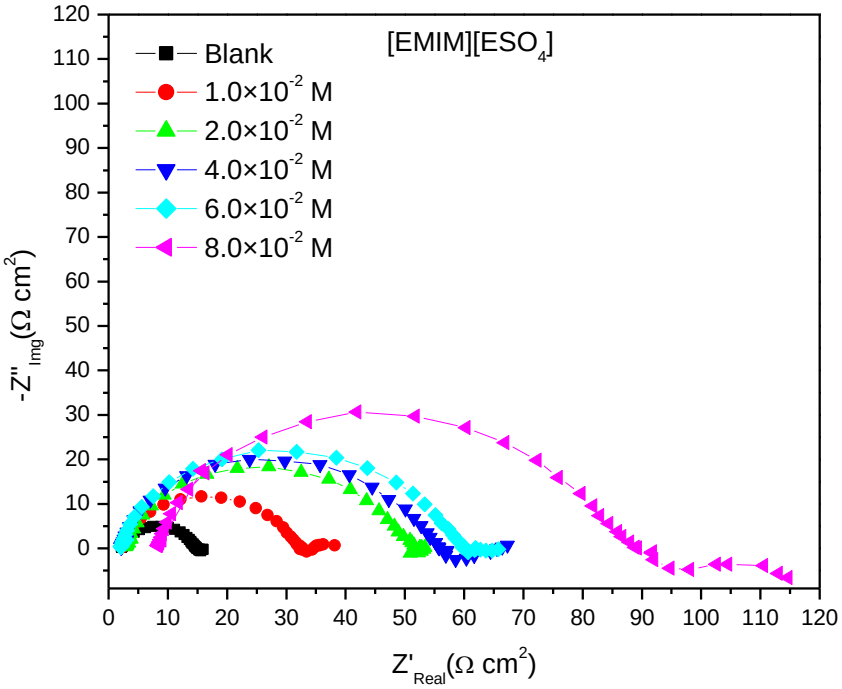

Figure 4.8: Nyquist plot of mild steel in 1.0 M HCl in the absence and presence of different concentrations of [EMIM][ESO_4] inhibitor compound.

© University of Venda

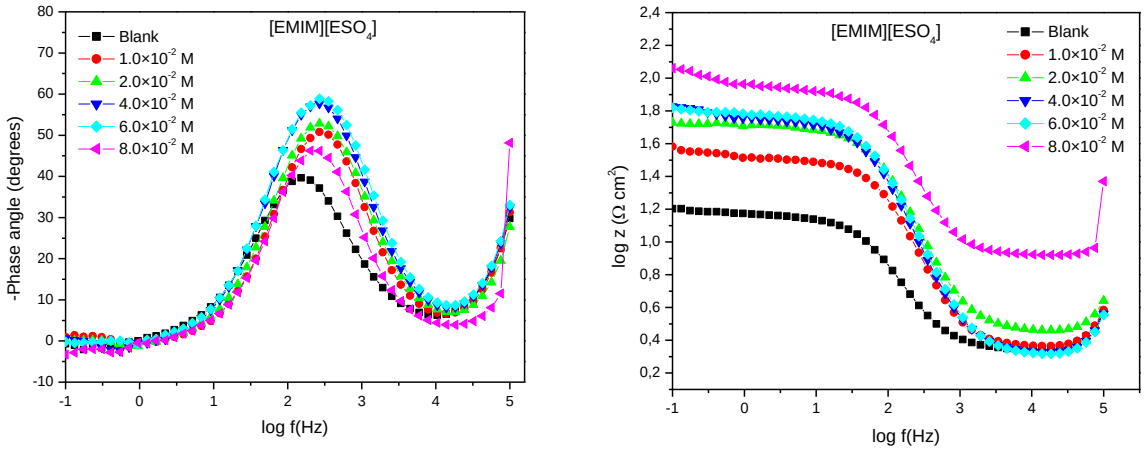

Figure 4.9: Bode plots of mild steel in 1.0 M HCl in the absence and presence of different concentrations of [EMIM][ESO_4] inhibitor compound.

The Nyquist plots showed both a depressed capacitive loop at high frequency and an inductive loop at low frequency. The high frequency capacitive loop is usually related to the charge-transfer and the double-layer capacitance while the low frequency inductive loop is related to the relaxation process of the adsorbed charged species [68]. The Nyquist plots have similar profiles which indicates that there is no change in corrosion mechanism with the addition of the inhibitor [69]. The depressed form in the high frequency capacitive loop is often referred to as frequency dispersion, and it arises due to solid surface roughness and inhomogeneities [70]. The capacitive loop increases in diameter with the increase in inhibitor concentration, this indicates the proportionality of the inhibition efficiency to the concentration of the inhibitor. The corrosion inhibition arises due to the formation of protective film on the mild steel surface [71]. The impedance parameters were determined by fitting the experimental results into a simple $R_s(R_{ct}CPE)$ equivalent circuit of the form in Figure 4.10. In this equivalent circuit, R_s is the solution resistance, *CPE* is the constant phase element and R_{ct} is the charge-transfer resistance. The *CPE* is a substitute for the capacitive element; its introduction is to ensure that a more accurate fit is obtained. The impedance function of *CPE* is defined by the expression:

$$Z_{CPE} = \frac{1}{Y_0(j\omega)^n} \tag{35}$$

where Y_0 is the *CPE* constant, ω is the angular frequency, j is imaginary number, and n is a *CPE* exponent which is used as a measure of the surface roughness or heterogeneity [72].

© University of Venda

Depending on the value of n, the *CPE* can represent resistance ($n = 0$, $Y_0 = R$), capacitance ($n = 1$, $Y_0 = C$), inductance ($n = -1$, $Y_0 = L$), or Warburg impedance ($n = 0.5$, $Y_0 = W$).

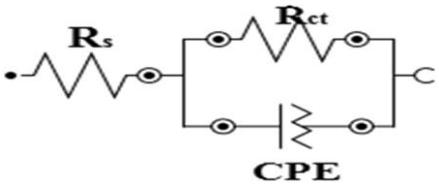

Figure 4.10: Equivalent circuit used diagram used to fit impedance spectra

The values of the electrochemical kinetic parameters for mild steel in 1.0 M HCl containing various concentrations of the studied ionic liquids are listed in Table 4.2. The inhibition efficiency ($\%IE_{EIS}$) was calculated using Equation 31. The values of the double layer capacitance (C_{dl}) were calculated from the charge-transfer resistance and *CPE* parameters, using Equation 36 below [73]:

$$C_{dl} = (Y_0 {R_{ct}}^{1-n})^{\frac{1}{n}} \quad (36)$$

The results in Table 4.2 reveal that an increase in the concentration of inhibitors causes an increase in the values of the charge-transfer resistance (R_{ct}) and the inhibition efficiency ($\%IE_{EIS}$) while the C_{dl} decrease with an increase in inhibitor concentration. The increase in R_{ct} is related to the increase in the surface coverage on the mild steel by the ionic liquids with an increase in inhibitor concentration [73]. The reduction in C_{dl} values can be attributed to the decrease in local dielectric constant and/or an increase in the thickness of the electrical double layer. This suggests that corrosion of mild steel is inhibited by adsorption of the ionic liquids at the mild steel / solution interface [74]. The values of n range from 0.88 to 0.78, this range is close to unity suggesting that the interface is of a capacitive nature. The results from the EIS measurements are comparable to a fair degree with those obtained from PDP.

© University of Venda

Table 4.2: Electrochemical parameters obtained from Nyquist and Bode plots of TDTB, TDTM and [EMIM][ESO_4].

Inhibitor	Inhibitor conc. (M)	R_s ($\Omega\ cm^2$)	R_{ct} ($\Omega\ cm^2$)	n	$(CPE)\ Y_0$ ($\times\ 10^6 s^n \Omega^{-1}\ cm^{-2}$)	C_{dl} ($\mu F cm^{-2}$)	%IE_{EIS}
Blank	-	2.25	12.70	0.88	508.00	247.15	-
TDTB	1.0×10^{-2}	2.81	46.50	0.88	203.93	105.47	72.69
	2.0×10^{-2}	3.95	49.40	0.86	209.40	98.88	74.29
	4.0×10^{-2}	3.84	101.00	0.56	114.00	56.46	87.43
	6.0×10^{-2}	6.11	126.00	0.81	754.40	24.59	89.92
	8.0×10^{-2}	3.65	133.00	0.84	898.30	38.89	90.45
TDTM	1.0×10^{-2}	2.21	32.40	0.83	317.00	127.43	60.80
	2.0×10^{-2}	3.36	44.00	0.79	248.00	76.81	71.13
	4.0×10^{-2}	2.56	64.80	0.85	150.00	67.07	80.40
	6.0×10^{-2}	4.27	108.00	0.78	99.10	28.18	88.24
	8.0×10^{-2}	1.92	130.00	0.82	74.90	26.36	90.23
[EMIM][ESO_4]	1.0×10^{-2}	2.35	30.60	0.87	456.00	243.57	58.49
	2.0×10^{-2}	2.93	48.30	0.87	333.00	175.76	73.71
	4.0×10^{-2}	2.16	55.00	0.87	388.00	216.15	76.91
	6.0×10^{-2}	2.10	57.9	0.87	343.00	194.95	78.07
	8.0×10^{-2}	8.34	83.50	0.86	197.00	99.27	84.79

4.1.3. Adsorption film analysis

FTIR is a useful technique which was used to investigate the possible chemical interaction between mild steel and the inhibitors [75]. The interaction was confirmed using FTIR spectra of the corrosion inhibitors as well as the adsorption formed on the mild steel surface when the metal is exposed to different inhibitors as shown in Figures 4.11 – 4.13.

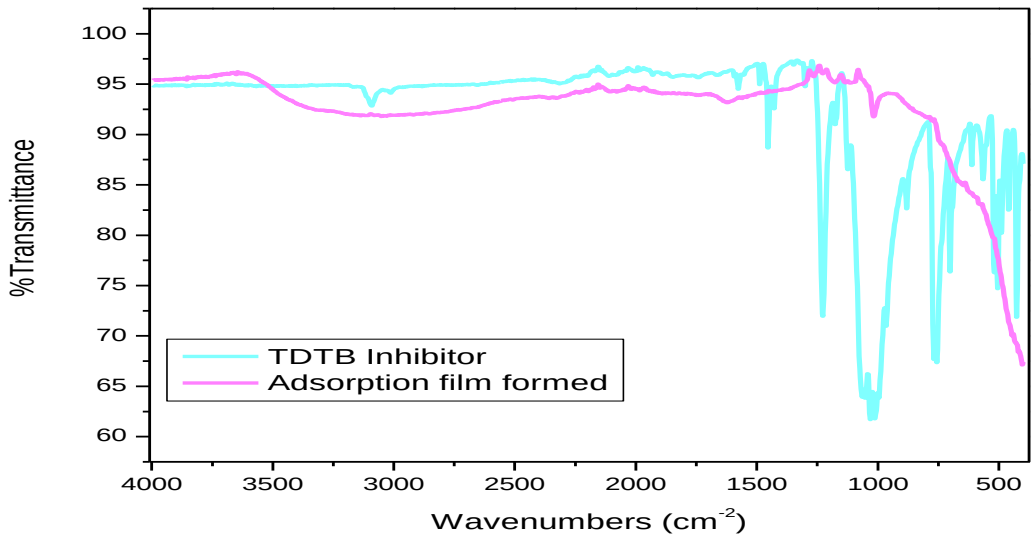

Figure 4.11: FTIR spectra of pure TDTB and the adsorption film formed on mild steel in the presence of the inhibitor TDTB.

© University of Venda

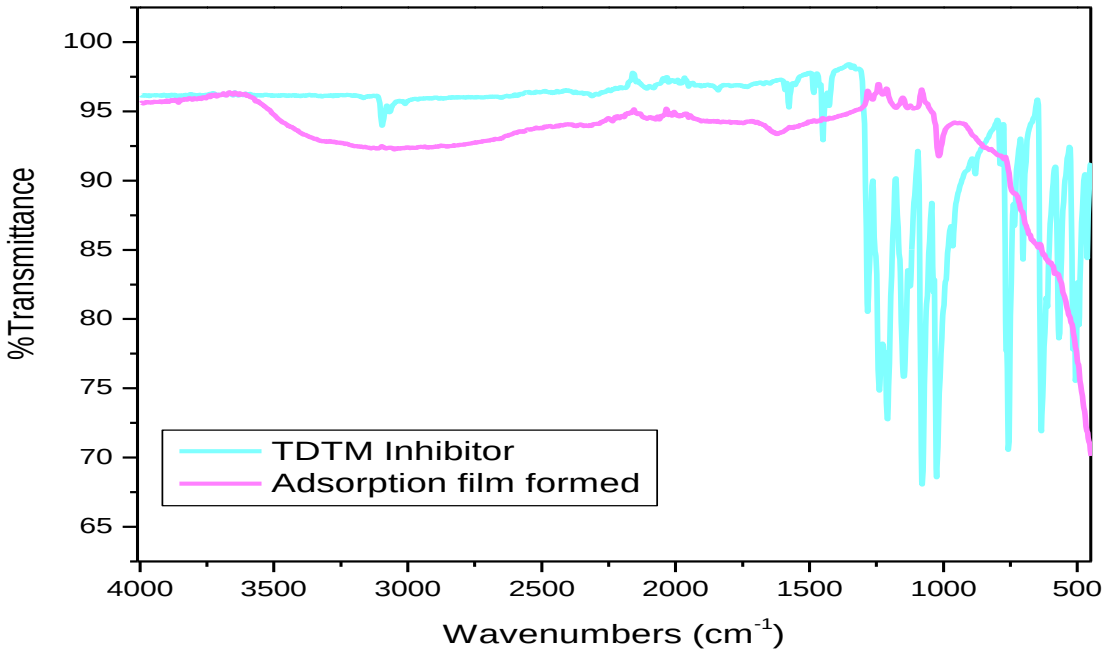

Figure 4.12: FTIR spectra of pure TDTM and the adsorption film formed on mild steel in the presence of the inhibitor TDTM.

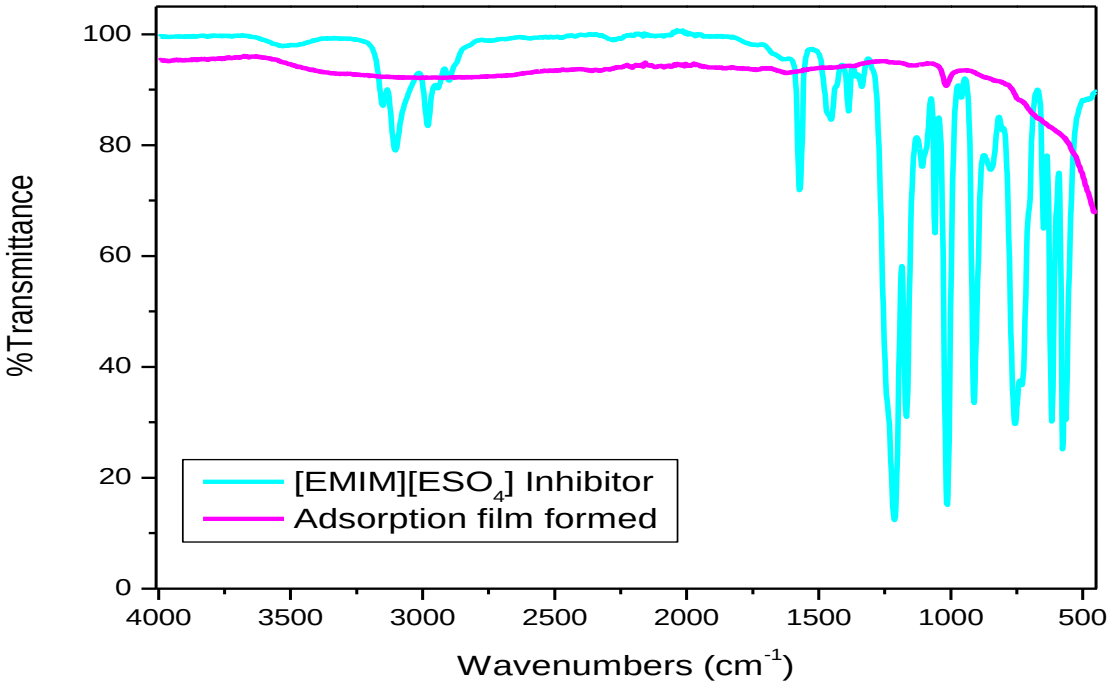

Figure 4.13: FTIR spectra of pure [EMIM][ESO_4] and the adsorption film formed on mild steel in the presence of the inhibitor [EMIM][ESO_4].

© University of Venda

Both TDTB and TDTM show similar features due to the identical cation they posses. The benzene rings in TDTB and TDTM represent regions of high electron density while in [EMIM][ESO_4], a region of electron density is represented by the imidazole ring. Chemical interaction is therefore likely to occur between these electron rich regions and the vacant d-orbitals of the mild steel [76]. Table 4.3 gives the IR peak assignments for some of the spectral bands observed in Figures 4.11 – 4.13. For TDTB and TDTM, the C-H stretch of the aromatic rings is observed at 3105 cm^{-1} and 3103 cm^{-1}, respectively. [EMIM][ESO_4] has peaks corresponding to the C-H stretch of the imidazole ring appearing at 3157 cm^{-1} and 3103 cm^{-1}. Bands of methylene (-CH_2) stretching are also observed at 2984 cm^{-1} and 2897 cm^{-1} in [EMIM][ESO_4] [75]. The bands corresponding to C=N stretching in [EMIM][ESO_4] are observed at 1577 cm^{-1}. Stretching freqencies for C=C were observed at 1459 cm^{-1}, 1457 cm^{-1} and 1468 cm^{-1} for TDTB, TDTM and [EMIM][ESO_4], respectively [64]. [EMIM][ESO_4] also shows bands corresponding to C-N stretching at 1219 cm^{-1}. Bands corresponding to O=S=O are observed in TDTM and [EMIM][ESO_4] at 1155 cm^{-1} and 1165 cm^{-1}, respectively [77].

There is a significant difference between the FTIR spectra of the pure inhibitors and the resulting adsorption film formed on the mild steel surface in the presence of the different inhibitors. The adsorption film spectra show a disappearance of all the prominant bands which were observed in the pure ILs. This indicates that some chemical interactions have occured between the mild steel and ILs.

Table 4.3: Peaks and their identification from FTIR spectra of the studied corrosion inhibitors.

Functional groups	**Peaks from FTIR spectra (cm^{-1})**		
	TDTB	**TDTM**	**[EMIM][ESO_4]**
Aromatic C-H	3105	3103	3157, 3103
Aliphatic C-H	–	–	2984, 2897
C=N	–	–	1577
C=C	1459	1457	1468
CF_3	–	1295	1338
C-N	–	–	1219
O=S=O	–	1155	1165
S-O	–	754	754

© University of Venda

4.1.4. Surface analysis

Scanning electron microscopy (SEM) is a useful technique which was used to study the surface morphology of the uncorroded and corroded mild steel specimens after they were immersed in 1.0 M HCl in the absence and presence of 8.0×10^{-2} M of the studied ILs. The SEM micrographs and the corresponding energy dispersive spectroscopy (EDS) spectra are shown in Figures 4.14 – 4.18 and Figures 4.19 – 4.23, respectively.

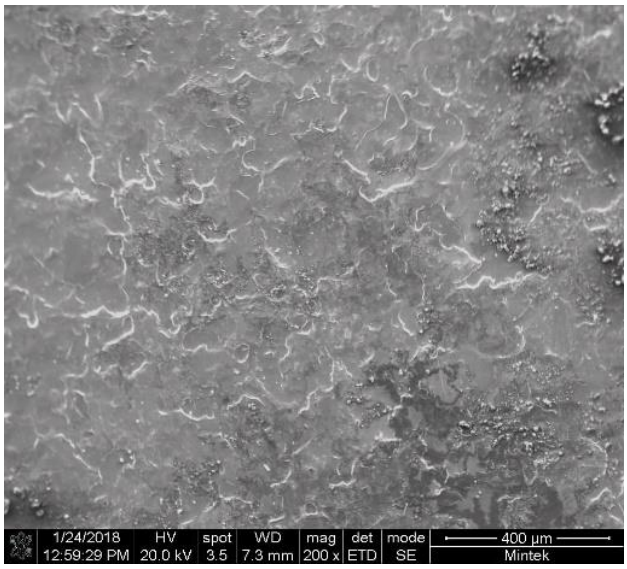

Figure 4.14: SEM micrograph of mild steel before exposure to 1.0 M HCl

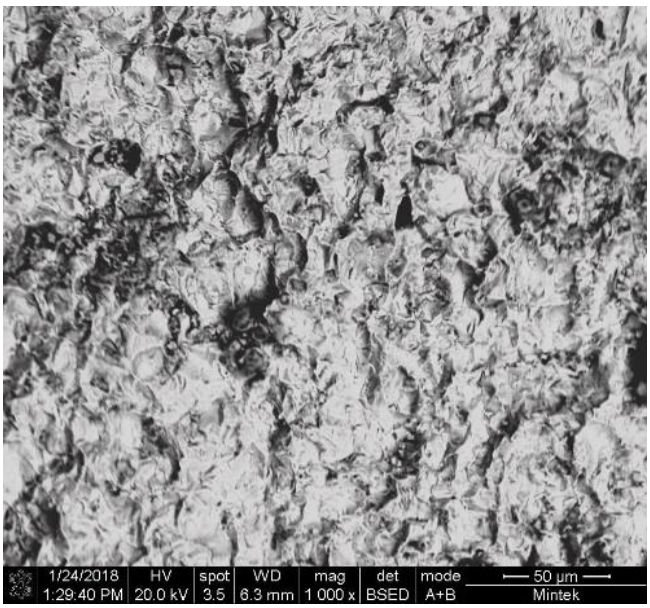

Figure 4.15: SEM micrograph of the surface of mild steel immersed in 1.0 M HCl uninhibited

© University of Venda

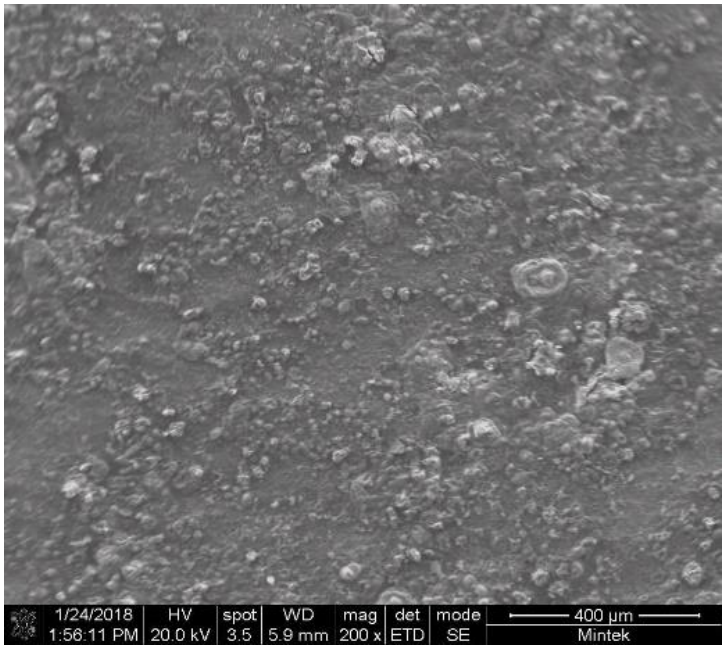

Figure 4.16: SEM micrograph of the surface of mild steel immersed in 1.0 M HCl in the presence of TDTB corrosion inhibitor.

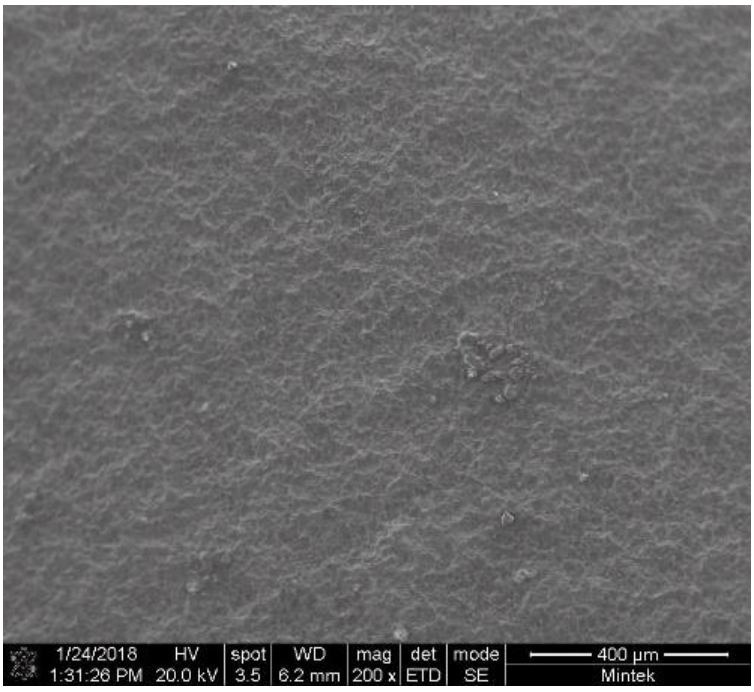

Figure 4.17: SEM micrograph of the surface of mild steel immersed in 1.0 M HCl in the presence of TDTM corrosion inhibitor.

© University of Venda

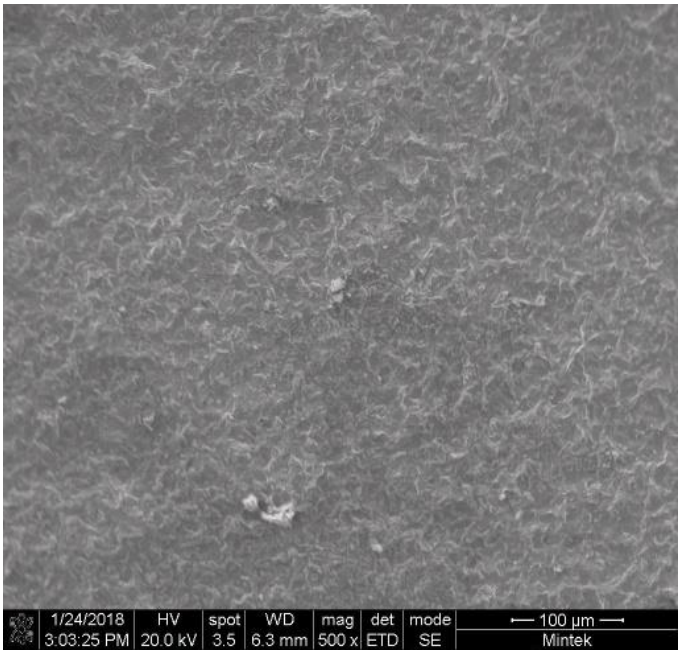

Figure 4.18: SEM micrograph of the surface of mild steel immersed in 1.0 M HCl in the presence of [EMIM][ESO_4] corrosion inhibitor.

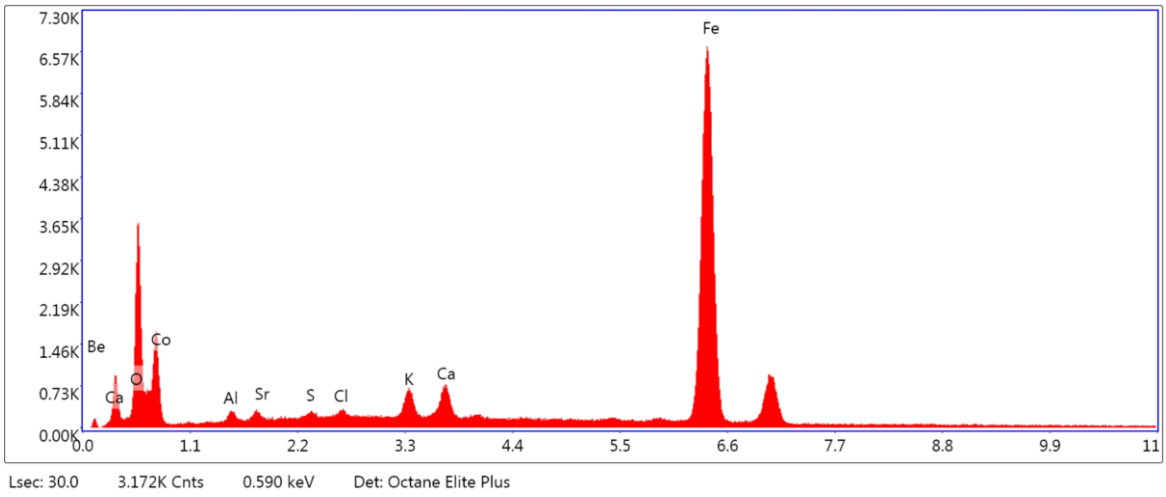

Figure 4.19: EDS spectrum of mild steel before exposure to 1.0 M HCl

© University of Venda

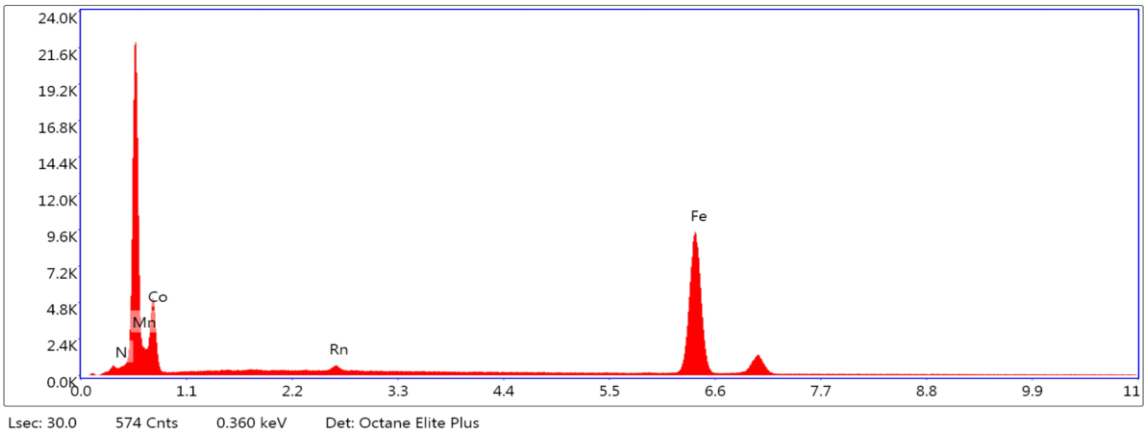

Figure 4.20: EDS spectrum of mild steel immersed in 1.0 M HCl uninhibited.

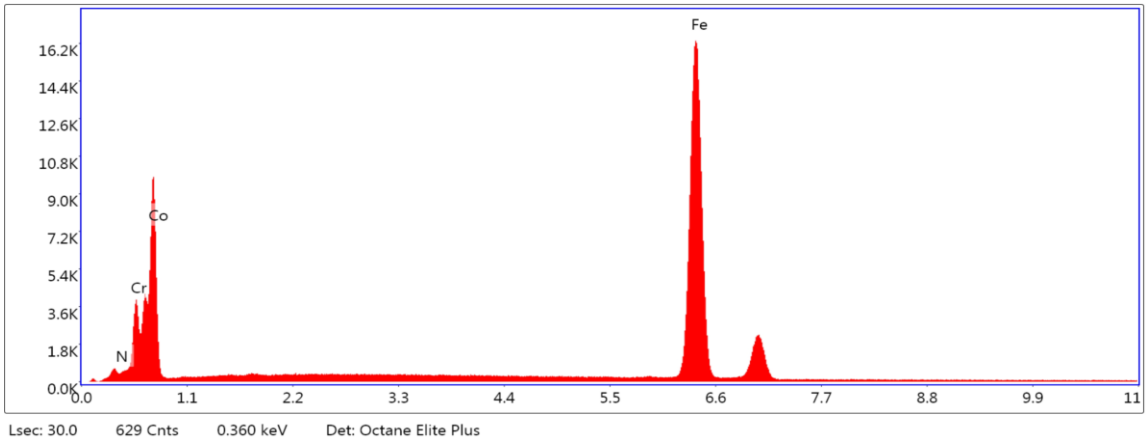

Figure 4.21: EDS spectrum of mild steel immersed in 1.0 M HCl in the presence of TDTB corrosion inhibitor.

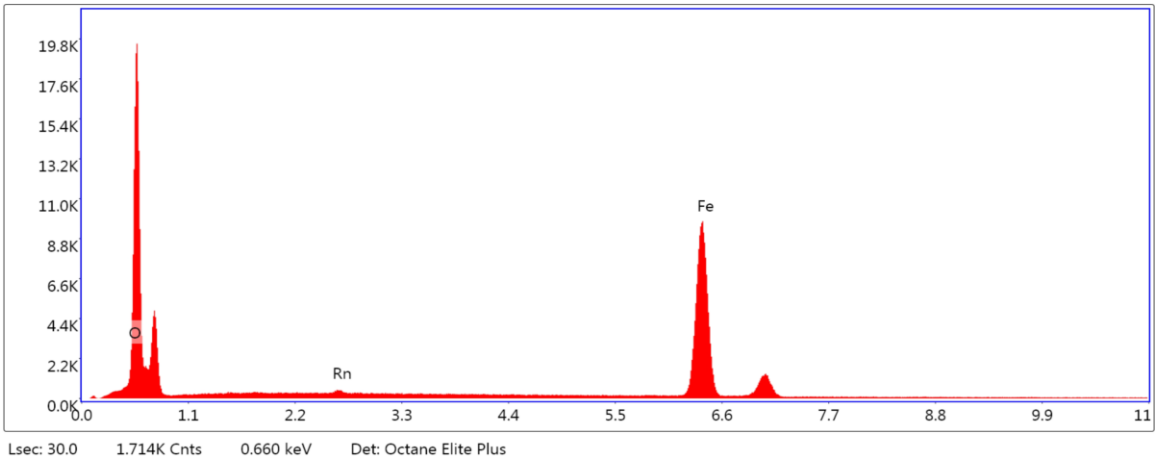

Figure 4.22: EDS spectrum of mild steel immersed in 1.0 M HCl in the presence of TDTM corrosion inhibitor.

© University of Venda

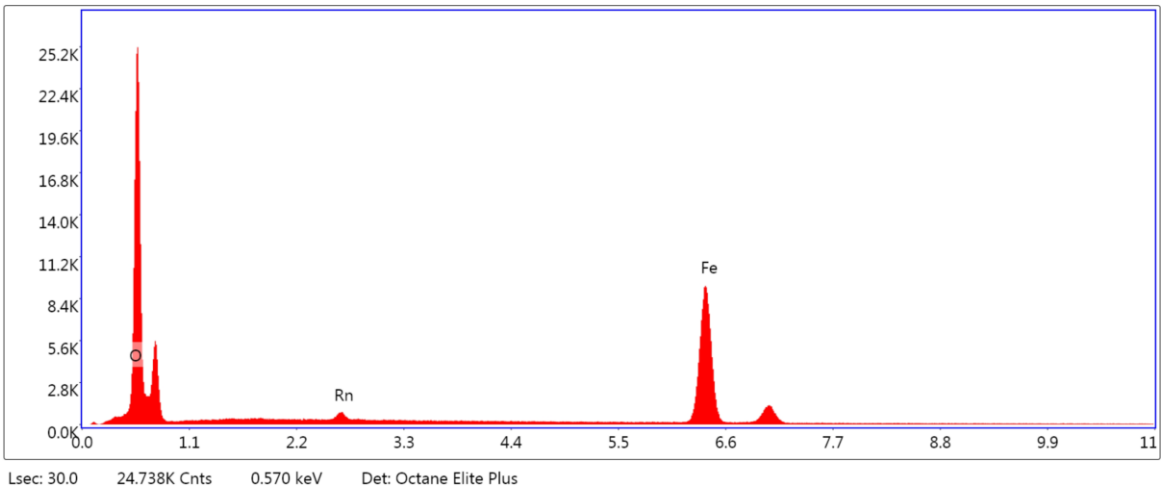

Figure 4.23: EDS spectrum of mild steel immersed in 1.0 M HCl in the presence of [EMIM][ESO_4] corrosion inhibitor.

Figure 4.14 shows the characteristic surface of mild steel prior to immersion in 1.0 M HCl, besides the minor damages which may have resulted during the polishing process, the surface appears smooth and uniform. Figure 4.15 shows a highly damaged surface full of cavities due to the corrosive attack of 1.0 M HCl solution. In the presence of the studied ILs, the damage on the mild steel surface (Figures 4.16 – 4.18) was observed to be relatively less than in the uninhibited mild steel surface. This implies that the inhibitors adsorb on to the surface of the metal resulting in the formation of a protective film which reduces the contact between the mild steel and the aggressive medium.

The corresponding EDS spectra were used to further analyse the surface of the mild steel specimens. The spectra are shown in Figures 4.19 – 4.23. The data for the plain mild steel (i.e. before exposure to 1.0 M HCl) shows that Fe is the major constituent of mild steel with other elements such as K, Ca, S, etc. present as minor constituents. The data also reveals the presence of Cl which is present in minor amounts (0.17 wt%). This might be due to contamination of the surface during the sample preparation process. The EDS spectrum for mild steel in uninhibited HCl shows a pronounced Mn peak, with the presence of Rn in minor amounts. There is a disappearance of most of the elemental peaks which were present in the plain mild steel. The data for mild steel immersed in TDTM and [EMIM][ESO_4] shows pronounced oxygen peaks. The amount of oxygen in MS-TDTM and MS-[EMIM][ESO_4] spectra, is 23.05 wt% and 21.56 wt%, respectively. The presence of oxygen could be due to the adsorption of the anions of these ILs which contain oxygen, hence forming a protective layer. The MS-TDTB does not show any peaks which could be responsible for protective layer formation. Further information in this regard may be revealed by quantum chemical studies

© University of Venda

which provide deeper insight into the possible functional groups from the inhibitor molecules that may interact with the surface of the metals.

4.1.5. Effect of inhibitor concentration on inhibitory behaviour for mild steel

The variations of the inhibition efficiencies with inhibitor concentration are represented in Figures 4.24 – 4.26 and Table 4.4. It can be noted that for all inhibitors at all temperatures the inhibition efficiency increases with an increase in concentration of inhibitor molecules. For all the inhibitors, the highest inhibition efficiency is observed at the highest concentration i.e. 8.0 × 10^{-2} M for TDTB, TDTM and [EMIM][ESO_4]. With an increase in inhibitor concentration, there is a greater tendency of adsorption of more inhibitor molecules at the metal / solution interface which results in higher %IE.

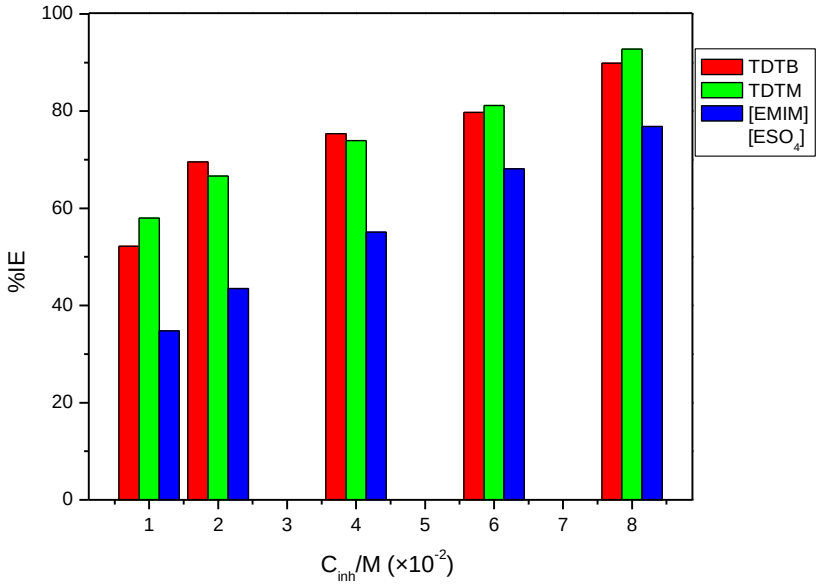

Figure 4.24: Variations of the weight loss percentage inhibition efficiencies (%IE) with various concentrations of the utilized corrosion inhibitors at 30°C.

© University of Venda

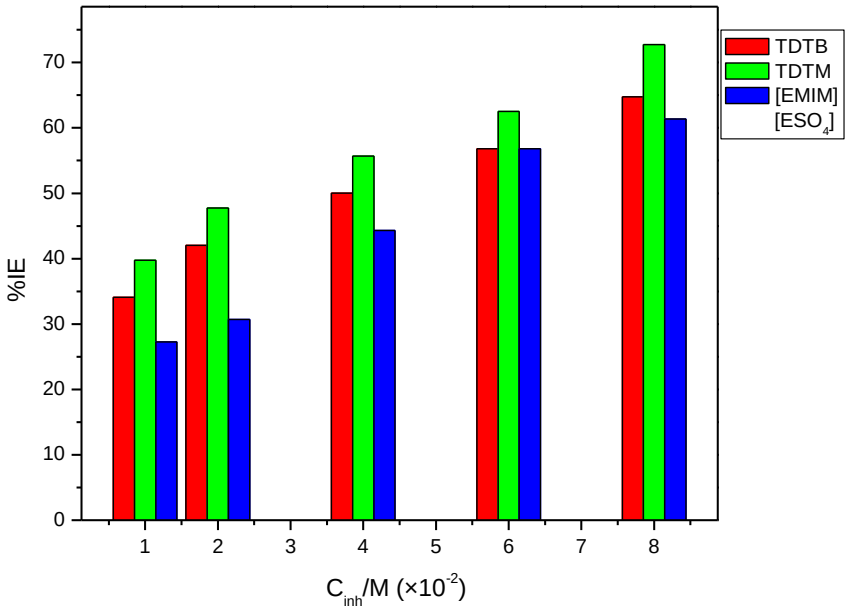

Figure 4.25: Variations of the weight loss percentage inhibition efficiencies (%IE) with various concentrations of the utilized corrosion inhibitors at 40°C.

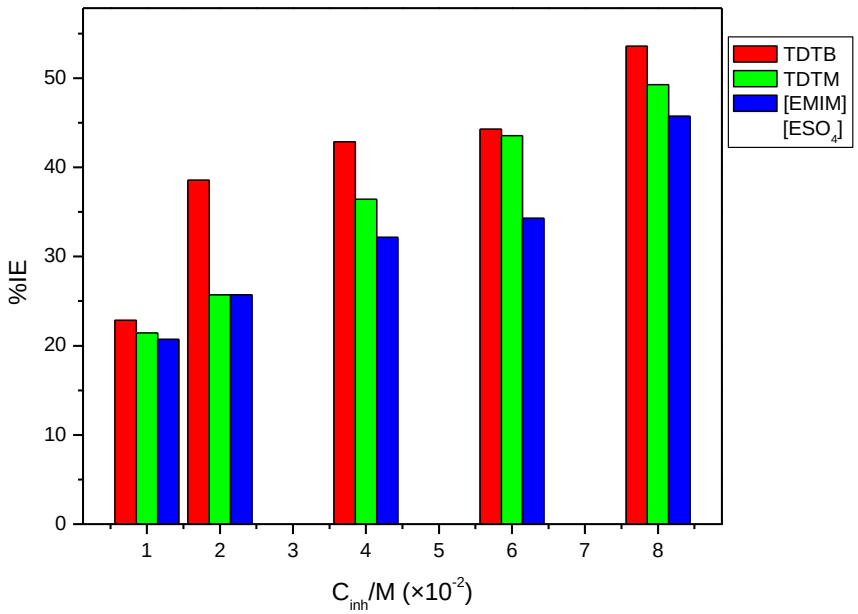

Figure 4.26: Variations of the weight loss percentage inhibition efficiencies (%IE) with various concentrations of the utilized corrosion inhibitors at 50°C.

© University of Venda

At 30°C, similar trends in inhibition efficiency with an increase in concentration are observed for all the inhibitors. TDTB and TDTM are observed to have similar inhibition efficiencies, which could imply that the difference in anions does not affect the adsorption behaviour of the ILs. The variations with concentration are illustrated in Figures 4.24 – 4.26. With an increase in temperature, the inhibition efficiencies of all three inhibitors are observed to decrease. For instance, the inhibitor TDTM with an inhibition efficiency of 92.75% at 30°C has an inhibition efficiency of 72.72% at 40°C. [EMIM][ESO_4] which has an inhibition efficiency of 76.81% at 30°C has an inhibition efficiency of 61.36% at 40°C.

Inhibition efficiencies decrease further with an increase in temperature to 50°C. A similar behaviour, i.e. decrease of inhibition efficiency with increase in temperature was reported by Alkhathlan et al [45]. This behaviour was attributed to the equilibrium which exists between adsorption and desorption processes that occur spontaneously on the metal surface. It was reported that with an increase in temperature, the equilibrium between adsorption and desorption shifts towards desorption until a new equilibrium is reached. Shifting of the equilibrium towards desorption means that less inhibitor molecules cover the metal surface hence resulting in lower %IE at higher temperatures [45].

Table 4.4: Percentage inhibition efficiencies and corrosion rate values obtained from the weight loss of mild steel in 1.0 M HCl in the absence and presence of various concentrations of inhibitors.

Inhibitor	**Inhibitor conc. (M)**	**Temperature**					
		30°C		**40°C**		**50°C**	
		%IE_{WL}	**C_R (g cm^{-2} h^{-1})**	**%IE_{WL}**	**C_R (g cm^{-2} h^{-1})**	**%IE_{WL}**	**C_R (g cm^{-2} h^{-1})**
Blank	0.0	–	0.0069	–	0.0088	–	0.0140
TDTB	1.0×10^{-2}	52.17	0.0033	34.09	0.0058	22.86	0.0108
	2.0×10^{-2}	69.56	0.0021	42.05	0.0051	38.57	0.0086
	4.0×10^{-2}	75.36	0.0017	50.01	0.0044	42.86	0.0080
	6.0×10^{-2}	79.71	0.0014	56.82	0.0038	44.29	0.0078
	8.0×10^{-2}	89.85	0.0007	64.77	0.0031	53.57	0.0065
TDTM	1.0×10^{-2}	57.97	0.0029	39.77	0.0053	21.43	0.0110
	2.0×10^{-2}	66.67	0.0023	47.73	0.0046	25.71	0.0104
	4.0×10^{-2}	73.91	0.0018	55.68	0.0039	36.42	0.0089
	6.0×10^{-2}	81.16	0.0013	62.50	0.0033	43.57	0.0079
	8.0×10^{-2}	92.75	0.0005	72.72	0.0024	49.29	0.0071
[EMIM][ESO_4]	1.0×10^{-2}	34.78	0.0045	27.27	0.0064	20.71	0.0111
	2.0×10^{-2}	43.48	0.0039	30.68	0.0061	25.71	0.0104
	4.0×10^{-2}	55.07	0.0031	44.32	0.0049	32.14	0.0095
	6.0×10^{-2}	68.12	0.0022	56.82	0.0038	34.29	0.0092
	8.0×10^{-2}	76.81	0.0016	61.36	0.0034	45.71	0.0076

© University of Venda

4.1.6. Effect of temperature and kinetic parameters

The interaction between the metal and the acidic media can be modified by temperature of the environment. Generally, the corrosion rate increases with an increase in temperature. Temperature variation can therefore be used to obtain information regarding the mode of adsorption of the inhibitor molecules on the metal surface [78]. The dependence of the corrosion rate can be evaluated by the Arrhenius equation (Equation 37) and transition state equation (Equation 38) as follows:

$$\text{Log}\, C_R = \log A - \frac{E_a}{2.303RT} \tag{37}$$

$$C_R = \frac{RT}{Nh}\exp\left(\frac{\Delta S^*}{R}\right)\exp\left(-\frac{\Delta H^*}{RT}\right) \tag{38}$$

where, C_R is the corrosion rate (in gcm^{-2}hr^{-1}). E_a is the apparent activation energy, A is the pre-exponential factor, R is the universal gas constant, T is the absolute temperature, ΔS^* is the entropy of activation, ΔH^* is the enthalpy of activation, N is the Avogadro's number (6.02252 × 10^{23} mol^{-1}) and h is the Plank's constant (6.626176 × 10^{-34} Js). Arrhenius and transition state plots for mild steel corrosion in 1.0 M HCl in the absence and presence of the three ILs are given in Figures 4.27 – 4.32 and the corresponding activation parameters (E_a, ΔH^* and ΔS^*) are listed in Table 4.5.

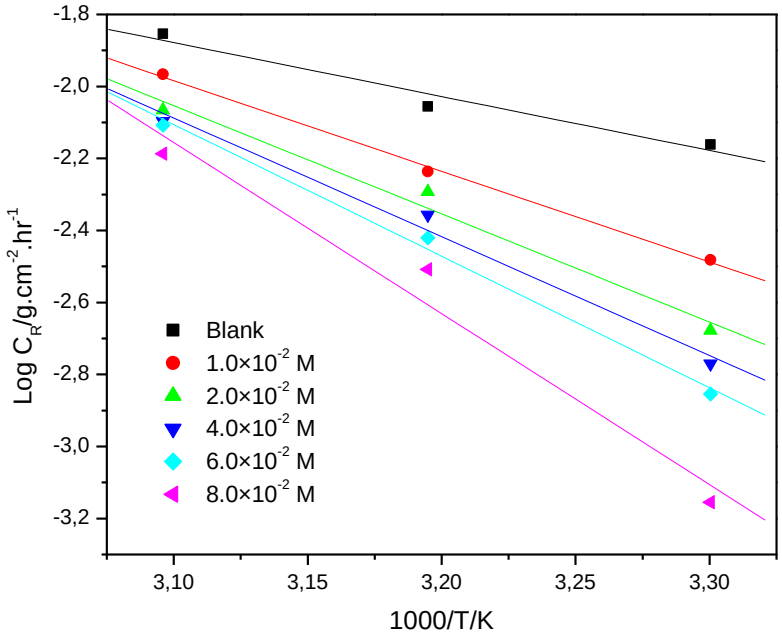

Figure 4.27: Arrhenius plots for the corrosion of mild steel in 1.0 M HCl in the absence and presence of various concentrations of TDTB corrosion inhibitor.

© University of Venda

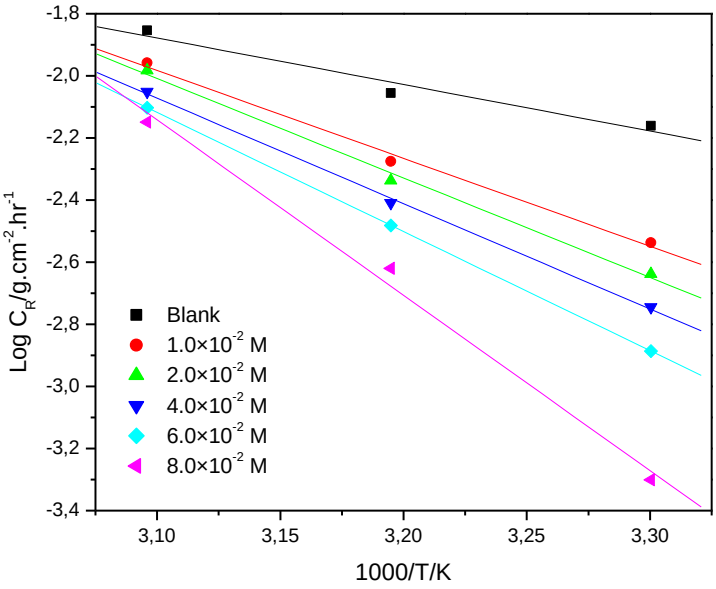

Figure 4.28: Arrhenius plots for the corrosion of mild steel in 1.0 M HCl in the absence and presence of various concentrations of TDTM corrosion inhibitor.

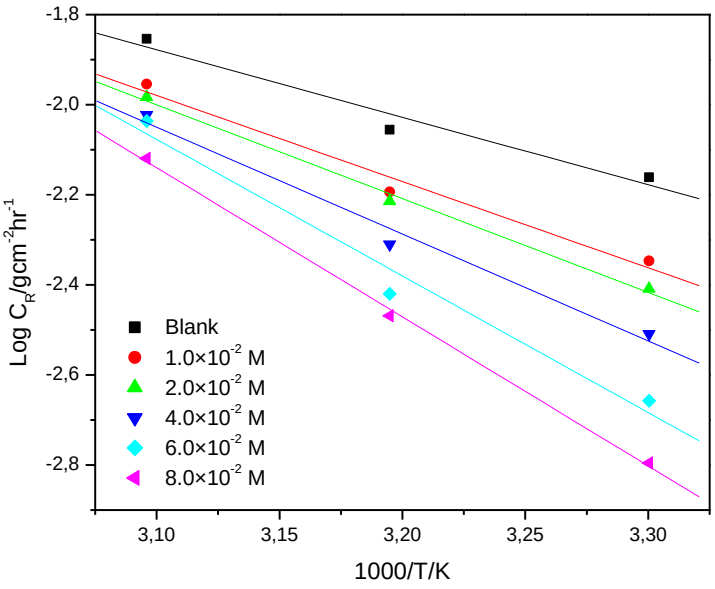

Figure 4.29: Arrhenius plots for the corrosion of mild steel in 1.0 M HCl in the absence and presence of various concentrations of [EMIM][ESO_4] corrosion inhibitor.

© University of Venda

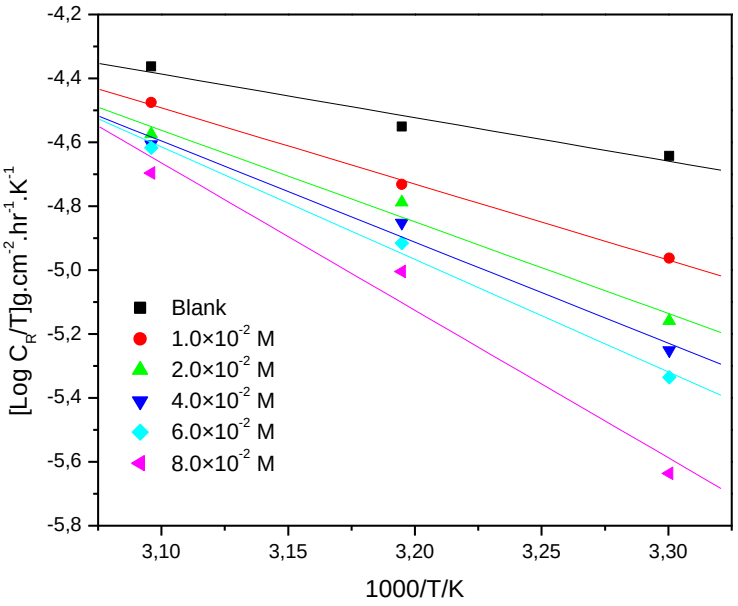

Figure 4.30: Transition state plots for the corrosion of mild steel in 1.0 M HCl in the absence and presence of various concentrations of TDTB corrosion inhibitor.

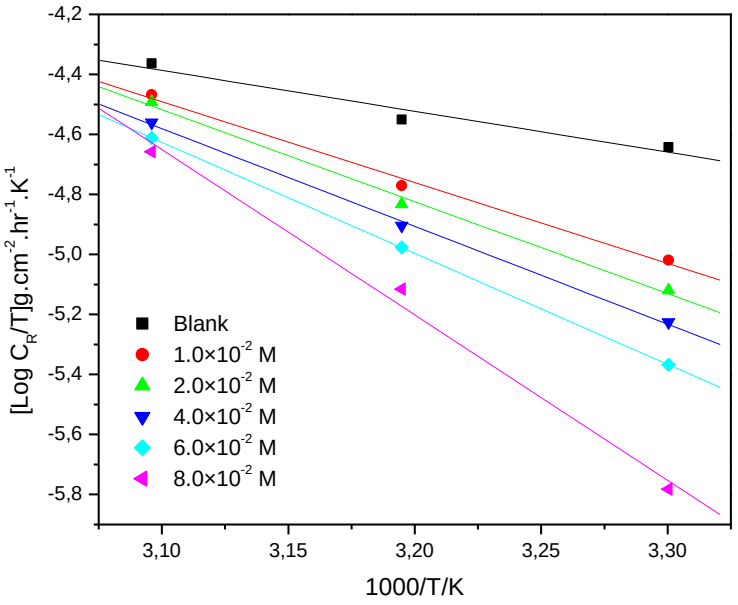

Figure 4.31: Transition state plots for the corrosion of mild steel in 1.0 M HCl in the absence and presence of various concentrations of TDTM corrosion inhibitor.

© University of Venda

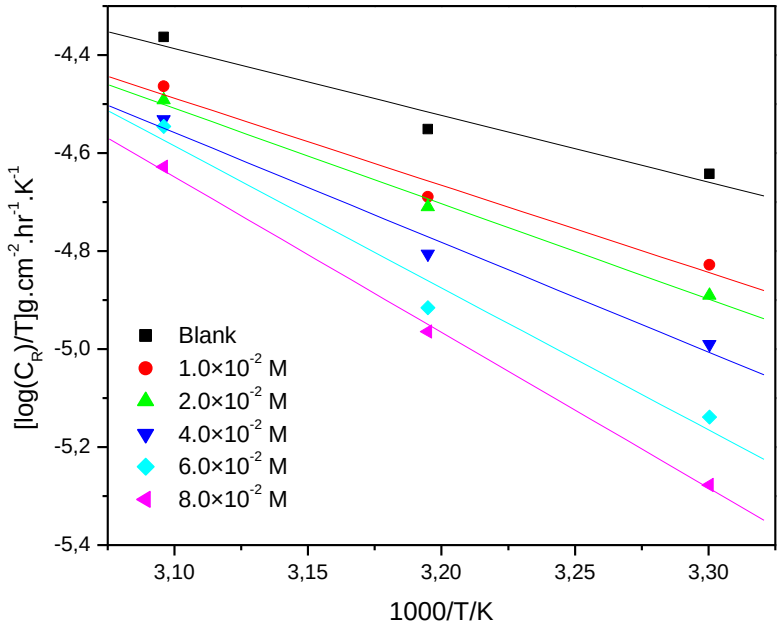

Figure 4.32: Transition state plots for the corrosion of mild steel in 1.0 M HCl in the absence and presence of various concentrations of [EMIM][ESO_4] corrosion inhibitor.

Table 4.5: Activation parameters derived from Arrhenius and transition state plots.

Inhibitor	Inhibitor Conc. (M)	Activation Energy E_a (kJ mol^{-1})	Enthalpy of Activation ΔH^* (kJ mol^{-1})	Entropy of Activation ΔS^* ($JK^{-1}mol^{-1}$)
Blank	0.0	28.69	26.08	-200.70
TDTB	1.0×10^{-2}	48.20	45.60	-142.22
	2.0×10^{-2}	57.51	56.91	-114.72
	4.0×10^{-2}	63.16	60.55	-97.86
	6.0×10^{-2}	69.99	67.39	-77.02
	8.0×10^{-2}	90.97	88.37	-12.93
TDTM	1.0×10^{-2}	54.18	51.58	-123.69
	2.0×10^{-2}	61.33	58.72	-102.02
	4.0×10^{-2}	64.99	62.39	-91.87
	6.0×10^{-2}	73.43	70.83	-66.59
	8.0×10^{-2}	108.14	105.54	40
[EMIM][ESO4]	1.0×10^{-2}	36.64	34.04	-177.98
	2.0×10^{-2}	39.86	37.26	-168.40
	4.0×10^{-2}	45.47	42.87	-151.97
	6.0×10^{-2}	58.05	55.45	-113.47
	8.0×10^{-2}	63.36	60.76	-98.23

© University of Venda

The results in Table 4.5 show that the values of E_a for inhibited systems are higher than those of the uninhibited system. The increase in E_a in the presence of the ILs is usually attributed to the formation of an adsorption film which forms by the physical adsorption of inhibitor molecules, this film results in an increase in the energy barrier for the corrosion process [79, 80]. The results showed a positive sign for E_a and ΔH^* values, this reflects the endothermic nature of the mild steel corrosion process, suggesting that the dissolution process is difficult [81].

The entropy of activation values is almost all negative for the uninhibited and inhibited systems. This indicates that the activated complex in the rate determining step involves association rather than dissociation meaning that there is a reduction in disorder in going from the reactants to the activated complex [82].

4.1.7. Thermodynamic parameters: Adsorption isotherms

Adsorption isotherms provide information on the interaction between the inhibitor molecules and mild steel surface. In order to obtain this information, the weight-loss results were fitted into various adsorption isotherms. The best description of the adsorption behaviour was found in the Langmuir adsorption isotherm, this is confirmed by the values of the regression coefficients (r^2). The values of r^2 and slopes are reported in Table 4.6.

Table 4.6: Langmuir adsorption parameters for the corrosion of mild steel in 1.0 M HCl at various temperatures in the presence of TDTB, TDTM and [EMIM][ESO_4].

Inhibitor	Temperature (°C)	r^2	Slope	K_{ads} (M^{-1})	ΔG^0_{ads} (kJ mol^{-1})
TDTB	30	0.991	1.032	103.08	-21.80
	40	0.985	1.356	49.44	-20.60
	50	0.974	1.642	38.79	-20.61
TDTM	30	0.984	1.002	97.98	-21.67
	40	0.979	1.231	57.90	-20.34
	50	0.978	1.592	33.34	-18.95
[EMIM][ESO4]	30	0.975	1.057	42.00	-19.56
	40	0.963	1.240	30.00	-19.29
	50	0.930	1.919	26.00	-19.49

The Langmuir isotherm gives a direct relationship between the concentration of inhibitor and the degree of adsorption i.e. surface coverage of inhibitor molecules on the mild steel surface, according to Equation 39:

$$\frac{\theta}{1-\theta} = K_{ads}\, C_{inh} \qquad (39)$$

© University of Venda

where K_{ads} is the equilibrium constant of adsorption process, C_{inh} is the molar concentration of the inhibitor used in acid solution and θ is the degree of surface coverage.

The equation can be rearranged to:

$$\frac{C_{inh}}{\theta} = \frac{1}{K_{ads}} + C_{inh} \quad (40)$$

The Langmuir adsorption isotherm plots for TDTB, TDTM and [EMIM][ESO_4] at the various temperatures are shown in Figures 4.33 – 4.35. From the intercept of the Langmuir plots, the values of K_{ads} can be calculated and related to the Gibbs free energy of adsorption in the following equation:

$$K_{ads} = \frac{1}{55.5}\exp\left(-\frac{\Delta G^{\circ}_{ads}}{RT}\right) \quad (41)$$

Equation 41 can also be expressed as:

$$\Delta G^{\circ}_{ads} = -RT\ ln(55.5K_{ads}) \quad (42)$$

where ΔG°_{ads} is the Gibbs free energy of adsorption, the value 55.5 is the molar concentration of water in solution and T is the temperature in Kelvin.

The values of ΔG°_{ads} for the ILs are listed in Table 4.6. The negative sign of these values indicates spontaneity of the adsorption process and the stability of the adsorbed layer on the mild steel surface [83, 84]. Generally, values of ΔG°_{ads} around -20 kJ mol^{-1} or less negative are consistent with electrostatic interaction between the charged inhibitor molecules and the charged metal surface while those more negative than -40 kJ mol^{-1} are consistent with chemisorption where charge sharing or transfer from the inhibitor molecule to the metal surface occurs to form a coordinate type of bond [83]. In this study, ΔG°_{ads} values are around -20 kJ mol^{-1}; this indicates that the inhibitors are physically adsorbed on the mild steel surface.

© University of Venda

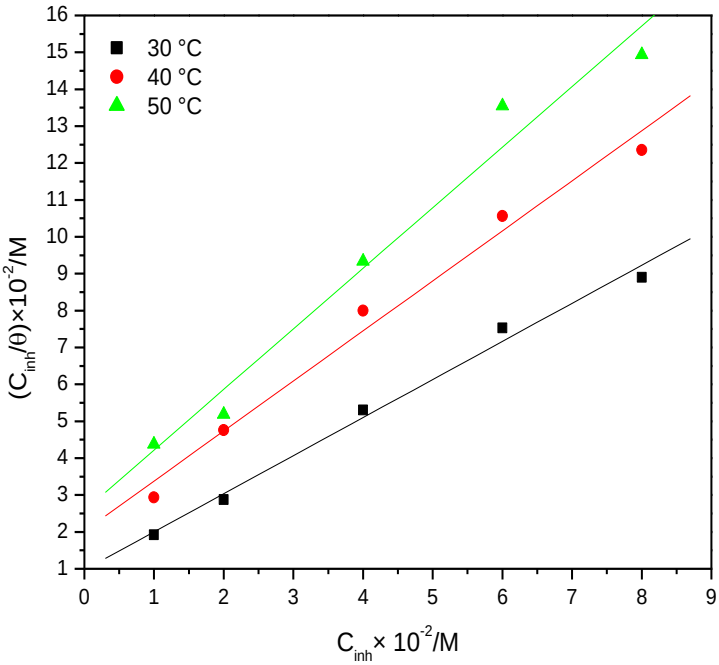

Figure 4.33: Langmuir adsorption isotherms for the corrosion of mild steel in 1.0 M HCl at various temperatures for TDTB corrosion inhibitor.

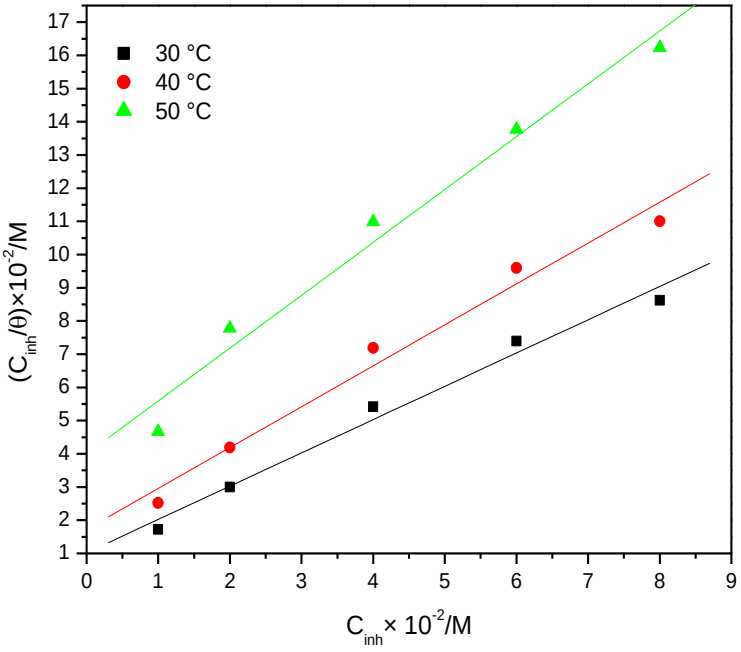

Figure 4.34: Langmuir adsorption isotherms for the corrosion of mild steel in 1.0 M HCl at various temperatures for TDTM corrosion inhibitor.

© University of Venda

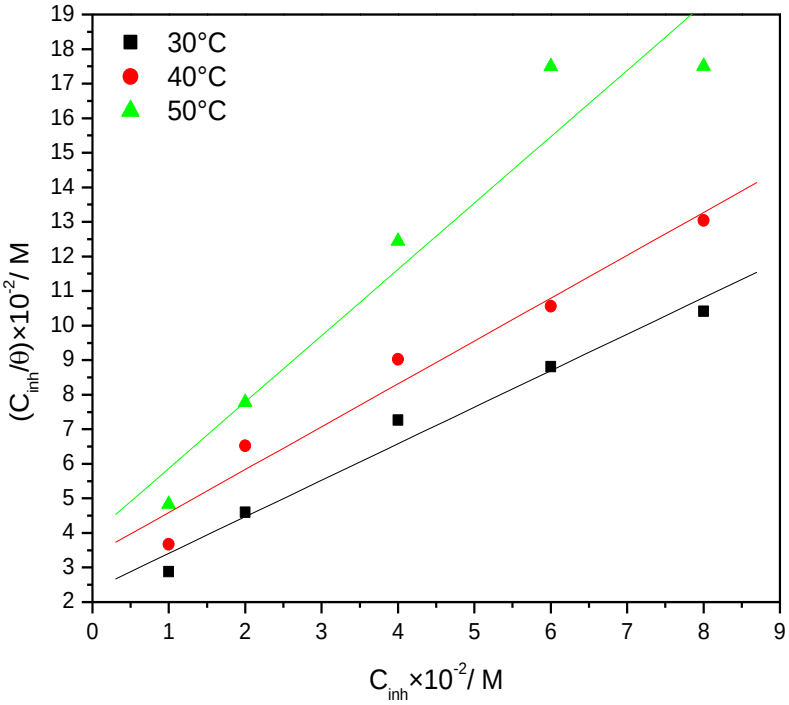

Figure 4.35: Langmuir adsorption isotherms for the corrosion of mild steel in 1.0 M HCl at various temperatures for [EMIM][ESO_4] corrosion inhibitor.

© University of Venda

4.2. Zinc

4.2.1. Potentiodynamic polarization (PDP)

The potentiodynamic polarization technique was used to gain an understanding of the corrosion process of zinc as well as the inhibitor behaviour of the three ionic liquids i.e. TDTB, TDTM and [EMIM][ESO_4]. The measurements were carried out at 30°C in the absence and presence of different concentrations of the ILs. Figures 4.36 – 4.38 are the polarization curves which were obtained, these show an anodic region which represents the dissolution of zinc and a cathodic region which corresponds to the cathodic reduction of hydrogen ions.

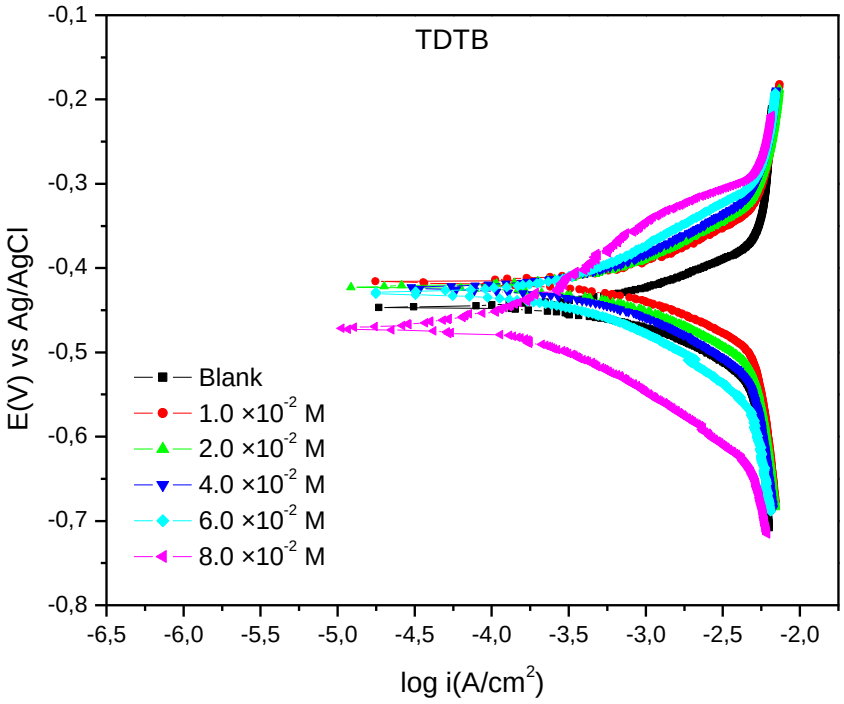

Figure 4.36: Tafel plots for zinc in 1.0 M HCl in the absence and presence of different concentrations of TDTB inhibitor compound.

© University of Venda

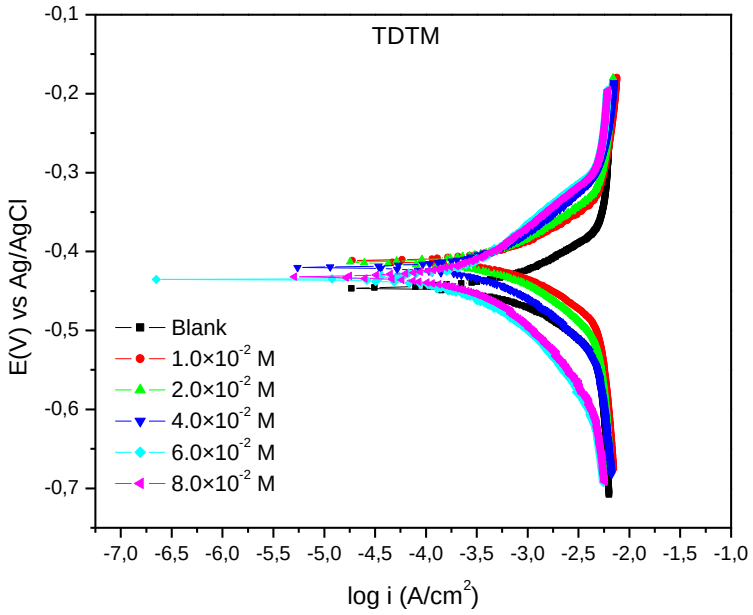

Figure 4.37: Tafel plots for zinc in 1.0 M HCl in the absence and presence of different concentrations of TDTM inhibitor compound.

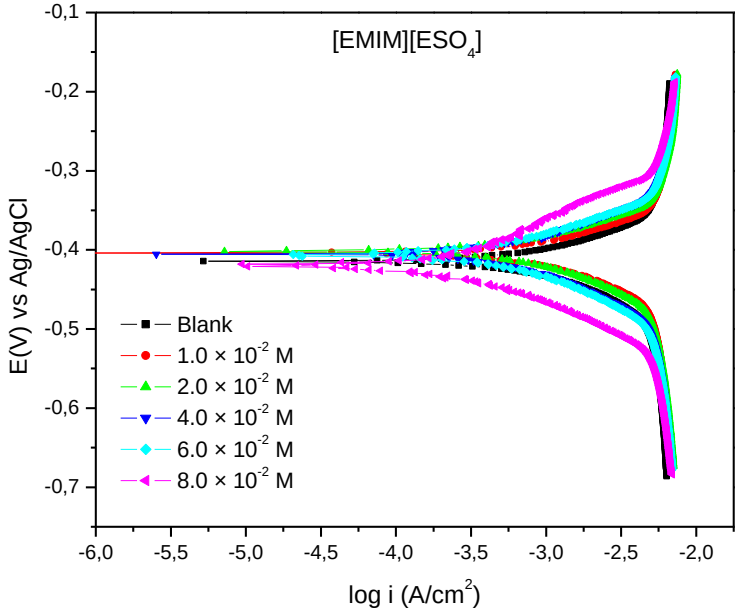

Figure 4.38: Tafel plots for zinc in 1.0 M HCl in the absence and presence of different concentrations of [EMIM][ESO_4] inhibitor compound.

© University of Venda

The linear segments of the PDP curves were further extrapolated to obtain the electrochemical kinetic parameters (E_{corr}, i_{corr} , β_a and β_c) listed in Table 4.7. The measured i_{corr} values were used to calculate the percentage inhibition efficiency using the relationship expressed in Equation 30.

Table 4.7: Potentiodynamic polarization (PDP) parameters using different inhibitors.

Inhibitor	Inhibitor conc. (M)	-E_{corr} (mV vs. Ag/AgCl)	i_{corr} (mA cm^{-2})	R_p (Ω cm^2)	b_a (mV dec^{-1})	b_c (mV dec^{-1})	%IE_{PDP}
Blank	–	415	1.38	17.91	97	136	–
TDTB	1×10^{-2}	417	0.64	25.22	126	116	53.62
	2×10^{-2}	423	0.60	34.00	117	101	56.52
	4×10^{-2}	424	0.48	41.41	130	107	65.22
	6×10^{-2}	430	0.17	59.78	153	118	87.68
	8×10^{-2}	471	0.09	141.39	194	77	93.48
TDTM	1×10^{-2}	411	0.79	24.93	128	122	42.75
	2×10^{-2}	414	0.60	31.86	118	115	56.52
	4×10^{-2}	421	0.39	45.87	136	119	71.74
	6×10^{-2}	436	0.35	80.39	154	138	74.64
	8×10^{-2}	433	0.15	74.71	127	117	89.13
[EMIM][ESO_4]	1×10^{-2}	404	1.22	16.61	82	108	11.42
	2×10^{-2}	402	0.92	20.62	87	89	33.26
	4×10^{-2}	406	0.83	26.74	92	110	39.43
	6×10^{-2}	407	0.63	30.10	84	91	54.22
	8×10^{-2}	421	0.37	62.86	128	93	72.96

The results shown in Table 4.7 do not show any trend in the E_{corr} values. This observation suggests that the ILs are mixed type inhibitors [66, 67]. The Tafel slopes β_a and β_c gave more information about the mechanism of inhibition. The values of β_a and β_c show that both the anodic and cathodic reactions have been affected by the inhibitors. However, no uniform trend is observed in these values. For the inhibitors TDTB and [EMIM][ESO_4], there is a similar influence on the anodic and cathodic reactions, while TDTM has a more significant influence on the anodic reaction than on the cathodic reaction. Values of β_a and β_c for all the inhibitors confirm a mixed type inhibition mechanism with TDTM being predominantly anodic.

© University of Venda

4.2.2. Electrochemical impedance spectroscopy (EIS)

Electrochemical impedance spectroscopy is a useful technique which can provide information on surface properties, electrode kinetics and mechanism of corrosion inhibition [85]. Impedance measurements were carried out on zinc in inhibited and uninhibited HCl solutions containing various concentrations of TDTB, TDTM and [EMIM][ESO_4] at open-circuit potential after 30 minutes of immersion. The Nyquist and Bode plots obtained from these measurements are shown in Figures 4.39 – 4.44.

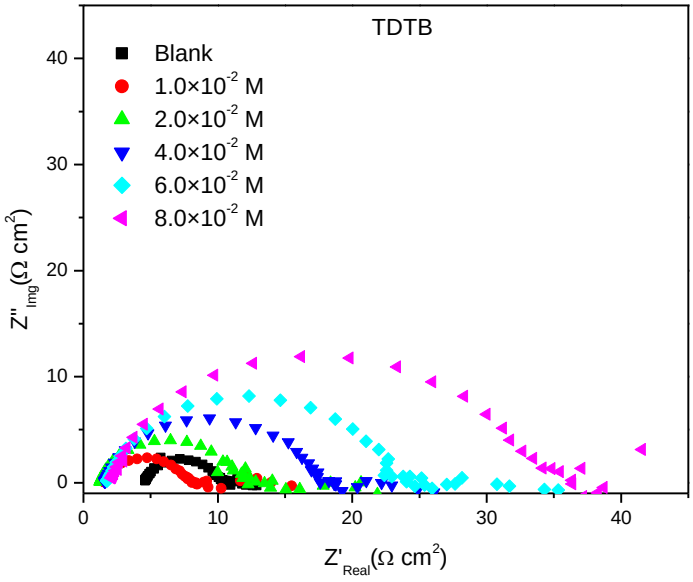

Figure 4.39: Nyquist plot of zinc in 1.0 M HCl in the absence and presence of different concentrations of TDTB inhibitor compound.

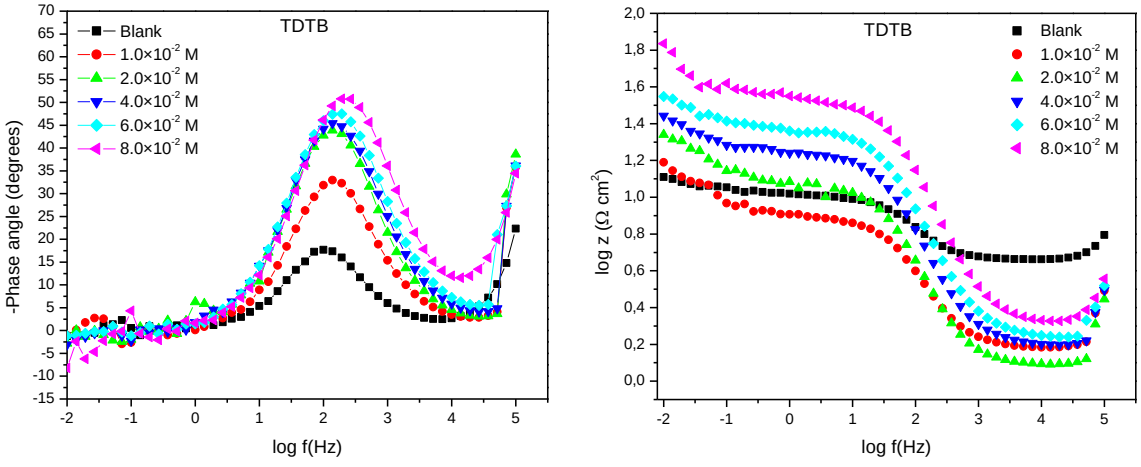

Figure 4.40: Bode plots of zinc in 1.0 M HCl in the absence and presence of different concentrations of TDTB inhibitor compound.

© University of Venda

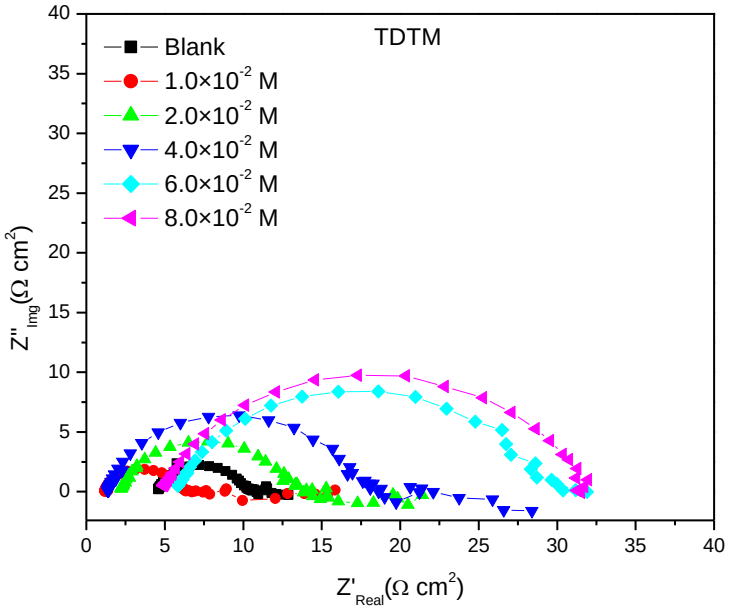

Figure 4.41: Nyquist plot of zinc in 1.0 M HCl in the absence and presence of different concentrations of TDTM inhibitor compound

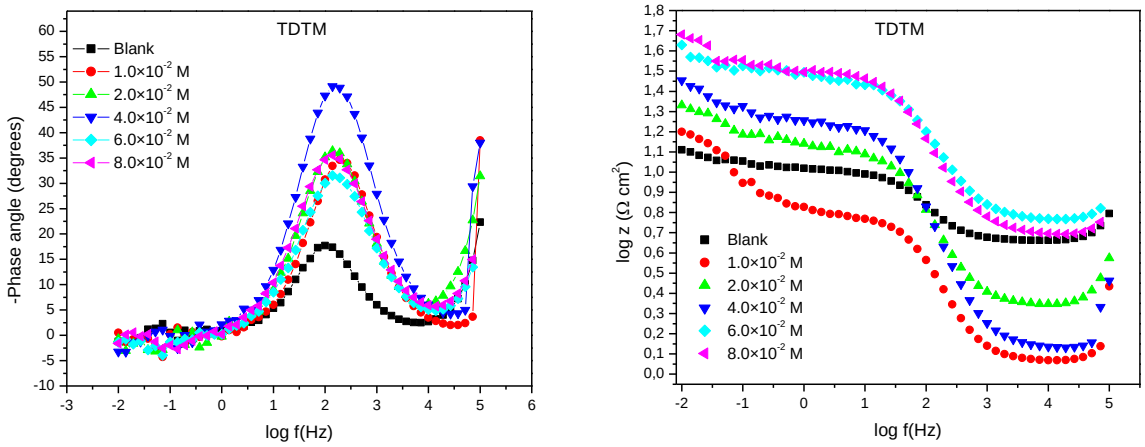

Figure 4.42: Bode plots of zinc in 1.0 M HCl in the absence and presence of different concentrations of TDTM inhibitor compound.

© University of Venda

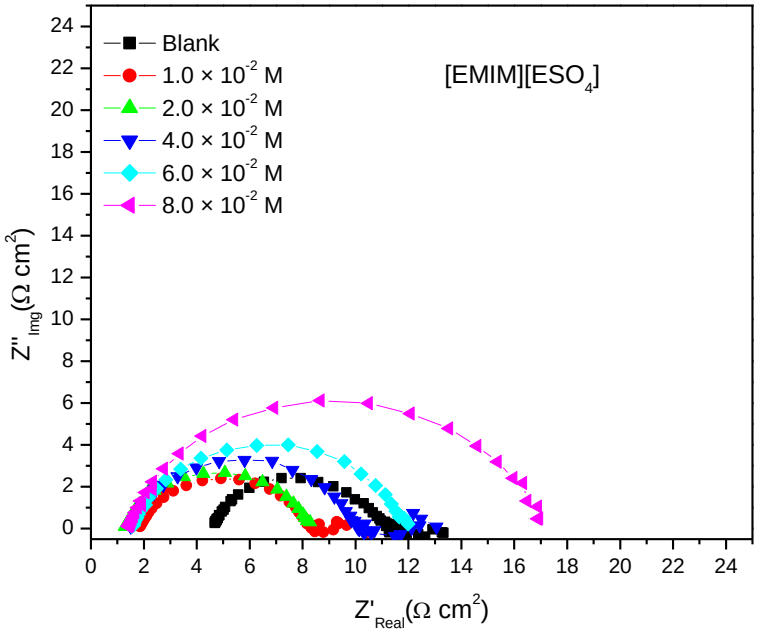

Figure 4.43: Nyquist plot of zinc in 1.0 M HCl in the absence and presence of different concentrations of [EMIM][ESO_4] inhibitor compound.

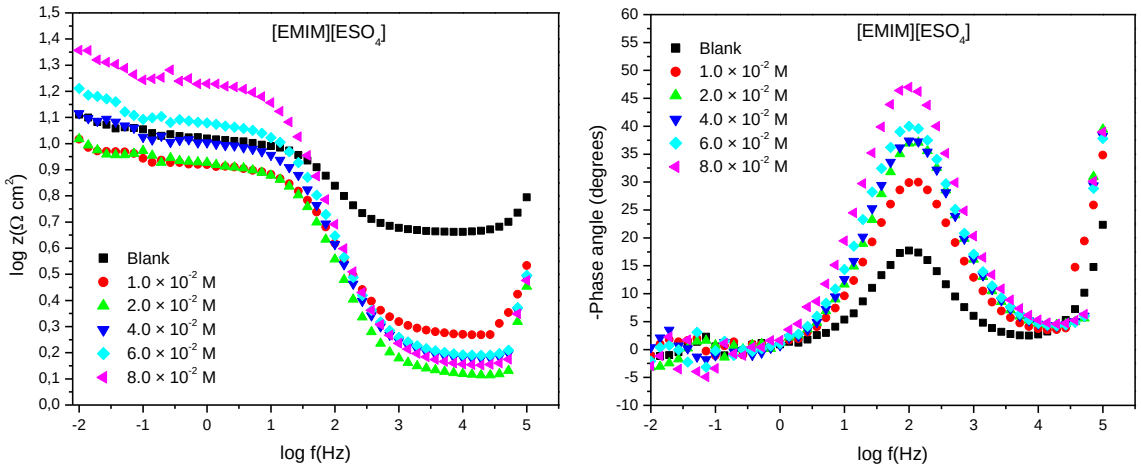

Figure 4.44: Bode plots of zinc in 1.0 M HCl in the absence and presence of different concentrations of [EMIM][ESO_4] inhibitor compound.

© University of Venda

The Nyquist spectra are characterised by a large high- frequency capacitive loop. The capacitive loops exhibit imperfect semi-circular shapes, this phenomenon is referred to as frequency dispersion which is commonly attributed to factors such as adsorption of inhibitor, inhomogeneity of the electrode surface and surface roughness [72, 86, 87]. The Nyquist plots were used to derive the characteristic impedance parameters as shown in Table 4.8.

Table 4.8: Electrochemical parameters obtained from Nyquist and Bode plots of TDTB, TDTM and [EMIM][ESO_4].

Inhibitor	**Inhibitor conc. (M)**	$R_s(\Omega\ cm^2)$	$R_{ct}(\Omega\ cm^2)$	**n**	$(CPE)Y_0$ $(\times 10^6 s^n \Omega^{-1}\ cm^{-2})$	C_{dl} $(\mu F cm^{-2})$	**%IE_{EIS}**
Blank	-	4.63	6.33	0.78	1785.70	509.04	–
TDTB	1.0×10^{-2}	1.53	12.33	0.77	2135.00	603.31	47.43
	2.0×10^{-2}	1.24	17.04	0.81	1258.40	484.97	63.97
	4.0×10^{-2}	1.59	23.57	0.82	786.42	305.94	73.14
	6.0×10^{-2}	1.77	25.89	0.82	578.32	228.85	82.36
	8.0×10^{-2}	2.06	39.99	0.82	355.42	131.98	84.17
TDTM	1.0×10^{-2}	1.15	12.82	0.74	2530.10	612.65	50.62
	2.0×10^{-2}	2.21	17.98	0.79	1037.60	331.89	64.79
	4.0×10^{-2}	1.37	26.31	0.85	629.36	284.22	75.94
	6.0×10^{-2}	5.77	29.65	0.77	494.40	130.44	78.65
	8.0×10^{-2}	4.89	36.91	0.77	497.12	144.82	82.85
[EMIM][ESO_4]	1.0×10^{-2}	1.89	6.80	0.81	1665.30	565.09	6.91
	2.0×10^{-2}	1.33	7.44	0.83	1514.20	597.49	14.92
	4.0×10^{-2}	1.53	9.19	0.82	1402.00	539.47	31.12
	6.0×10^{-2}	1.57	11.17	0.82	1266.40	508.75	43.33
	8.0×10^{-2}	1.45	16.79	0.84	1006.60	456.51	62.30

The impedance kinetic parameters were obtained by fitting the impedance data into a simple Randle's equivalent circuit of the form $R_s(R_{ct}CPE)$ as shown in Figure 4.10. The impedance function of the *CPE* is shown in Equation 35, and the inhibition efficiency (%IE_{EIS}) was calculated using Equation 31. The results obtained from the fitting of impedance data are listed in Table 4.8. Inspection of Table 4.8 reveals that the R_{ct} values of the inhibited systems are generally higher than the corresponding values of the uninhibited system. In the inhibited system, it is observed that the R_{ct} values increase with an increase in the concentration of the inhibitor molecules. This is due to an increase in the number of inhibitor molecules covering the surface of the metal [73]. The C_{dl} values of the inhibited system, on the other hand, are lower than the values of the uninhibited system. The C_{dl} values of the studied ILs generally decrease with an increase in concentration of the inhibitor, this indicates a decrease in the dielectric constant and/or an increase in the thickness of the electrical double layer [74].

© University of Venda

4.2.3. Adsorption film analysis

The FTIR technique was used to carry out spectroscopic analysis of the pure ILs as well as the adsorption films formed on the zinc metal surface after exposure to 1.0 M HCl in the presence of 8.0×10^{-2} M of the ILs. The FTIR spectra are shown in Figures 4.45 – 4.47.

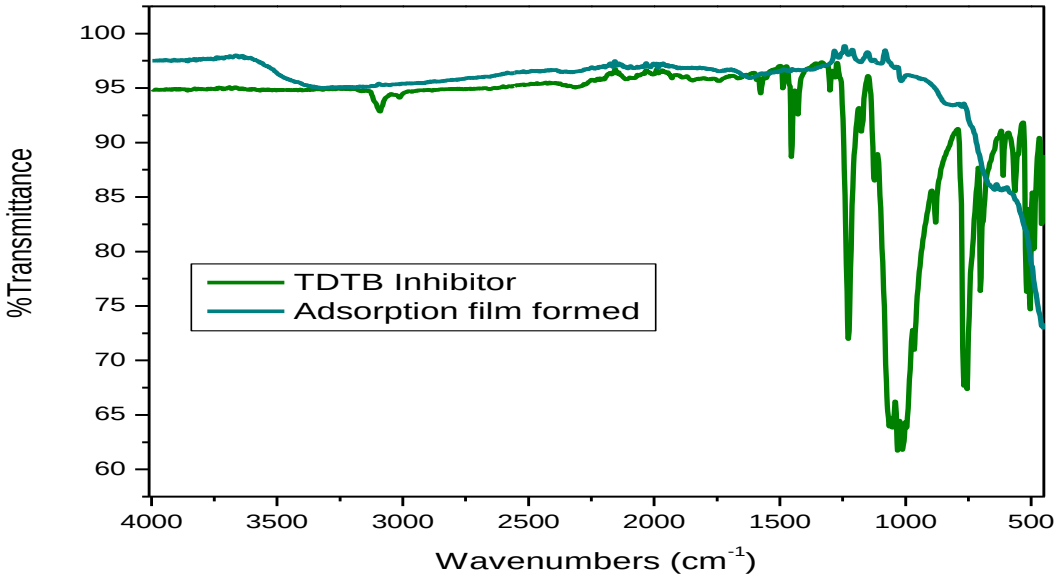

Figure 4.45: FT-IR spectra for the studied corrosion inhibitors and adsorption films formed on zinc in 1.0 M HCl using TDTB corrosion inhibitor.

© University of Venda

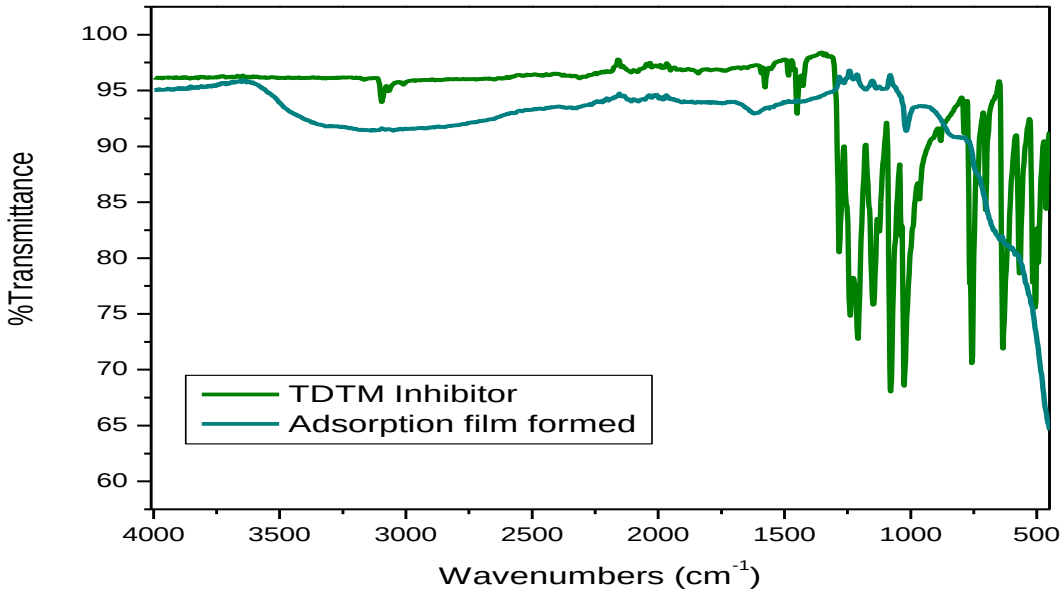

Figure 4.46: FT-IR spectra for the studied corrosion inhibitors and adsorption films formed on zinc in 1.0 M HCl using TDTM corrosion inhibitor.

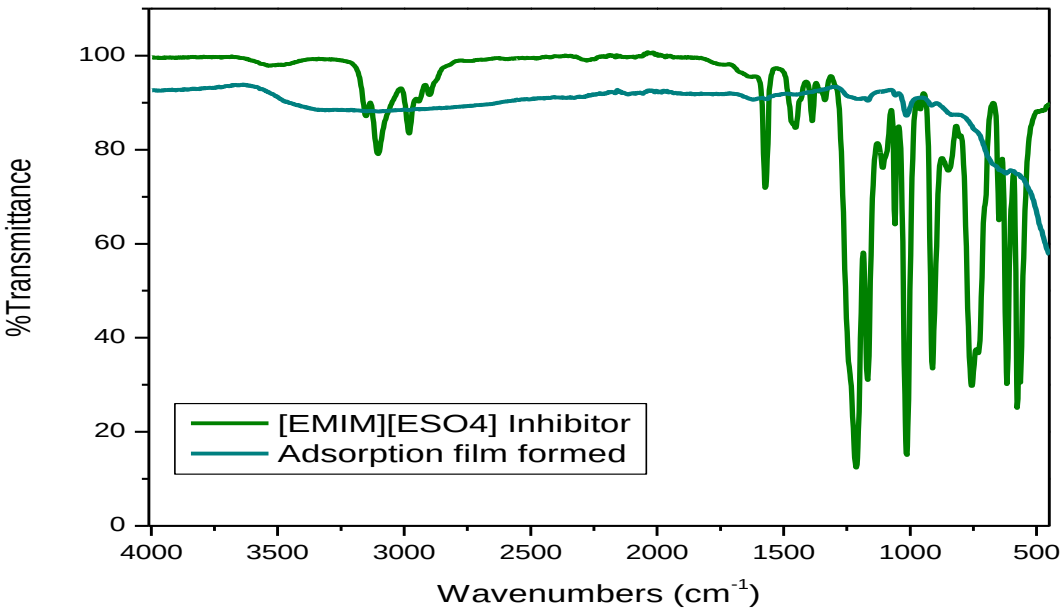

Figure 4.47: FT-IR spectra for the studied corrosion inhibitors and adsorption films formed on zinc in 1.0 M HCl using [EMIM][ESO_4] corrosion inhibitor.

© University of Venda

TDTB and TDTM show similar FTIR spectra due to the identical cation they possess. There are minor differences which occur in the fingerprint region due to their differences in anions. [EMIM][ESO_4] possesses a different cation and anion relative to TDTB and TDTM, these differences are observed both in the high and low wavenumbers. [EMIM][ESO_4] shows adsorption bands at 3157 cm^{-1} and 3103 cm^{-1} corresponding to C–H stretch of the imidazole ring while TDTB and TDTM show relatively weaker bands at 3105 cm^{-1} and 3103 cm^{-1}. The characteristic adsorption bands of the ILs are listed in Table 4.3. The FTIR spectrum of the TDTB adsorption film shows the disappearance of the characteristic absorption bands; this indicates that the functional groups represented by these bands acted as adsorption sites resulting in the formation of a TDTB-Zn complex. TDTM and [EMIM][ESO_4] adsorption film spectra also show the disappearance of characteristic band implying that TDTM-Zn and [EMIM][ESO_4] have been formed.

4.2.4. Surface analysis

The morphology of the zinc surface in the absence and presence of 8.0×10^{-2} M of TDTB, TDTM and [EMIM][ESO_4] was characterised using scanning electron microscope. The SEM micrographs and the corresponding EDS spectra are shown in Figures 4.48 – 4.52 and Figures 4.53 – 4.57, respectively.

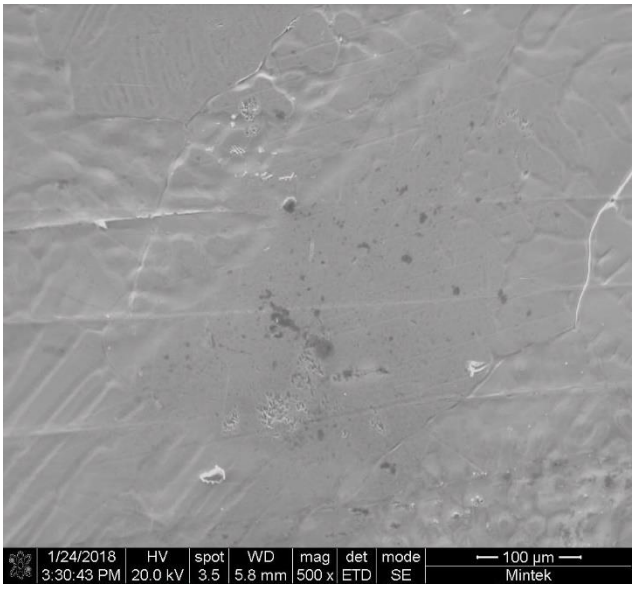

Figure 4.48: SEM micrograph of zinc before exposure to 1.0 M HCl

© University of Venda

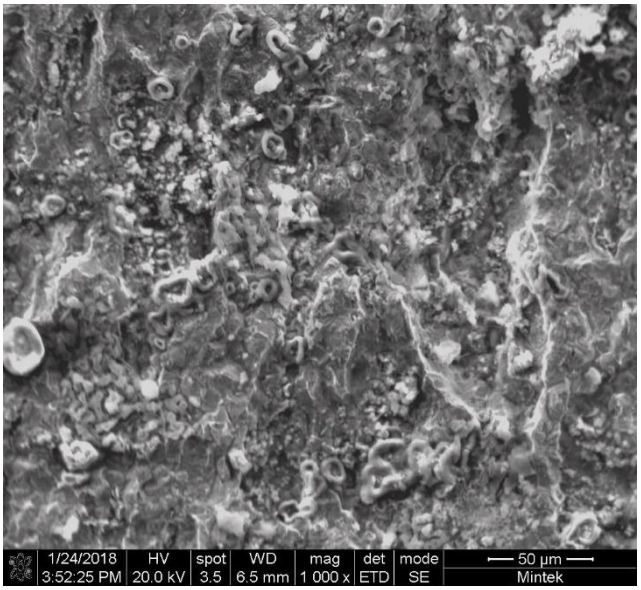

Figure 4.49: SEM micrograph of the surface of zinc immersed in 1.0 M HCl uninhibited

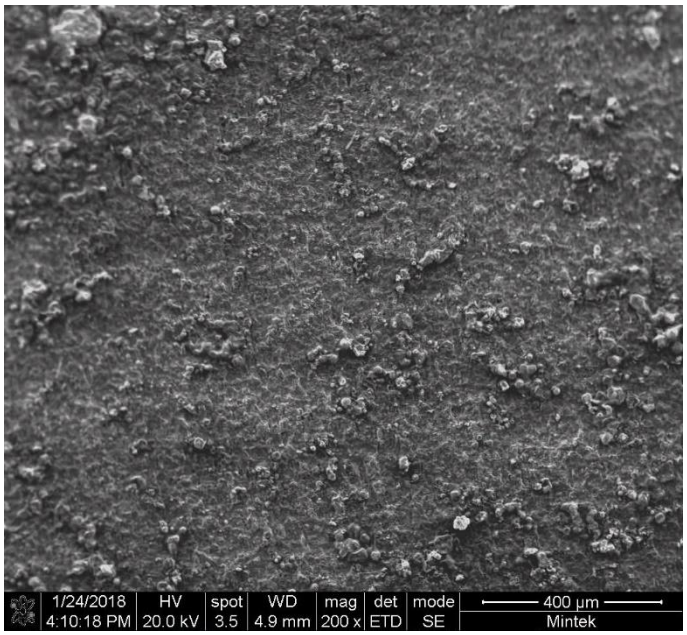

Figure 4.50: SEM micrograph of the surface of zinc immersed in 1.0 M HCl in the presence of TDTB corrosion inhibitor.

© University of Venda

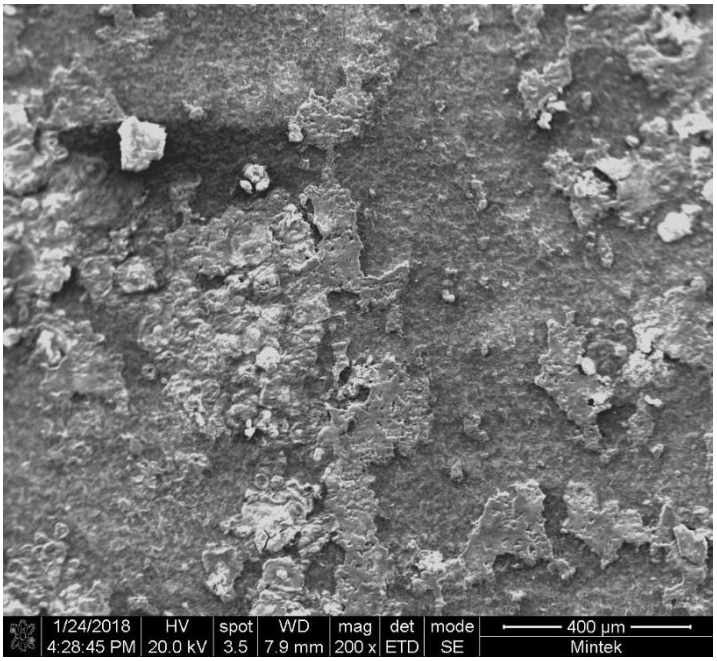

Figure 4.51: SEM micrograph of the surface of zinc immersed in 1.0 M HCl in the presence of TDTM corrosion inhibitor.

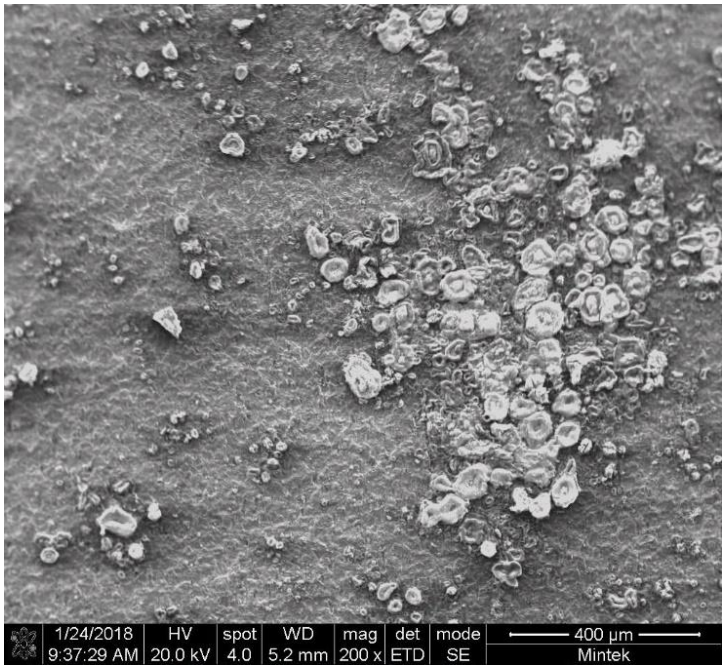

Figure 4.52: SEM micrograph of the surface of zinc immersed in 1.0 M HCl in the presence of [EMIM][ESO_4] corrosion inhibitor.

© University of Venda

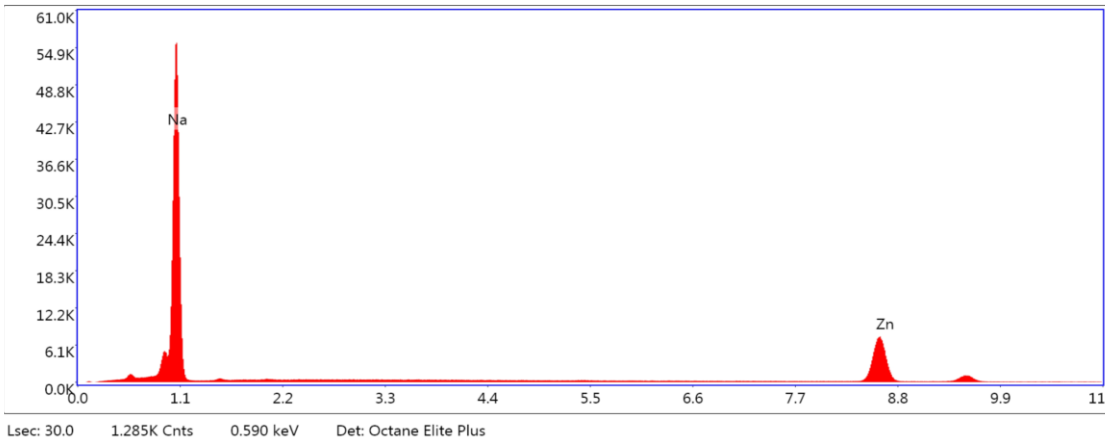

Figure 4.53: EDS spectrum of zinc before exposure to 1.0 M HCl.

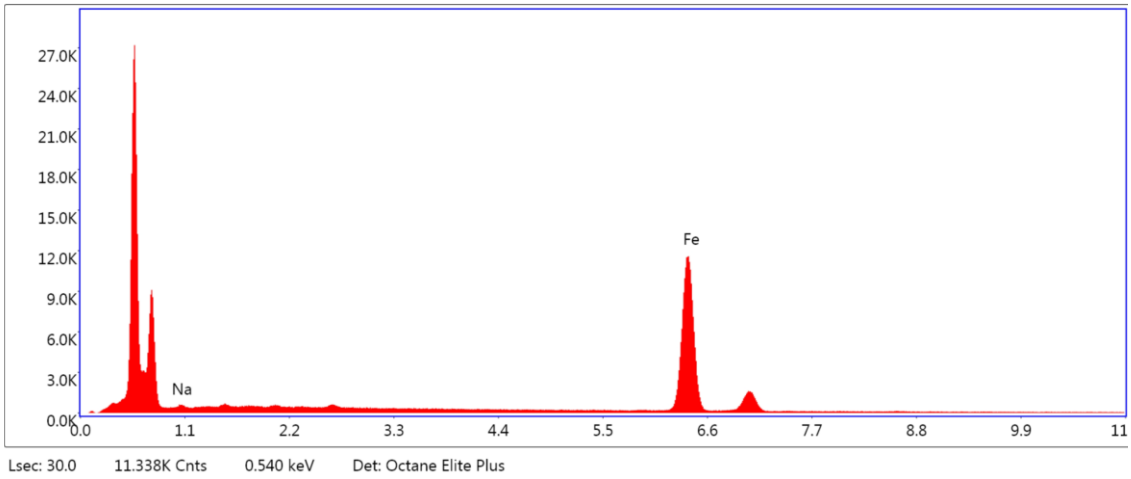

Figure 4.54: EDS spectrum of zinc immersed in 1.0 M HCl uninhibited.

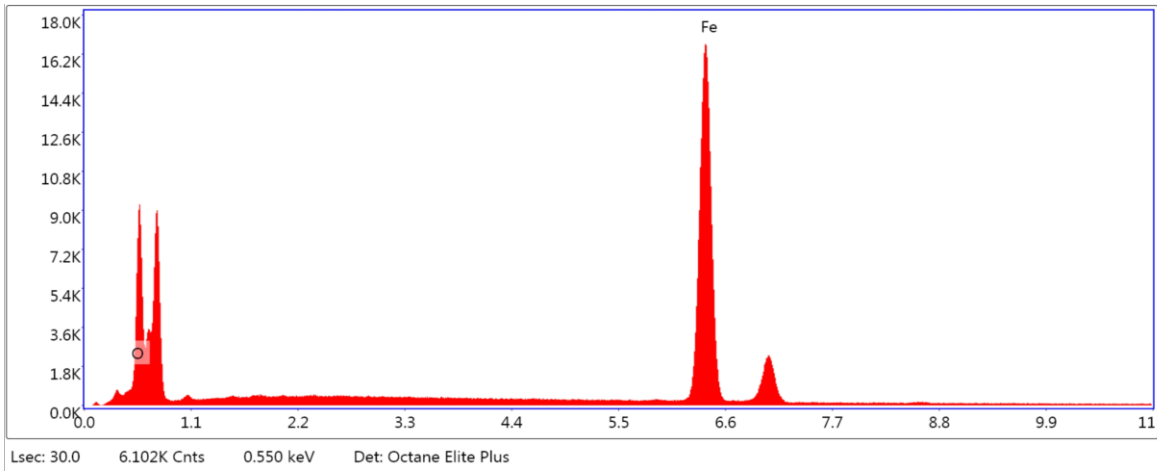

Figure 4.55: EDS spectrum of zinc immersed in 1.0 M HCl in the presence of TDTB corrosion inhibitor.

© University of Venda

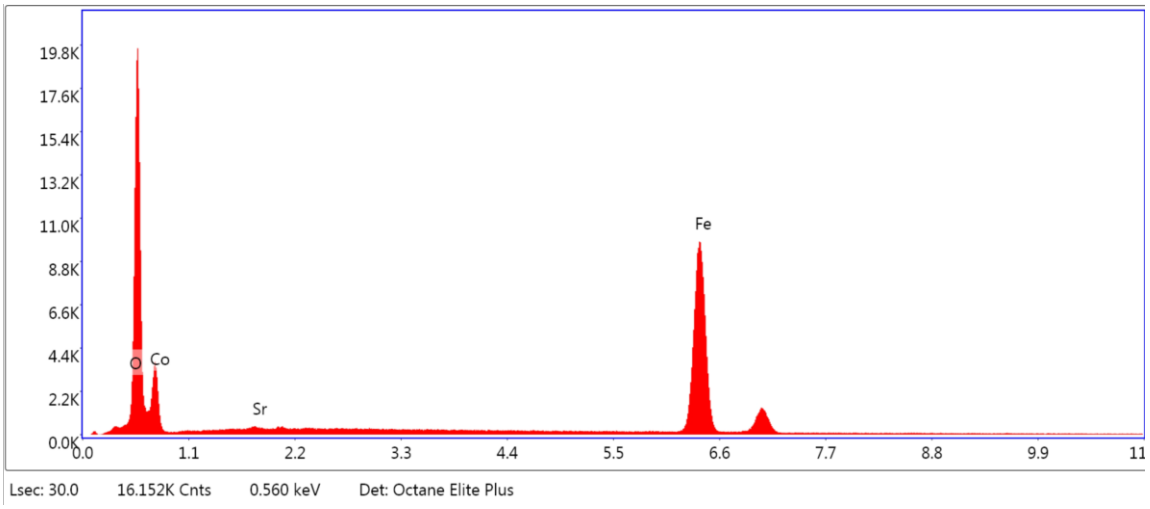

Figure 4.56: EDS spectrum of zinc immersed in 1.0 M HCl in the presence of TDTM corrosion inhibitor.

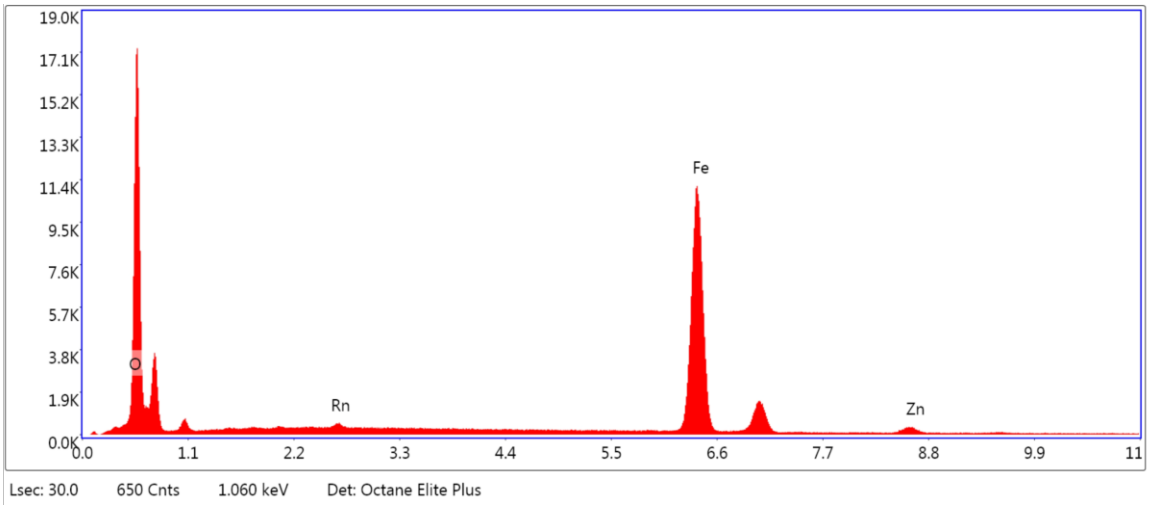

Figure 4.57: EDS spectrum of zinc immersed in 1.0 M HCl in the presence of [EMIM][ESO_4] corrosion inhibitor.

© University of Venda

The surface of zinc before exposure to the acidic medium is shown in Figure 4.48; the surface appears smooth with some minor scratches which may be due to the polishing process. After the zinc metal has been exposed to uninhibited 1.0 M HCl, the surface appears to be aggressively attacked (Figures 4.49). This is indicated by the presence of cavities and pits. The number of cavities and pits is observed to decrease with the introduction of the corrosion inhibitors as shown in Figures 4.50 – 4.52, whereby the surface of the zinc metal appears less damaged than in the uninhibited case. This implies that a protective film was formed on the zinc surface by the inhibitors. The corresponding EDS data reveals that the surface of the untreated zinc specimen consists of Zn and Na as the main constituents. Exposing the metal to uninhibited HCl resulted in the appearance of Fe in the EDS spectrum implying that the metal specimen consisted of Fe (the metal must have contained a considerable amount of Fe). Introduction of the corrosion inhibitors resulted in the appearance of O peaks, even in the TDTB spectrum (TDTB does not contain oxygen in its molecular structure, hence appearance of oxygen may be due to the contamination of the metal surface). In the case of TDTM and [EMIM][ESO_4], oxygen may indicate adsorption of the anions on to the surface of the zinc metal in order to form a protective film.

4.2.5. Effect of inhibitor concentration on inhibitory behaviour for zinc

The variation of the inhibition efficiencies with inhibitor concentration at different temperatures are illustrated in Figures 4.58 – 4.60 and Table 4.9.

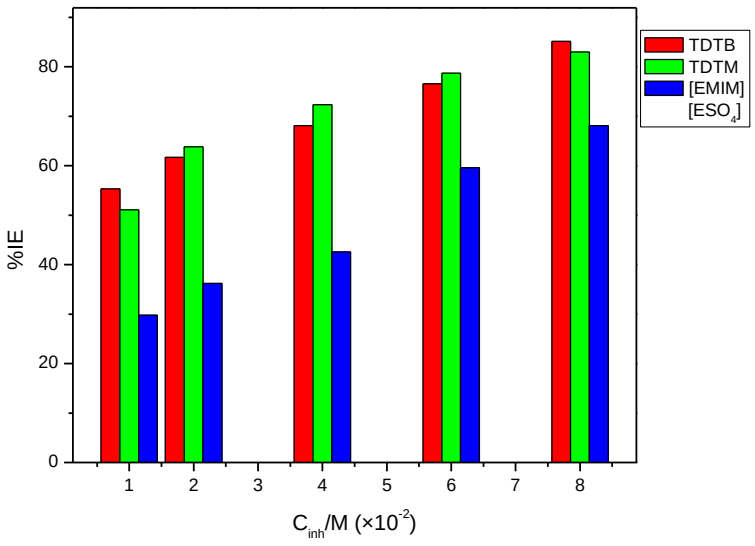

Figure 4.58: Variations of the weight loss percentage inhibition efficiencies with various concentrations of the utilized corrosion inhibitors at 30°C.

© University of Venda

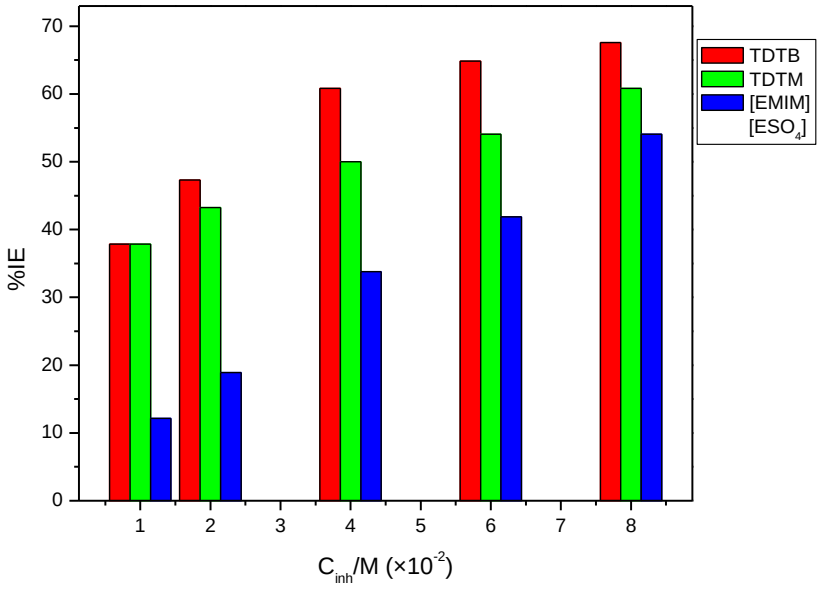

Figure 4.59: Variations of the weight loss percentage inhibition efficiencies with various concentrations of the utilized corrosion inhibitors at 40°C.

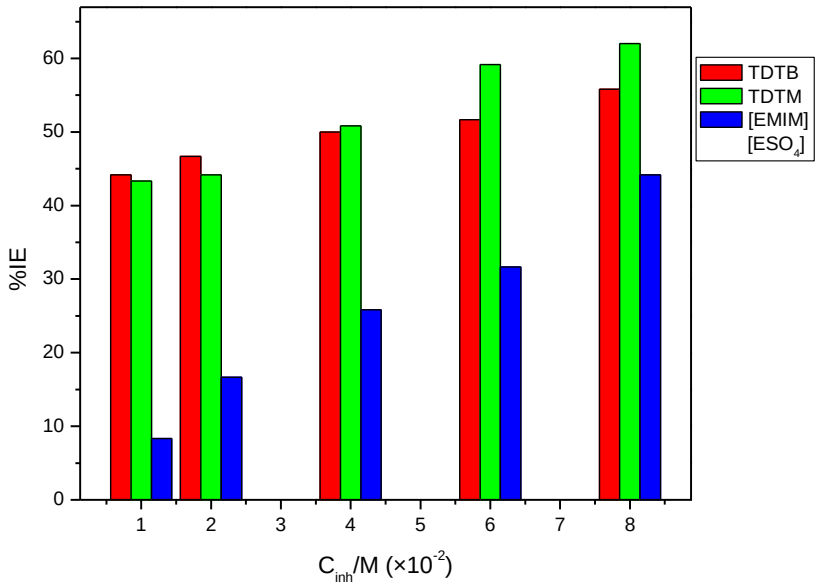

Figure 4.60: Variations of the weight loss percentage inhibition efficiencies with various concentrations of the utilized corrosion inhibitors at 50°C.

© University of Venda

Table 4.9: Percentage inhibition efficiencies and corrosion rates values obtained from the weight loss of zinc in 1.0 M HCl in the absence and presence of various concentrations of inhibitors.

Inhibitor	Inhibitor conc. (M)	Temperature					
		30°C		40°C		50°C	
		$\%IE_{WL}$	C_R (g cm^{-2} h^{-1})	$\%IE_{WL}$	C_R (g cm^{-2} h^{-1})	$\%IE_{WL}$	C_R (g cm^{-2} h^{-1})
Blank	0.0	–	0.0047	–	0.0074	–	0.012
TDTB	1.0×10^{-2}	55.32	0.0021	37.84	0.0046	44.17	0.0067
	2.0×10^{-2}	61.70	0.0018	47.30	0.0039	46.67	0.0064
	4.0×10^{-2}	68.09	0.0015	60.81	0.0029	50.00	0.0060
	6.0×10^{-2}	76.59	0.0011	64.86	0.0026	51.67	0.0058
	8.0×10^{-2}	85.11	0.0007	67.57	0.0024	55.83	0.0053
TDTM	1.0×10^{-2}	51.06	0.0023	37.84	0.0046	43.33	0.0068
	2.0×10^{-2}	63.82	0.0016	43.24	0.0042	44.17	0.0067
	4.0×10^{-2}	72.34	0.0013	50.00	0.0037	50.83	0.0059
	6.0×10^{-2}	78.72	0.0010	54.05	0.0034	59.17	0.0049
	8.0×10^{-2}	82.98	0.0008	60.81	0.0029	62.00	0.0045
[EMIM][ESO4]	1.0×10^{-2}	29.79	0.0033	12.16	0.0065	8.33	0.011
	2.0×10^{-2}	36.17	0.0030	18.92	0.0060	16.67	0.010
	4.0×10^{-2}	42.55	0.0027	33.78	0.0049	25.83	0.0089
	6.0×10^{-2}	59.57	0.0019	41.89	0.0043	31.67	0.0082
	8.0×10^{-2}	68.09	0.0015	54.05	0.0034	44.17	0.0067

When zinc is exposed to the HCl solution in the presence of the studied ILs, the inhibition efficiencies at constant temperature are observed to vary with concentration of inhibitor. For instance, the inhibition efficiency of TDTB at 30°C increases from 55.32% at 1.0×10^{-2} M to 85.11% at 8.0×10^{-2} M. Similarly, in the presence of [EMIM][ESO_4], the inhibition efficiency increases from 29.79% at 1.0×10^{-2} M to 68.09% at 8.0×10^{-2} M. An increase in the concentration of inhibitor molecules means that a greater number of inhibitor molecules are covering the metal surface. This results in the reduction of the contact between the metal surface and the aggressive medium hence reducing the corrosion rate. This trend is observed for all the temperatures. However, the inhibition efficiencies for all the inhibitors at constant concentration decrease with increase in temperature. For instance, at 8.0×10^{-2} M, TDTB has the following %IE values 85.11%, 67.57% and 55.83% at temperatures 30°C, 40°C and 50°C, respectively. This trend is due to the increase in corrosion rate with increase in temperature (as shown in Table 4.9), and the desorption of inhibitor molecules which results in less inhibitor molecules covering the surface of the metal.

© University of Venda

4.2.6. Effect of temperature and kinetic parameters

Inspection of Table 4.9 reveals that temperature greatly influences the corrosion rate as well as the inhibition efficiency. It is observed that the corrosion rate increases with temperature while the inhibition efficiency decreases with temperature. The variations of corrosion rate with temperature can therefore be used to obtain useful information regarding the mode of adsorption of the inhibitor molecules. The effect of temperature on the corrosion rate and the inhibition efficiency of zinc was studied at the concentration range 1.0×10^{-2} M to 8.0×10^{-2} M of the inhibitors TDTB, TDTM and [EMIM][ESO_4] at temperatures 30°C, 40°C and 50°C for immersion period of 15 hrs. The corrosion rate was related to the temperature using the Arrhenius and transition state equations i.e. Equation 34 and Equation 35, respectively. From these equations, the Arrhenius and transition state plots (as shown in Figures 4.61 – 4.66) were obtained and used to calculate the following kinetic parameters: E_a, ΔH^* and ΔS^*. The values of these parameters are listed in Table 4.10.

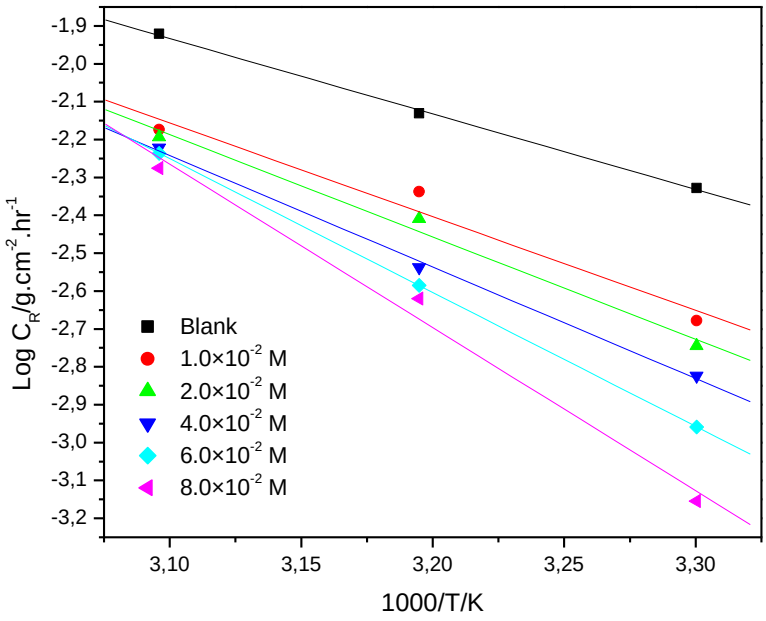

Figure 4.61: Arrhenius plots for the corrosion of zinc in 1.0 M HCl in the absence and presence of various concentrations of TDTB corrosion inhibitor.

© University of Venda

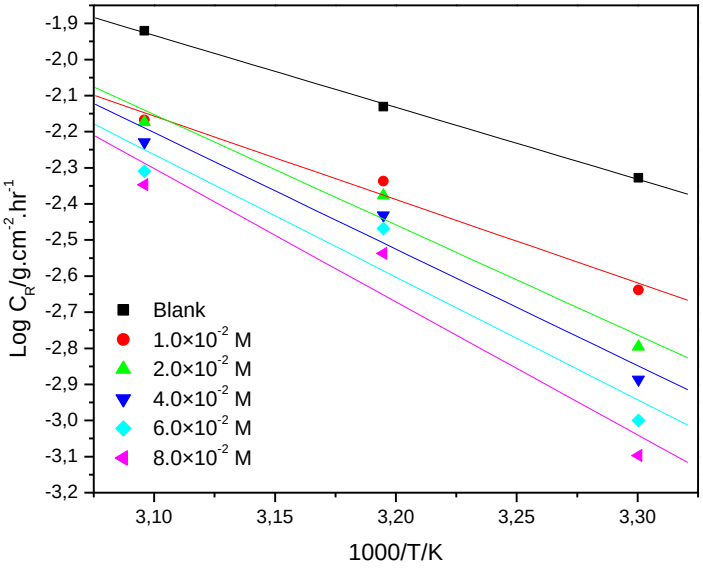

Figure 4.62: Arrhenius plots for the corrosion of zinc in 1.0 M HCl in the absence and presence of various concentrations of TDTM corrosion inhibitor.

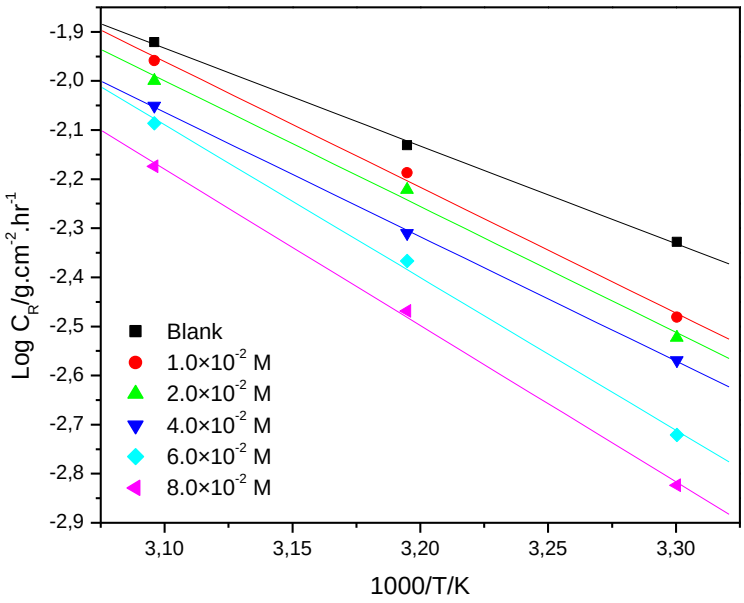

Figure 4.63: Arrhenius plots for the corrosion of zinc in 1.0 M HCl in the absence and presence of various concentrations of [EMIM][ESO_4] corrosion inhibitor.

© University of Venda

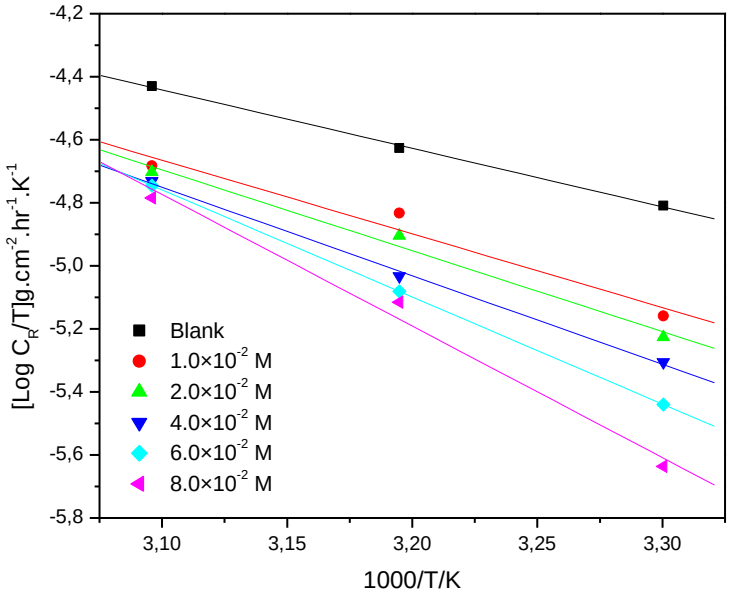

Figure 4.64: Transition state plots for the corrosion of zinc in 1.0 M HCl in the absence and presence of various concentrations of TDTB corrosion inhibitor.

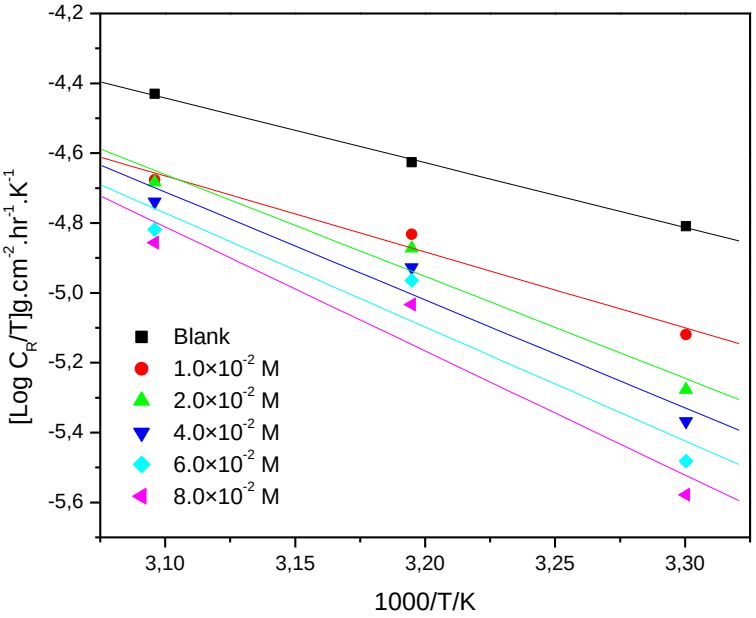

Figure 4.65: Transition state plots for the corrosion of zinc in 1.0 M HCl in the absence and presence of various concentrations of TDTM corrosion inhibitor.

© University of Venda

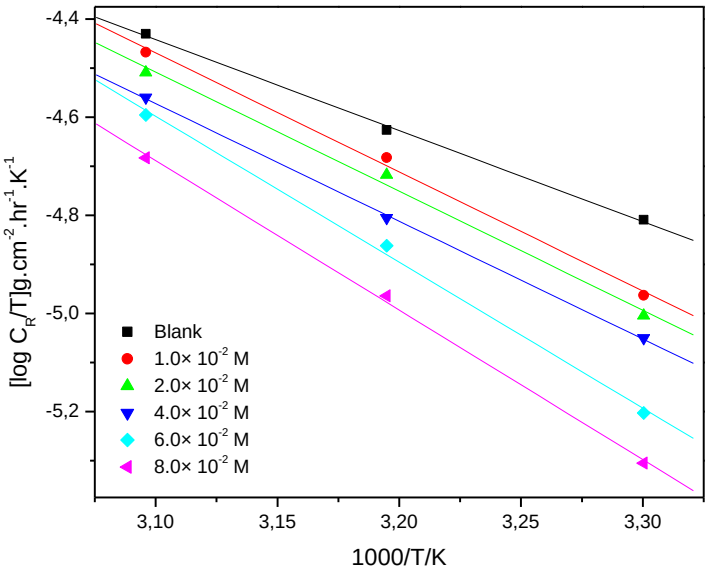

Figure 4.66: Transition state plots for the corrosion of zinc in 1.0 M HCl in the absence and presence of various concentrations of [EMIM][ESO_4] corrosion inhibitor

Table 4.10: Activation parameters derived from Arrhenius and transition state plots.

Inhibitor	Inhibitor Conc. (M)	Activation Energy E_a (kJ mol^{-1})	Enthalpy of Activation ΔH^* (kJ mol^{-1})	Entropy of Activation ΔS^* (JK^{-1}mol^{-1})
Blank	0.0	38.12	35.52	-172.53
TDTB	1.0×10^{-2}	47.37	44.77	-148.11
	2.0×10^{-2}	51.72	49.12	-135.21
	4.0×10^{-2}	56.36	53.76	-121.88
	6.0×10^{-2}	67.65	65.05	-87.04
	8.0×10^{-2}	82.54	79.94	-41.18
TDTM	1.0×10^{-2}	44.23	41.63	-157.87
	2.0×10^{-2}	58.47	55.87	-113.63
	4.0×10^{-2}	61.7	59.18	-104.33
	6.0×10^{-2}	65.02	62.42	-95.45
	8.0×10^{-2}	70.63	68.03	-78.81
[EMIM][ESO_4]	1.0×10^{-2}	49.04	46.44	-139.18
	2.0×10^{-2}	49.05	46.45	-139.89
	4.0×10^{-2}	48.52	45.92	-142.77
	6.0×10^{-2}	59.56	56.96	-109.05
	8.0×10^{-2}	60.94	58.34	-106.50

The results in Table 4.10 show that the value of E_a for zinc in the uninhibited system is 38 kJ mol^{-1}. When an inhibitor such as TDTM is introduced with a concentration of 1.0×10^{-2} M, the E_a increases to 44.23 kJ mol^{-1}. E_a continues to increase as more inhibitor molecules are

© University of Venda

introduced. At 8.0×10^{-2} M, E_a is observed to be 70.63 kJ mol^{-1}. TDTB and [EMIM][ESO_4] exhibit similar tends in E_a values. The apparent activation energy represents the energy barrier of the reaction, an increase in this value suggests that the energy barrier is increased when the inhibitor molecules are introduced hence reducing the rate of zinc dissolution [51, 83].

The enthalpy of activation gives information about whether the zinc dissolution process is endothermic or exothermic. The positive signs of the ΔH^* values as shown in Table 4.10 suggest that the dissolution of zinc is an endothermic reaction. The values of ΔH^* are observed to increase with an increase in inhibitor concentration, this indicates that the energy barrier of the reaction is increased hence making the dissolution process difficult [81]. The highest values of ΔH^* are observed at the highest inhibitor concentration (8.0×10^{-2} M) for all the inhibitors, this indicates that this concentration is the optimal concentration for greatest reduction in zinc dissolution. This corresponds to the high %IE values obtained at this concentration.

The entropy of activation (ΔS^*) values are negative in both the inhibited and uninhibited systems. This indicates that the activated complex in the rate determining step for all the systems involves association rather than dissociation meaning that there is a reduction in disorder on going from the reactants to the activated complex [82].

4.2.7. Thermodynamic parameters: Adsorption isotherms

The type of mechanism followed during the adsorption process can be determined by testing the weight loss data with several adsorption isotherms (i.e. Langmuir, Temkin, Freundlich, Frumkin). The adsorption isotherm that gave the best fit with r^2 values close to unity was chosen and used to calculate the adsorption parameters. For this study, the best description of the adsorption behaviour of the studied ILs was found to be given by the Langmuir adsorption isotherm. The relationship between the surface coverage and the concentration of the ILs was given by Equation 40. Langmuir plots were plotted as shown in Figures 4.67 – 4.69. The slopes, r^2, equilibrium constant of adsorption (K_{ads}) and Gibbs free energy of adsorption (ΔG°_{ads}) values are listed in Table 4.11.

© University of Venda

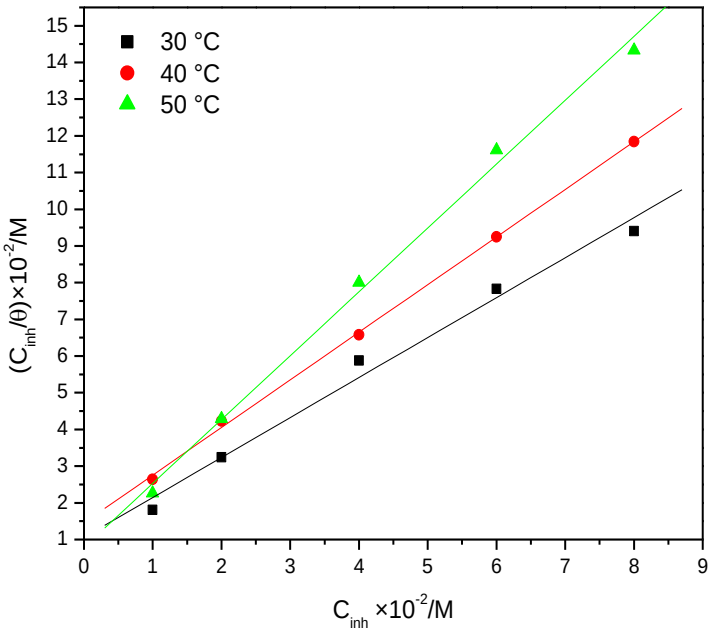

Figure 4.67: Langmuir adsorption isotherms for the corrosion of zinc in 1.0 M HCl at various temperatures for TDTB corrosion inhibitor.

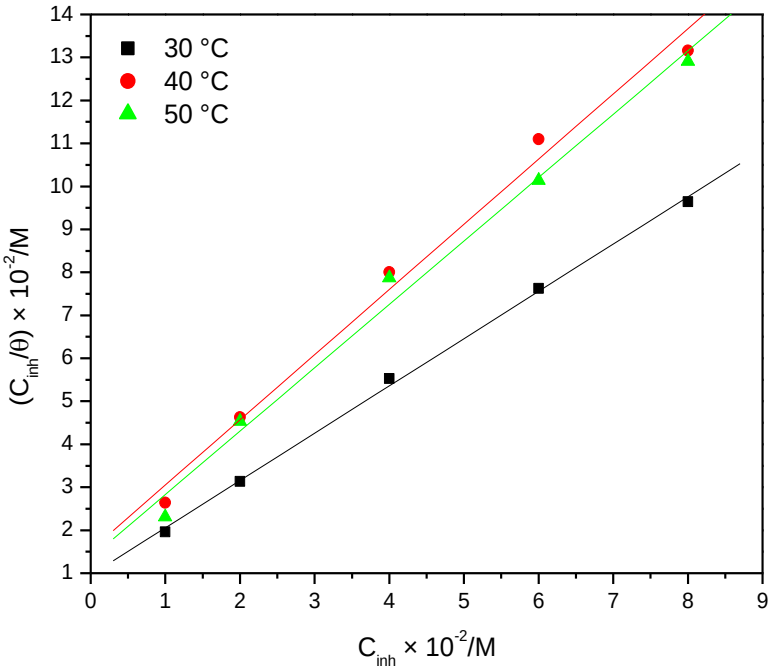

Figure 4.68: Langmuir adsorption isotherms for the corrosion of zinc in 1.0 M HCl at various temperatures for TDTM corrosion inhibitor.

© University of Venda

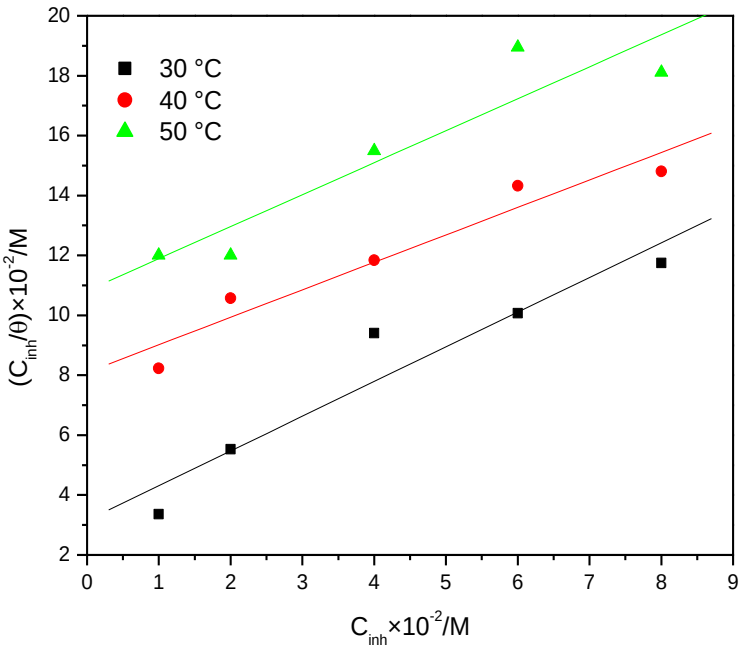

Figure 4.69: Langmuir adsorption isotherms for the corrosion of zinc in 1.0 M HCl at various temperatures for [EMIM][ESO_4] corrosion inhibitor.

Table 4.11: Langmuir adsorption parameters for the corrosion of zinc in 1.0 M HCl at various temperatures in the presence of TDTB, TDTM and [EMIM][ESO_4].

Inhibitor	Temperature (°C)	r^2	Slope	K_{ads} (M^{-1})	ΔG^0_{ads} (kJ mol^{-1})
TDTB	30	0.987	1.089	94.66	-21.58
	40	0.999	1.298	68.63	-21.46
	50	0.996	1.740	128.73	-23.83
TDTM	30	0.999	1.100	104.61	-23.27
	40	0.989	1.516	65.12	-21.32
	50	0.989	1.475	73.70	-20.95
[EMIM][ESO4]	30	0.917	1.158	31.67	-18.82
	40	0.934	0.917	12.35	-16.99
	50	0.870	1.068	9.24	-16.76

The values of r^2 and the slopes are close to unity. This signifies that a monolayer type of adsorption layer was formed on the metal surface [88, 89]. The values of K_{ads} and ΔG°_{ads} were calculated using Equations 41 and 42, respectively. The negative values of ΔG°_{ads} indicate that the adsorption process is spontaneous and that the layer adsorbed on the metal surface is stable [84]. As shown in Table 4.11 the ΔG°_{ads} values for all the inhibitors decreased with increase in temperature. This indicates that the %IE decreased with increase in temperature [90]. The values of ΔG°_{ads} for all the inhibitors are around -20 kJ mol^{-1}, this suggests that the

© University of Venda

adsorption can be attributed to electrostatic interactions between the charged metal and charged inhibitor molecules (i.e. physical adsorption occurred).

© University of Venda

CONCLUSIONS AND RECOMMENDATIONS

The inhibitory behaviours of 5-(Trifluoromethyl)dibenzothiophenium tetrafluoroborate [TDTB], 5-(Trifluoromethyl)dibenzothiophenium trifluoromethanesulfonate [TDTM] and 1-Ethyl-3-methylimidazolium ethyl sulfate [EMIM][ESO_4] were investigated using electrochemical [Potentiodynamic polarization (PDP), electrochemical impendence spectroscopy (EIS)], Fourier Transform Infrared spectroscopy (FTIR), Scanning Electron Microscopy (SEM) and gravimetric techniques.

The PDP results indicated that the compounds affected both the anodic and cathodic reactions for both mild steel and zinc metals, hence they can be classified as mixed-type inhibitors. In both metals, TDTM was found to significantly influence the anodic dissolution reaction more than the cathodic reaction. The EIS results also indicated that inhibition was achieved by the formation of an adsorption layer on the metal surfaces. The values of constant phase element exponent (*n*) were close to unity which is consistent with a capacitive interface. The FTIR data for adsorption films formed on both metals showed a disappearance of all prominent bands when compared to the pure ILs. These bands included C=N, O=S=O, C–N, for [EMIM][ESO_4], C=C, O=S=O, for TDTM and C=C for TDTB. This indicates that these functional groups acted as adsorption sites.

The SEM micrographs of the surfaces of mild steel and zinc showed a great improvement in the smoothness of the surfaces after the inhibitor molecules had been introduced to the aggressive medium. This indicates that an adsorption film formed which limited the interaction of the metal surface with the HCl solution.

At constant temperature, inhibition efficiency for all the inhibitors was observed to increase with an increase in concentration. At constant concentration, inhibition efficiency was observed to decrease with an increase in temperature. The Langmuir adsorption isotherm provided the best description of the adsorption process of the ILs. ΔG_{ads} values indicated that the adsorption process was spontaneous, and a physical adsorption mechanism was suggested for both metals.

The orders of inhibition efficiency at 8.0×10^{-2} M were TDTM > TDTB > [EMIM][ESO_4] and TDTB > TDTM > [EMIM]ESO_4] for mild steel and zinc, respectively. All inhibitors showed superior performance in mild steel than in zinc.

The ILs provided optimal inhibition at 30 °C hence they can be recommended for low temperature applications for both mild steel and zinc.

© University of Venda

REFERENCES

1. V.S. Sastri, E. Ghali, M. Elboujdaini, Corrosion prevention and protection: practical solutions, Wiley, Chichester, England, 2007, pp. 3 – 18.
2. P.R. Roberge, Corrosion engineering: principles and practice, McGraw-Hill, New York, 2008, pp. 13 – 428.
3. Z. Ahmad, Principles of corrosion engineering and corrosion control, Butterworth Heinemann, Oxford, UK, 2006, pp. 1 – 10.
4. R.G. Kelly, J.R. Scully, D.W. Shoesmith, R.G. Buchheit, Electrochemical techniques in corrosion science and engineering, Marcel Dekker, New York, 2003, pp. 1 – 54.
5. J.R. Scully, Electrochemical Impedance Spectroscopy for evaluation of organic coating deterioration and under film corrosion, Naval Civil Engineering Laboratory, Port Hueneme, CA, 1986, pp. 1 – 175.
6. D. Talbot, J. Talbot, Corrosion science and technology, Taylor and Francis, Boca Raton, FL, 2007, 1 – 192.
7. P.A. Schweitzer, Fundamentals of metallic corrosion: atmospheric and media corrosion metals, CRC Press, Boca Raton, FL, 2006, pp. 1 – 65.
8. M.C. Gonçalves, Materials for construction and civil engineering, Springer International Publishing, Switzerland, 2015, pp. 679 – 700.
9. K.E. Heusler, D. Landolt, S. Trasatti, Electrochemical corrosion nomenclature, *Pure Appl. Chem.*, 61 (1989) 19 – 22.
10. Corrosion of metals and alloys. Basic terms and definitions, EN ISO 8044: 2015.
11. M.G. Fontana, Corrosion engineering, McGraw-Hill Book Company, New York, 1986, pp. 1 – 350.
12. P.R. Roberge, Handbook of corrosion engineering, McGraw-Hill, New York, 2000, pp. 1 – 861.
13. L.L. Shreir, G.T. Burstein, R.A. Jarman, Corrosion, Butterworth-Heinemann, Oxford, 1994, pp. 1 – 990.
14. B.N. Popov, Corrosion engineering: principles and solved problems, Elsevier, Amsterdam, 2015, pp. 1 – 278.
15. H.H. Uhlig, R.W. Revie, Corrosion and corrosion control, J. Wiley, Hoboken, NJ, 2008, pp. 1 – 314.
16. J.R. Davis, Corrosion: Understanding the basics, ASM International, Materials Park, OH, 2011, pp. 20 – 370.
17. E. Bardal, Corrosion and protection, Springer, London, 2004, pp.1 – 259.

© University of Venda

18. A. Bahadori, Corrosion and materials: a guide for the chemical and petroleum industries, Wiley, Chichester, 2014, pp. 125 – 155.
19. X.G. Zhang, Corrosion and electrochemistry of zinc, Springer, New York, 1996.
20. K.A. Chandler, Marine and offshore corrosion: marine engineering series, Elsevier Ltd, Butterworth-Heinemann, 1985, pp. 39.
21. E. Mattsson, Basic corrosion technology for scientists and engineers, Institute of Materials, London, UK, 1996, pp. 1 – 107.
22. R.W. Revie, Uhlig's corrosion handbook, 3rd edition, John Wiley and Sons, Hoboken, NJ, 2011, pp. 1 – 299.
23. K. Elayaperumal, V.S. Raja, Corrosion failures, Wiley, Hoboken, NJ, 2015, pp. 2 – 70.
24. E. McCafferty, Introduction to corrosion science, Springer, New York, 2010, pp. 1 – 396.
25. D. Parker, "Skills transfer, capacity building imperative in corrosion control industry", Engineering News, 28 May 2009: Web. 15 July 2016.
26. G.H. Koch, M.P.H. Brongers, N.G. Thompson, Y.P. Virmani, J.H. Payer, Cost of corrosion and prevention strategies in the United States, C.C. Technologies Laboratories, Inc, USA, 2011.
27. D.A. Jones, Principles and Prevention of Corrosion, Prentice-Hall, Upper Saddle River, N.J., USA, 2nd edn, 1996, pp. 345.
28. D. Landolt, Corrosion and surface chemistry of metals, EPFL Press, Lausanne Switzerland, 2007, pp. 1 – 560.
29. A. Almubarak, W. Abuhaimed, A. Almazrouee, Corrosion behavior of the stressed sensitized austenitic stainless steels of high nitrogen content in seawater, *Int. J. Electrochem.*, 2013(2013) 1 – 7.
30. P.A. Schweitzer, Fundamentals of corrosion: mechanisms, causes and preventative methods, CRC Press, Boca Raton, FL, 2010, pp. 1 – 326.
31. V. Cicek, Cathodic protection, John Wiley and Sons, Inc., Hoboken, NJ, 2013, pp. 1 – 122.
32. S.H. Teoh, Engineering materials for biological applications, Word Scientific, New Jersey, 2007.
33. D.R. Askeland, P.P. Fulay, W.J. Wright, The science and engineering of materials, Cengage Learning, Stamford, CT, 2011, pp. 876.
34. P.A. Schweitzer, Atmospheric degradation and corrosion control, Marcel Dekker, New York, 1999, pp. 9 – 12.
35. S. Papavinasam, D. Abayarathna, Corrosion control in the oil and gas industry, Gulf Professional Publishing, 2014, pp. 249 – 710.

© University of Venda

36. V.M. Balsaraf, Applied Chemistry, volume 2, I.K. International Publishing House, New Delhi, 2009, pp. 1 – 3.
37. B.K. Ambasta, Chemistry for engineers, University Science Press, New Delhi, 2012, pp. 153 – 187.
38. V. Cicek, B. Al-Numan, Corrosion chemistry, Wiley, Hoboken, NJ, 2011, pp. 03 – 07.
39. A. Moncmanová, Environmental deterioration of materials, WIT Press, Southhampton, UK, 2007, pp. 27 – 138.
40. E.E. Stansbury, R.A. Buchanan, Fundamentals of electrochemical corrosion, ASM International, Materials Park, OH, 2000, pp. 1 – 268.
41. H. Ashassi-Sorkhabi, M. Es'haghi. Corrosion inhibition of mild steel in acidic media by [BMIm] Br Ionic liquid. *Mater. Chem. Phys.*,114(2009) 267 – 271.
42. S.S. Zumdahl, D.J. DeCoste, Chemical principles, Cengage Learning, Belmont, CA, 2013, pp. 500.
43. J.K. Wessel, Handbook of advanced materials, Wiley, Hoboken, NJ, 2004, pp. 487 – 540.
44. V.S. Sastri, E. Ghali, M. Elboujdaini, Corrosion prevention and protection: practical solutions, Wiley, Chichester, England, 2007, pp. 3 – 246.
45. H.Z. Alkhathlan, M. Khan, M.M.S. Abdullah, A.M. Al-Mayouf, A.A. Mousa, Z. A.M. Al-Othman, Launaea nudicaulis as a source of new and efficient green corrosion inhibitor for mild steel in acidic medium: a comparative study of two solvent extracts, *Int. J. Electrochem. Sci*., 9 (2014) 870 – 889.
46. S.K. Shukla, L.C. Murulana, E.E. Ebenso, Inhibitive effect of imidazolium based aprotic ionic liquids on mild steel corrosion in hydrochloric acid medium, *Int. J. Electrochem. Sci.*, 6 (2011) 4286 – 4295.
47. N.O. Obi-Egbedi, I. B. Obot, A. O. Eseola, Synthesis, characterization and corrosion inhibition efficiency of 2-(6-methylpyridin-2-yl)-1H-imidazo [4, 5-f][1, 10] phenanthroline on mild steel in sulphuric acid, *Arabian J. Chem*. 7(2) (2014): 197 – 207.
48. F. Ropital, T. Jones, Corrosion and degradation of metallic materials, Éd. Technip, Paris, 2010, pp. 98 – 233.
49. L, Garverick, Corrosion in the petrochemical industry, ASM International, Ohio, 1995, pp. 1 – 389.
50. Q.B. Zhang, Y.X. Hua, Corrosion inhibition of aluminum in hydrochloric acid solution by alkylimidazolium ionic liquids, *Mater. Chem. Phys.*, 119 (2010) 57 – 64.
51. Q. B. Zhang, Y. X. Hua, Corrosion inhibition of mild steel by alkylimidazolium ionic liquids in hydrochloric acid, *Electrochim. Acta*, 54(6) (2009) 1881 – 1887.
52. M. Freemantle, An introduction to ionic liquids, RSC Pub, Cambridge, UK, 2010, pp. 1 – 76.

© University of Venda

53. J. Kärkkäinen, Preparation and characterization of some ionic liquids and their use in the dimerization reaction of 2-methylpropene, University of Oulu, Oulu, 2007, pp. 1 – 112.
54. A. Kokorin, Ionic Liquids: Applications and Perspectives, InTech, Rijeka, Croatia, 2011, 29 – 95.
55. B. Kirchner, B. Clare, Ionic liquids, Springer Verlag, Heidelberg, 2009, pp. 1 – 36.
56. H. Ohno, Electrochemical aspects of ionic liquids, Wiley, Hoboken, NJ, 2005, pp. 5 – 26.
57. P.J. Dyson, T.J. Geldbach. Applications of ionic liquids in synthesis and catalysis, *Electrochem. Soc. Interface.*, 16 (2007) 50 – 53.
58. P. Wasserscheid, T. Welton, eds. Ionic liquids in synthesis, John Wiley & Sons, 2008, pp. 1 – 70.
59. P. Bonhote, A.P. Dias, N. Papageorgiou, K. Kalyanasundaram, M. Grätzel, Hydrophobic, highly conductive ambient-temperature molten salts, *Inorg. Chem.*, 35 (5) (1996), 1168 – 1178.
60. S.T. Handy, Room temperature ionic liquids: different classes and physical properties. *Curr. Org. Chem.*, 9 (10) (2005) 959 – 988.
61. B.C. Ranu, S. Banerjee, Ionic liquid as catalyst and reaction medium. The dramatic influence of a task-specific ionic liquid, [bmIm] OH, in michael addition of active methylene compounds to conjugated ketones, carboxylic esters, and nitriles, *Org. Lett.*, 7 (14) (2005) 3049 – 3052.
62. X. Zhou, H. Yang, F. Wang, [BMIM] BF4 ionic liquids as effective inhibitor for carbon steel in alkaline chloride solution *Electrochim. Acta*, 56 (2011) 4268 – 4275.
63. N.V. Likhanova, M. A. Domínguez-Aguilar, O. Olivares-Xometl, N. Nava-Entzana, E. Arce, H. Dorantes, The effect of ionic liquids with imidazolium and pyridinium cations on the corrosion inhibition of mild steel in acidic environment. *Corros. Sci.*, 52 (6) (2010) 2088 – 2097.
64. Y. Sasikumar, A.S. Adekunle, L.O. Olasunkanmi, I. Bahadur, R. Baskar, M.M. Kabanda, I.B. Obot, E.E. Ebenso, Experimental, quantum chemical and Monte Carlo simulation studies on the corrosion inhibition of some alkyl imidazolium ionic liquids containing tetrafluoroborate anion on mild steel in acidic medium. *J. Mol. Liq.*, 211 (2015) 105 – 118.
65. N.O. Obi-Egbedi, K. E. Essien, I. B. Obot, E. E. Ebenso, 1, 2-Diaminoanthraquinone as corrosion inhibitor for mild steel in hydrochloric acid: weight loss and quantum chemical study, *Int. J. Electrochem. Sci.*, 6 (2011) 913 – 930.

© University of Venda

66. M. Mahdavian, M.M. Attar, Electrochemical behaviour of some transition metal acetylacetonate complexes as corrosion inhibitors for mild steel, *Corros. Sci.*, 51 (2009) 409 – 414.
67. A.M. Abdel-Gaber, M. S. Masoud, E. A. Khalil, E. E. Shehata, Electrochemical study on the effect of Schiff base and its cobalt complex on the acid corrosion of steel, *Corros. Sci.,* 51 (12) (2009) 3021 – 3024.
68. A. Lecante, F. Robert, P.A. Blandinières, C. Roos, Anti-corrosive properties of S. tinctoria and G. ouregou alkaloid extracts on low carbon steel, *Curr. Appl. Phys.*, 11 (2011) 714 – 724.
69. F.M. Reisde, H.G. Melo, I. Costa, EIS investigation on Al 5052 alloy surface preparation for self assembling monolayer, *Electrochim. Acta*, 51 (2006) 1780 – 1788.
70. M. Lebrini, M. Lagrene, H. Vezin, M. Traisnel, F. Bentis, Experimental and theoretical study for corrosion inhibition of mild steel in normal hydrochloric acid solution by some new macrocyclic polyether compounds, *Corros. Sci.*, 49 (2007) 2254 – 2269.
71. M. Faustin, A. Maciuk, P. Salvin, C. Ross, M. Lebrini, Corrosion of C38 steel by alkaloids extract of Geissopermum laeve in 1 M hydrochloric acid: Electrochemical and phytochemical studies, *Corros. Sci.*, 92 (2015) 287 – 300.
72. L.O. Olasunkanmi, M.M. Kabanda, E.E. Ebenso, Quinoxaline derivatives as corrosion inhibitors for mild steel in hydrochloric acid medium: Electrochemical and quantum chemical studies, *Physica E*, 76 (2016) 109 – 126.
73. L.C. Murulana, A.K. Singh, S.K. Shukla, M.M. Kabanda, E.E. Ebenso, Experimental and quantum chemical studies of some bis(trifluoromethyl-sulfonyl) imide imidazolium-based ionic liquids as corrosion inhibitors from mild steel in hydrochloric acid solution, *Ind. Eng. Chem. Res.*, 51 (2012) 13282 – 13299.
74. R. Karthikaiselvi, S. Subhashini, Study of adsorption properties and inhibition of mild steel corrosion in hydrochloric acid media by water soluble composite poly (vinyl alcohol-*o*-methoxy aniline), *J. Assoc. Arab Univ. Basic Appl. Sci.*, 16 (2014) 74 – 82.
75. M.E. Mashuga, L.O. Olasunkanmi, A.S. Adekunle, S. Yesudass, M.M. Kabanda, E.E. Ebenso, Adsorption, thermodynamic and quantum chemical studies of1-hexyl-3-methylimidazolium based ionic liquids as corrosion inhibitors for mild steel in HCl, *Materials*, 8 (2015) 3607 – 3632.
76. L.C. Murulana, M.M. Kabanda, E.E. Ebenso, Experimental and theoretical studies of the corrosion inhibition of mild steel by some sulphonamides in aqueous HCl, *RSC Adv.*, 5 (2015) 28743 – 28761.
77. A.M. Atta, G.A. El-Mahdy, H.A. Al-Lohedan, A.O. Ezzat, Synthesis and application of hybrid polymer composites based on silver nanoparticles as corrosion protection for line pipe steel, *Molecules*, 19 (2014) 6246 – 6262.

© University of Venda

78. A.I. Onen, B.T. Nwufo, E.E. Ebenso, R.M. Hlophe, Titanium (IV) oxide as corrosion inhibitor for aluminium and mild steel in acidic medium, *Int. J. Electrochem. Sci.*, 5 (2010) 1563 – 1573.
79. A. Popova, E. Sokolova, S. Raicheva, M. Chritov, AC and DC study of the temperature effect on mild steel corrosion in acid media in the presence of benzimidazole derivatives, *Corros. Sci.*, 45 (2003) 33 – 58.
80. M. Bouklah, B. Hammouti, M. Lagrenée, F. Bentiss, Thermodynamic properties of 2,5-bis(4-methoxyphenyl)-1,3,4-oxadiazole as a corrosion inhibitor for mild steel in normal sulfuric acid medium, *Corros. Sci.*, 48 (2006) 2831 – 2842.
81. A.M. Al-Turkustani, Thermodynamic, chemical and electrochemical investigation pandanus tectorius extract as corrosion inhibitor for steel sulphuric acid solutions, *Eur. J. Chem.*, 4 (3) (2013) 303 – 310.
82. I.B. Obot, N.O. Obi-Egbedi, Adsoption properties and inhibition of mild steel corrosion in sulphuric acid solution by ketoconazole: experimental and theoretical investigation, *Corros. Sci.*, 52 (2010) 198 – 204.
83. F.M. Donahue, K. Nobe, Theory of organic corrosion inhibitors adsorption and linear free energy relationships, *J. Electrochem. Soc.*, 112 (9) (1965) 886 – 891.
84. F. Bentiss, M. Lebrini, H. Vezin, F. Chai, M. Traisnel, M. Lagrene, Enhanced corrosion resistance of carbon steel in normal sulfuric acid medium by some macrocyclic polyether compounds containing a 1,3,4-thiadiazole moiety AC impedance and computational studies, *Corros. Sci.*, 51 (2005) 2165 – 2173.
85. W.J. Lorenz, F. Mansfeld, Determined of corrosion rates by electrochemical DC and AC methods, *Corros. Sci.*, 21 (1981) 647 – 672.
86. A.K. Singh, M.A. Quraishi, Investigation of adsorption of isoniazid derivatives at mild steel/hydrochloric acid interface: Electrochemical and weight loss methods, *Mater. Chem. Phys.*, 123 (2010) 666 – 677.
87. A.K. Singh, M.A. Quraishi, The effect of some bis-thiadiazole derivatives on the corrosion of mild steel in hydrochloric acid, *Corros. Sci.*, 52 (2010) 1373 – 1385.
88. A.Y. El-Etre, M. Abdallah, Z.E. El-Tantawy, Corrosion inhibition of some metals using lawsonia extract, *Corros. Sci.*, 47 (2005) 385 – 395.
89. F. Bentiss, M. Traisnel, M. Lagrenee, The substituted 1,3,4-oxadiazoles: a new class of corrosion inhibitors of mild steel in acidic media, *Corros. Sci.*,42 (2000) 127 – 146.
90. I. Ahamad, M.A. Quraish, Mebendazole: new and efficient corrosion inhibitor for mild steel in acid medium, *Corros. Sci.*, 52 (2010) 651 – 656.

© University of Venda